

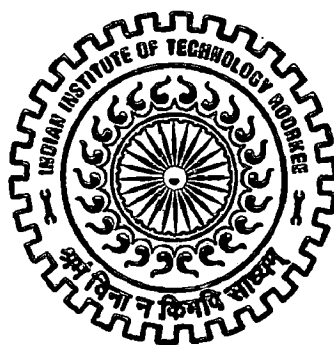
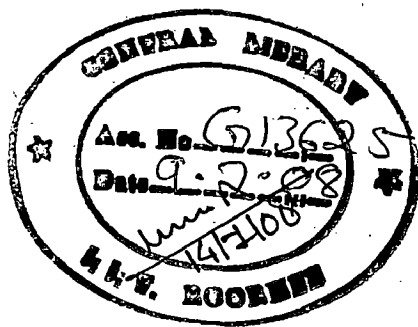
NICKEL COMPLEXES OF PYRAZOLYL BORATE AND THEIR CATALYTIC ACTIVITIES

A DISSERTATION

*Submitted in partial fulfillment of the
requirements for the award of the degree
of*
MASTER OF TECHNOLOGY
in
ADVANCED CHEMICAL ANALYSIS

By

SAURABH GOYAL



DEPARTMENT OF CHEMISTRY
INDIAN INSTITUTE OF TECHNOLOGY ROORKEE
ROORKEE - 247 667 (INDIA)

JUNE, 2007



INDIAN INSTITUTE OF TECHNOLOGY ROORKEE
ROORKEE

CANDIDATE'S DECLARATION

I hereby declare that the work which is being presented in the thesis entitled "NICKEL COMPLEXES OF PYRAZOLYL BORATE AND THEIR CATALYTIC ACTIVITIES" in partial fulfillment of the requirements for the award of the degree of Master of Technology with specialization in "Advanced Chemical Analysis" submitted in the Department of Chemistry, Indian Institute of Technology Roorkee, Roorkee is an authentic record of my own work carried out during the period from July 2006 to June 2007 under the guidance of Dr. Udai P. Singh, Associate Professor, Department of Chemistry, Indian Institute of Technology Roorkee, Roorkee.

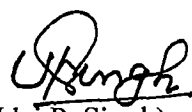
The matter embodied in this thesis to the best of my knowledge has not been submitted for the award of any other degree of this or any other Institute.

Date: 29.06.07

Place: Roorkee


(SARABH GOYAL)

This is to certify that the above statement made by the candidate is correct to the best of my knowledge.


(Udai P. Singh)
Associate Professor
Department of Chemistry
Indian Institute of Technology Roorkee
Roorkee - 247 667 (India)

ACKNOWLEDGEMENT

Perseverance, inspiration and motivation have always plays a key role in the success of any venture. At this level of understanding, it is often difficult to understand the wide spectrum of knowledge without proper guidance and advice. Hence it gives me great pleasure to express my deep sense to my supervisor Dr. U. P. Singh, Associate Professor, Indian Institute of Technology Roorkee for their restorative guidance, encouragement and valuable suggestion with his inspiring ideas all through this work.

I wish to express my sincere thanks to Dr. Ravi Bhushan, Professor and Head, Department of Chemistry, Indian Institute of Technology Roorkee, Dr R. K. Datta (Coordinator for M. Tech programme) for giving me excellent support and guidance.

I express my gratitude to all my teachers at the Department of Chemistry. I wish to thank Mr. Vaibhave Aggarwal, Mr. Raj Kumar, Mr. Rajeev Kumar, Ms. Pooja Tyagi, Ms. Sujata and Ms. Nidhi Goyal for their constructive support and cooperating with me during the dissertation work and helping me in all possible manners.

I thank I.I.T Roorkee for providing me all the necessary facilities, and MHRD, New Delhi for financial assistance.


SAURABH GOYAL

ABSTRACT

Addition of potassium hydrotris(3-phenyl-5-methyl-pyrazolyl)borate ligand $[K\text{Tp}^{\text{Ph, Me}}]$ to a solution of NiCl_2 and 3-phenyl-5-methyl-pyrazole $[\text{pz}^{\text{Ph, Me}}\text{H}]$ in dichloro methane and methanol yields the structurally characterized complex **2** $[\text{Ni}(\text{Tp}^{\text{Ph, Me}})(\text{pz}^{\text{Ph, Me}})\text{Cl}]$ which is further reacted with different substituted benzoates to form complexes type $[\text{Ni}(\text{Tp}^{\text{Ph, Me}})(\text{pz}^{\text{Ph, Me}})(\text{X-OBz})]$ ($\text{X} = \text{H, Me, OMe, NO}_2, \text{Cl, F, CHO, CN, NH}_2, \text{OH}$). IR spectroscopy confirms that $\text{Tp}^{\text{Ph, Me}}$ ligand is α^3 coordinated in all the complexes and the benzoates are coordinated as monodentate terminally. Also the reaction of complex **2** with $\text{NaN}_3, \text{KCN, KSCN}$ in methanol and toluene yields $[\text{Ni}(\text{Tp}^{\text{Ph, Me}})(\text{pz}^{\text{Ph, Me}})(\text{Y})]$ ($\text{Y} = \text{N}_3, \text{NCS, CN}$) the IR spectra shows the monodentate terminal binding of these ligands. The magnetic susceptibility studies suggest that complexes **2-16** are paramagnetic with two unpaired electrons. The X-ray crystallographic studies of **2-5, 7** and **13-15** reveals the distorted square pyramidal nickel centre. Thermogravimetric measurements were also carried out to all the complexes to check their thermal stabilities. Finally the SOD activity of complexes **2-16** for 50% inhibition of superoxide ions in biological system shows the activity of complexes at different levels.

CONTENTS

CANDIDATES'S DECLARATION	i
ACKNOWLEDGEMENT	ii
ABSTRACT	iii
1. INTRODUCTION	1
2. EXPERIMENTAL SECTION	
2.1 Chemicals and suppliers	17
2.2 The make and model of instruments	18
2.3 Procedure	18
2.3.1a Synthesis of 3-phenyl-5-methyl pyrazole	18
2.3.1b Synthesis of potassium hydrotris(3-phenyl-5-methyl-pyrazolyl)borate	18
2.3.2 Synthesis of $[\text{Ni}(\text{Tp}^{\text{Ph,Me}})(\text{pz}^{\text{Ph,Me}})\text{Cl}]$	19
2.3.3 Synthesis of $[\text{Ni}(\text{Tp}^{\text{Ph,Me}})(\text{pz}^{\text{Ph,Me}})(\text{OBz})]$	19
2.3.4 Synthesis of $[\text{Ni}(\text{Tp}^{\text{Ph,Me}})(\text{pz}^{\text{Ph,Me}})(p\text{-Cl-OBz})]$	19
2.3.5 Synthesis of $[\text{Ni}(\text{Tp}^{\text{Ph,Me}})(\text{pz}^{\text{Ph,Me}})(p\text{-F-OBz})]$	20
2.3.6 Synthesis of $[\text{Ni}(\text{Tp}^{\text{Ph,Me}})(\text{pz}^{\text{Ph,Me}})(p\text{-NO}_2\text{-OBz})]$	20
2.3.7 Synthesis of $[\text{Ni}(\text{Tp}^{\text{Ph,Me}})(\text{pz}^{\text{Ph,Me}})(p\text{-Me-OBz})]$	20
2.3.8 Synthesis of $[\text{Ni}(\text{Tp}^{\text{Ph,Me}})(\text{pz}^{\text{Ph,Me}})(p\text{-MeO-OBz})]$	20
2.3.9 Synthesis of $[\text{Ni}(\text{Tp}^{\text{Ph,Me}})(\text{pz}^{\text{Ph,Me}})(p\text{-NH}_2\text{-OBz})]$	20
2.3.10 Synthesis of $[\text{Ni}(\text{Tp}^{\text{Ph,Me}})(\text{pz}^{\text{Ph,Me}})(p\text{-HO-OBz})]$	21
2.3.11 Synthesis of $[\text{Ni}(\text{Tp}^{\text{Ph,Me}})(\text{pz}^{\text{Ph,Me}})(p\text{-CHO-OBz})]$	21
2.3.12 Synthesis of $[\text{Ni}(\text{Tp}^{\text{Ph,Me}})(\text{pz}^{\text{Ph,Me}})(p\text{-CN-OBz})]$	21
2.3.13 Synthesis of $[\text{Ni}(\text{Tp}^{\text{Ph,Me}})_2]$	21
2.3.14 Synthesis of $[\text{Ni}(\text{Tp}^{\text{Ph,Me}})(\text{pz}^{\text{Ph,Me}})(\text{N}_3)]$	21
2.3.15 Synthesis of $[\text{Ni}(\text{Tp}^{\text{Ph,Me}})(\text{pz}^{\text{Ph,Me}})(\text{NCS})]$	22
2.3.16 Synthesis of $[\text{Ni}(\text{Tp}^{\text{Ph,Me}})(\text{pz}^{\text{Ph,Me}})(\text{CN})]$	22

Chapter -1

INTRODUCTION

Introduction:

For a long time, Nickel has been the only element of the “late” 3d transition metals for which a biological role could not be definitely established. The reason for this oversight was manifold: nickel ions do not exhibit a very characteristic light absorbance in the presence of physiologically relevant ligands. In addition, it has now been shown that Ni is often only one of the several components of complex enzymes, which may otherwise contain several coenzymes as well as additional inorganic material. Nickel is an essential nutrient for selected microorganisms where it participates in a variety of cellular processes. Many microbes are capable of sensing cellular nickel ion concentrations and taking up this nutrient via nickel-specific permeases or ATP-binding cassette-type transport systems. The metal ion is specifically incorporated into nickel-dependent enzymes, often via complex assembly processes requiring accessory proteins and additional non-protein components, in some cases accompanied by nucleotide triphosphate hydrolysis. For instance, nickel centres remained undetected for a long time due to their frequent association with Fe/S clusters. However applying more sensitive detection methods in atomic absorption or emission spectroscopy (AAS or AES), magnetic measuring (SQUID) or EPR spectroscopy using ⁶¹Ni enriched material, some nickel containing enzymes of plant and microorganisms have now been established and partly characterized. Low concentrations of nickel (0.015 mg per kg) in the diet resulted in decreased weight gains in growing rats in comparison with nickel supplemented control animals. Nickel deficiency appeared to decrease the absorption of iron by rats, with resultant development of anemia, and also caused 29-82% decrease in the activity of dehydrogenase enzymes and 45% decrease in the activity of enzymes of amino acids metabolism in liver. In both liver and serum of nickel deficient rats, the concentration of glucose and glycogen were decreased by 90% [1]. In female goats and minipigs, nickel deficiency caused decrease conception rates after artificial insemination. The offspring from these nickel deficient dams had reduced birth weight and weight gains during suckling when compared to nickel-supplemented controls animals.

Only in the late 1960s, it was nickel beginning to be considered as a necessary component for the growth of some anaerobic bacteria. In 1975 the metal was reported to occur in plant urease and also provided the first documentation of nickel activity on a molecular level [2]. To date, nine nickel-containing enzymes are known: urease, NiFe-

hydrogenase, carbon monoxide dehydrogenase, acetyl-CoA decarbonylase/synthase, methyl coenzyme M reductase, certain superoxide dismutases, some glyoxylases, aci-reductone dioxygenase, and methylenediurease. Seven of these enzymes have been structurally characterized, revealing distinct metalcenter environments in each case [3]. Whereas the urease enzymes of bacteria and plant contains 5- or 6- coordinate Ni(II) bound to N, O-ligands, both the hydrogenases of many bacteria and the CO dehydrogenase of anaerobic bacteria contain Ni which is mainly coordinated by sulphur ligands. The methyl-coenzymes M reductase of methanogenic bacteria features a nickel tetrapyrrole complex as the prosthetic group, the coenzyme F430. Another tetrapyrrole complex with an as yet unspecified function, the nickel containing tunichlorin, was isolated from a tunicate species [4].

Nickel is now recognised as an essential trace element for bacteria, plants, animals and humans [5]. While the role of this metal in animal biochemistry is still not well defined, to date four bacterial enzymes have been found to be Ni dependent urease (also found in plants), carbon monoxide dehydrogenase (CODH), hydrogenase (H₂-ase) and methyl-S-coenzyme-M methyl reductase (MCR), which employs a Ni-containing prosthetic group. The Ni environment within each protein is different, however the Ni centres are believed to reside within the active sites of all these enzymes and to be intimately involved in there catalytic cycles. Several aspects of the chemistry of these biological Ni ions are unusual in the context of the known coordination chemistry of nickel: three of the four enzymes are known to contain redox-active nickel centres that can cycle between +3, +2, and/or +1 oxidation states, in thiolate-rich or tetrapyrrole ligand environments that were not previously thought to favor metal-centered redox processes in the Ni complexes.

Urease is a metalloenzyme that catalyses the hydrolysis of urea to form ammonia and carbamate. This hydrolysis has not been observed without the enzyme, so the rate enhancement produces by urease is $>10^{14}$. Thus, the catalytic mechanism that yields this rate enhancement is an interesting problem. This mechanism is likely to involve the two-nickel ions present in the urease active site, as well as amino acid residues, possibly acting as general acids and bases. The observed pH profile of activity is bell-shaped with two pKa's: a lower pKa of 6.5 and higher pKa of 9.0, indicating that the protonation state of two groups effect urease activity. Based on crystallographic and kinetic studies of the urease from *Klebsiella aerogenes*, which includes the structure of the wild type enzymes at ambient

temperature, a 1.6 Å resolution wild-type structure at cryogenic temperature, and several mutant structures, furthers a detailed mechanism for urease [6]. In this proposal, the residue His 219, along with the first Ni ion, binds the urea oxygen, positioning the urea molecule and polarizing the carbonyl. The second nickel without the aid of general base, stabilizes a hydroxide ion, which attack the urea carbon. One of the amide nitrogens of urea is protonated by the general acid His 320, and ammonia is eliminated. This key histidine act as an acid and must be in its protonated form for activity, even though it has been assigned a pKa of 6.5 which is lower than the pH optimum for enzyme. Thus, the active protonation state of urease is reverse-protonated, meaning that a group with a lower pKa must be protonated and a group with a higher pKa must be deprotonated for activity. The higher pKa of 9.0 has been interpreted as being due to the metal-bound hydroxide, which must be deprotonated for activity.

The 2.2 Å resolution X-ray crystal structure of *Klebsiella aerogenes* urease revealed a trimer of trimers containing three di-Ni active sites [7]. The two Ni ions are located 3.5 Å apart and bridged by a carbamate formed by reaction of the activating CO₂ with Lys 217. The active site has coupled Ni(II) ions, Ni-1 is coordinated by two N (His^{α246}, His^{α272}) and one O (O of carbamylated Lys^{α217}), and Ni-2 is coordinated by two N (His^{α134}, His^{α136}) and three O (Asp^{α360}, water and carbamylated Lys^{α217}).

The holoenzyme of jackbeans urease consists of six equivalent subunits; each subunit (91 kDa) contains two close but apparently different nickel ions [8]. EXAFS measurements have only nitrogen and oxygen ligands in the first coordination spheres and have suggested coordination numbers of five and or six in agreement with the magnetic and absorption spectroscopic studies. Measurement of the magnetic susceptibility point to an equilibrium between high spin and low spin forms, which would be typical for five coordinate or disordered six coordinate Ni(II) due to small and variable energy difference between dz² and dx²-dy² orbitals.

On the basis of model studies, the proposed reaction mechanism involves an electrophilic attack of one of the nickel centers on the carbonyl oxygen atom and a nucleophilic attack of a nickel hydroxo species on the carbonyl carbon center. Similar mechanistical hypothesis exists for the function for Zn-containing hydrolytic enzymes where

protons often functions as the electrophilic species. Hydrolytic zinc enzymes thus required only one metal center to provide the hydroxide nucleophile in an H₂O activation step. It is not entirely obvious why hydrolytic nickel centre are present only in urease; e.g. it is possible to substitute nickel for zinc in well characterized zinc-containing enzymes such as carboxypeptidase A (CPA) and carbonic anhydrase (CA). Perhaps the less stringent stereochemical requirements regarding selectivity and the large number of potentially coordinating hetro atoms in urea favor Ni(II) centers over typically lower coordinate Zinc(II).

The electronic spectrum of urease shows d-d absorptions at λ_{max} (ϵ_{max}) = 1600 nm ($10 \text{ M}^{-1}\text{cm}^{-1}$), 910 (13), 745(46) and 407(sh), [3] consistent with octahedral or high spin five coordinate Ni ions bound by N- and O-donor ligands. While it is clear from the above data that urease Ni is ligated by N and O donors only, the coordination geometry about each Ni ion, the distance between the metal centers and the nature of many bridging ligand remain to be determined. On the basis of comparisons with dinuclear Ni complexes containing bridging carboxylate [9, 10-13] or carbonate ligands, [14, 15] or by employment of molecular models, the bridging intermediate in the proposed urease hydrolysis mechanism is thought to possess a Ni²⁺-Ni separation of approximately 3.4, 4.2 or 6.0 Å depending upon the Ni-O-C angle, the presence of carboxylate or imidazolate bridge between the Ni ions in this species would require a Ni²⁺-Ni distance of < 4.0 and 5.3 Å, respectively.

Methyl-CoM reductase is the key enzyme in the energy metabolism of strictly anaerobic archaea called methanogens [16]. Methyl-CoM reductase has a molecular mass of about 300 kDa and is composed of three different types of subunits α , β , γ arranged as a hexamer of $(\alpha\beta\gamma)_2$ composition. The multi subunit complex contains two molecule of Ni-porphinoid coenzyme F430, coenzyme M (mercaptoethane suffonate) and coenzyme B (mercapto heptanothreonine phosphate). The enzyme catalyzes the final reaction of the methanogenic pathway by reducing methyl-CoM to methane with coenzyme B as electron donor forming the hetrodisulphide CoM-S-S-CoB. The crystal structure of methyl-CoM reductase from *Methanobacterium thermoautoropium* has been determind to 1.45 Å resolution. The overall structure is characterized by a series of α helices. The active site and the binding site of the coenzymes are formed by subunit α , α' , β and γ indicating that the entire hexamer is required for enzymatic activity.

The coenzyme F₄₃₀ is anchored to the protein matrix mainly by hydrogen bonds between carboxylate groups of the tetrapyrrole ring and main chain amide groups of residues from subunits α , α' , β and γ . The Ni atom is axially coordinated to the side chain amide oxygen atom of Gln α' 147. Coenzyme M and B and the active sites are located on the other side of the Ni-porphinoid plane. The binding of coenzyme B shields the active sites from bulk solvent by locking a channel leading from the protein surface to the active site.

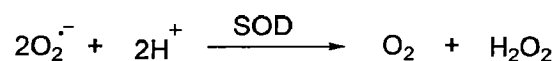
Methyl-CoM reductase catalyses the final reaction step in the formation of methane by methanogenic archaea, the reduction of methyl-coenzyme M with coenzyme B to methane and the hetrodisulfide of coenzyme M and coenzyme B [17].

Hydrogenase is an enzyme, which catalyse the oxidation and reduction of molecular hydrogen. Two type of hydrogenase, iron only and iron-nickel hydrogenases have been found in the sulphate-reducing bacteria. The three dimensional structure of the nickel iron hydrogenase from *Desulfovibrio gigas* at 2.85 Å, showing the location, coordination and geometry of the metal center in the hetrodimer [18]. In contrast to the Fe hydrogenases, the nickel enzyme possess a variety of compositions, molecular weights, activation behaviour and redox potentials [19]. Some of the nickel hydrogenases contain selenium, likely in the form of selenocysteine, some contain flavin (FMN or FAD), and all contain iron-sulfur centers, but in amounts ranging from 4 to 14 iron atoms per Ni atom. Among the different Ni hydrogenases, there is a proper pattern of protein composition, to which many, but not all, seem to confirm (especially those enzymes originating from purple eubacteria). There are two protein subunits of approximate molecular masses 30 and 60 kDa, with the nickel probably residing in the latter subunit. The hydrogenase of the sulphate-reducing bacterium *Desulfovibrio gigas* is among the best investigated. *D. gigas* hydrogenase contain a single unit Ni, two Fe₂S₄ clusters, and one Fe₃S₄ cluster. Of primary interest is the Ni site, which is thought to be the site of H₂ activation. EPR signals attributable to mononuclear nickel have been used in numerous investigations of the role of Ni in hydrogenases.

Carbon monoxide dehydrogenase (CODH)/acetyl CoA synthase (ACS) is a bifunctional enzyme responding for CO oxidation and acetate synthesis, respectively, in acetogens and other anaerobes. While the active site for each process are distinct, their chemical composition are similar, each contains a nickel ion and an Fe₄S₄ cluster. The A-

cluster of CODH/ACS from *Clostridium thermoaceticum* catalyzes the synthesis of acetyl CoA by condensing the methyl group from methylcobalamin with CO, and CoA [20]. The C-cluster is active site responsible for the reversible oxidation of CO to CO₂. The A-cluster is a [Ni-X-Fe₄S₄] center. The nickel ion resides in the distorted square planar coordination sphere of two sulphur and two nitrogen/oxygen based ligands [21]. The ligand(s) bridging the Ni center to the Fe₄S₄ cluster, though not yet identified, is proposed to be either a cysteine residue or an inorganic sulphide.

Superoxide dismutase (SODs) are metalloenzymes involve in the protecting cells from oxidative damage arising from superoxide radical, or reactive oxygen species produced from superoxide.



Generated by a single-electron transfer to dioxygen, superoxide radicals are produced in large amounts in respiration and photosynthesis, during an immune response by phagocytes, etc. [22, 23]. SODs play an important protective role in aerobes which encounter toxic O₂^{·-} radicals during their metabolism. The presence of SOD in the intracellular environment reduces oxidative stress and can play a key role in moderating the aging process. SOD is therefore used as an antioxidative therapeutic agent. Other medical applications involve treatment of arthritis and prevention of side effects of cancer treatment and injury to transplant organs during surgery. Given that mutations in SOD are associated with 20% of the cases of familiar amyotrophic lateral sclerosis (FALS), [24-27] the enzyme is used to block the development of this paralytic disorder. To date, three independent SOD classes are known, based on their cofactor metal ion: Cu- and Zn-dependent SODs (CuZnSODs), SODs that use Fe or Mn, or either of the two (FeSODs, MnSODs, or Fe/MnSODs), and Ni-dependent enzymes (NiSODs). While CuZnSODs are the most abundant superoxide scavengers in living nature, found in all eucaryotes and many procaryotes, [28] the recently discovered NiSOD class is confined to *Streptomyces*, soil bacteria [29-31] and cyanobacteria [32].

The amino acid sequence of the NiSOD deduced from the nucleotide sequence of the structure gene *sodN* from *Streptomyces seoulensis* has been reported, which has no homology with other SODs [32]. X-ray crystallographic structure determinations [33, 34]

reveal a homohexameric NiSOD, possessing a three-fold symmetry axis. Composed of a four-helix bundle in the all-antiparallel topology, the monomer subunit is a quite small 117 amino acid protein. The residues of the N-terminal loop form the metal-coordinating “Ni-hook” which is disordered in the absence of a bound metal ion [35-37]. Conserved between the known NiSODs, the Ni-hook His1-Cys2-X-X-Pro5-Cys6-Gly7-X-Tyr9 motif (Figure 1) was proposed as a diagnostic of this enzyme class. The amine of N-terminal His1, the deprotonated backbone amide of Cys2, and the thiolates of Cys2 and Cys6 form a square planar framework of the Ni coordination sphere. This N₂S₂ ligand field with the metal incorporation into the backbone nitrogens and thiolate sulfurs is reminiscent of nickel coordination. The NiSOD activity (kcat) was determined to be 1.3 x 10⁹ M⁻¹S⁻¹ per Ni. The proposed two step redox mechanism of NiSOD for superoxide inhibition is given as below [38]:

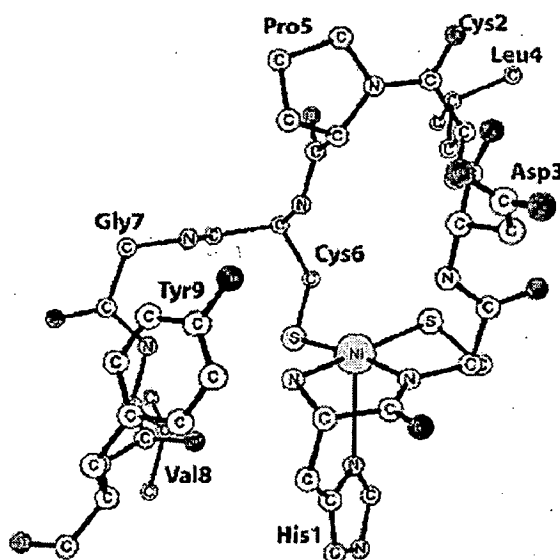
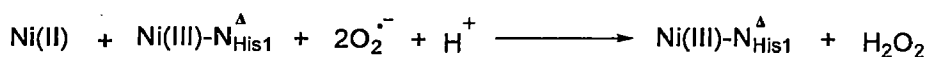
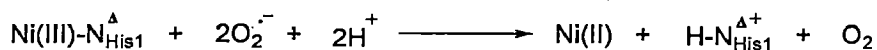


Fig.1.1 Crystal Structure of NiSOD

Also a large number of enzymes are dependent on a divalent lewis acid ion such as Ca, Mg, Fe or Zn. These metal ions are often readily removed by a chelating agent such as

EDTA or bpy, and many of the resultant apoenzymes have been reconstituted with non-native cations Ni^{2+} can act as both a mechanistic and structural probe in such cases, since the native metal ions often have no available spectroscopic or magnetic handle [5]. The fact that the Ni enzymes thus obtained often retain complete or partial activity demonstrates that Ni^{2+} can indeed carry out the roles proposed for it in urease, namely polarization of a C=O bond and activation of a coordinated water molecule towards deprotonation. The best characterized of these synthetic Ni proteins is Ni-carboxypeptidase A (Ni-CPA), whose native enzyme catalyzes the hydrolysis of peptide amide bonds and contain the five coordinated center within the active site, the carboxylate ligand being asymmetrically bound [39].

Ni-CPA shows ca. 50% of the activity of the native enzyme toward amide hydrolysis. The spectroscopic and magnetic properties of the Ni enzyme were originally thought to arise from an octahedral Ni ion but also consistent with a high spin five coordinate Ni center [40, 41]. A single crystal X-ray structure determination of Ni-CPA showed that Ni complex exhibits a more regular square pyramidal geometry compared with the native Zn site. Carboxylate inhibitors binds directly to the Ni^{2+} ion in Ni-CPA, the precise role played by metal ions in imide hydrolysis by CPA is still unclear. In contrast to the above results, Ni substituted carbonic anhydrase shows greatly reduced activity for CO_2 hydration. The electronic spectra and magnetic properties of this enzyme have been interpreted on the basis of an octahedral Ni(II) ion containing at least one aqua ligand with a five coordinate species possibly being observed at higher pH [42] or in the presence of inorganic anions [43], this contrast with the Td site in the native enzyme. The low activity of Ni-CA has been rationalized on the preferred bidentate mode of coordination of the CO_2 hydrolysis product bicarbonate to a Ni(II) center of approximately monodentate to Zn^{2+} [44, 45].

Oxygen activation by various late first row transitional metals is common to many metalloenzymes. Although redox active nickel enzymes are known, no oxygen activating nickel enzymes have been discovered, and only recently have Ni-containing superoxide dismutase been characterised. However, several Ni(II) complexes with "biologically relevant" ligands have been shown to react with oxygen, resulting Ni(II) species. These one electron reactions generally result in the oxidative ligand decomposition. Our goal is to develop Ni(II) complexes that will undergo two electron reactions with O_2 , producing a

peroxide level intermediate that will likely to be more sensitive in its reactivity than the superoxide level intermediates formed in the one electron reactions. This may be accomplished either by oxidation of a mononuclear Ni(II) to Ni(IV), or of a dinuclear Ni(II)₂ to Ni(III)₂ oxidation (a strategy used in many oxygen activating metalloenzyme with Fe, Cu, and Mn). In order to accomplish that, we must understand the factors that determine the metal electron stoichiometry in these reactions. To this end, we have synthesized and undertaken spectroscopic and reactivity studies of a series of nickel complexes with hindered tris(pyrazolyl)borate and different benzoate salts.

The poly(pyrazolyl)borate ligand has more than 40 years old history as it was first time reported by S. Trofimenko in 1960's [46]. The pyrazole nucleus is thermally and hydrolytically very stable. As a ligand, it coordinates to metals and metalloids through the 2-N. Due to these attractive features the coordination chemistry of pyrazole and of its derivatives have attracted much attention. As poly(pyrazolyl)borates are vigorously developed hence these are used to provide steric shielding to the metal center and also for creating the synthetic equivalent enzymes for various catalytic activity. The ligands can be tetradentate, tridentate, bidentate or monodentate depending on the number of donor substituents on boron and the steric congestion around the metal. Nitrogen heterocyclics other than pyrazole can be used such as pyrrole, imidazole, indole and indizole. In addition, tripodal ligand can have central atoms other than boron such as carbon, phosphorus or gallium. The ligands also can bind metals through sulphur, phosphorus or other donor atoms. The pyrazolylborates / scorpionate chemistry signify a very large and growing area. These ligands are extremely versatile because the number of donor atoms in each ligand can be varied from two to three while going from the bidentate ligands to the potentially tridentate ligands. The steric properties of the ligands can be altered by changing the substituents on the pyrazolyl rings. These ligands have been used extensively to prepare complexes of the transition metals [47].

Hydrotris(pyrazolyl)borate ligands (TpR), are used in a wide range of inorganic studies because of the coordination properties (steric and electronic), which can be tuned in a systematic manner by choosing appropriate substituents on the pyrazolyl rings. TpR form a coordinatively unsaturated tetrahedral species with 1st row transition metal complexes, which is interconverted with five- and six-coordinate structures via coordination/dissociation

of donor(s). In addition to the traditional view of TpR as a ligand system isoelectronic with cyclopentadienyls ($\square 5-C_5R_5$), the TpR ligand is now recognized as a unique ancillary ligand suitable for bioinorganic studies, because the tripodal ligand can mimic the coordination environment created by three imidazolyl groups from histidine residues, which is frequently found in the active sites of metalloenzymes [48]. With the increasing applicability of TpR ligands in combination with a wide range of transition metal ions, various 3,5-substituted tris(pyrazolyl)borate nickel(II) complexes have been prepared and characterised in both the solid state and solution and found that Tp ligands can coordinate metal centres in facial fashion (commonly known as k^3N,N',N''). The occurrence of this bonding mode implies that all the pyrazole units are bound to the same metal centre. These are found catalytically active in many elementary steps occurring in olefin polymerisation (e.g. C-C and C-H bond formation/cleavage/coordination). The catalytic performance of various 3,5-substituted Nickel(II) compounds has been tested in ethylene polymerisation. The nickel catalysts activated with methylaluminoxane (MAO) produce polyethylene with moderate to good activity [49].

Hydrotris(pyrazolyl)borate ligands (TpR) are widely used in the design of functional molecules, catalysis of chiral induced asymmetric synthesis, liquid crystal materials, molecular 'electronic devices' and biomimetic chemistry. Half-sandwich mononuclear complexes with the mono-hydrotris(pyrazolyl)borate ligand and small molecules or anions can be considered as the complexes of metalloenzymes such as carbonic anhydrase (CA) [50] and nitrite reductases (NiR) [51], and as the precursors for the syntheses of various multinuclear model complexes [52, 53].

The advantageous characteristics of this ligand are as follows:

1. Preventing formation of bis-chelated complexes completely.
2. High solubility in non-coordinating solvents such as toluene and pentane.
3. Highly shielding effect of isopropyl groups to stabilize unusual coordinating structures.
4. Moderate steric hindrance to allow formation of dimeric complexes.
5. Strong electron donating property.

Kunrath et al. studied that the reaction of $HB(3\text{-mesitylpyrazolyl})_3\text{-(Tp}^{Ms})$, $HB(3\text{-mesitylpyrazolyl})_2(5\text{-mesitylpyrazolyl})\text{-(Tp}^{Ms*})$ with $NiCl_2 \cdot 6H_2O$ affords $Tp^{Ms}NiCl$ (1) and

$\text{Tp}^{\text{Ms}*}\text{NiCl}$ (2) in good yield. The compound 2 undergoes an isomerization process to form $[\{\text{Tp}^{\text{Ms}***}\text{NiCl}\}_2]$ (3) ($\text{Tp}^{\text{Ms}***}$) $\text{HB}(5\text{-mesitylpyrazolyl})_2(3\text{-mesitylpyrazolyl})\text{-}$ in 68% yield. Treatment of the tris(pyrazolyl)-borate nickel compounds 1 and 2 with alkylaluminum cocatalysts such as methylalumoxane (MAO) and trimethylaluminum (TMA) in toluene generates active catalysts for ethylene oligomerization. The compound 1 shows turnover frequencies in the range of $(2.2\text{-}43.1) \times 10^3 \text{ h}^{-1}$. Oligomerization reaction conditions can be adjusted that lead to selectivities as high as 81% for butene-1 [53].

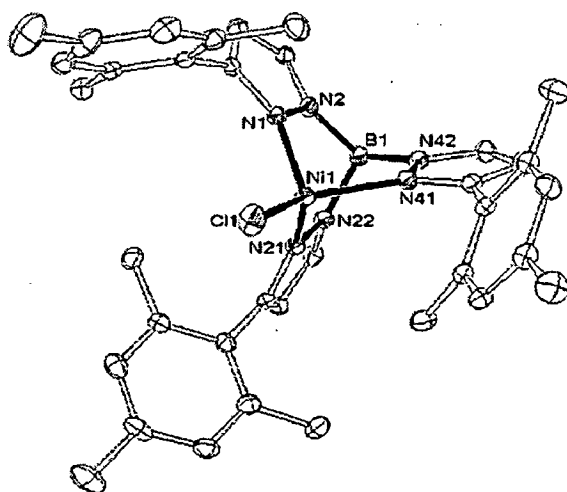


Fig.1.2 Molecular structure of $[\text{Tp}^{\text{Ms}}\text{NiCl}]$

Santi et al. prepared and characterised the various 3,5-substituted tris(pyrazolyl)borate nickel(II) and palladium(II) complexes both the solid and solution state where [tris(pyrazolyl)borate is tris(3,5-dimethylpyrazolyl)borate (Tp^*), tris(3-*t*-butyl-5-methylpyrazolyl)borate ($\text{Tp}^{\text{t-Bu,Me}}$) or tris(3-cumyl-5-methyl pyrazolyl)borate ($\text{Tp}^{\text{Cum,Me}}$)]. The crystal structures of the tetrahedral complex $[\text{k}3\text{N},\text{N}',\text{N}''\text{-Tp}^{\text{t-Bu,Me}}\text{NiCl}]$ and of the trigonal-bipyramidal derivative $[\text{k}3\text{N},\text{N}',\text{N}''\text{-Tp}^{\text{Cum,Me}}\text{NiCl}(3\text{-methyl-5-cumylpyrazole})]$ have been determined by X-ray diffraction analysis. The catalytic performance of all compounds has been tested in ethylene polymerisation. The nickel catalysts activated with methylaluminoxane (MAO) produce polyethylene with moderate to good activity, while the palladium compounds show scarce activity [48].

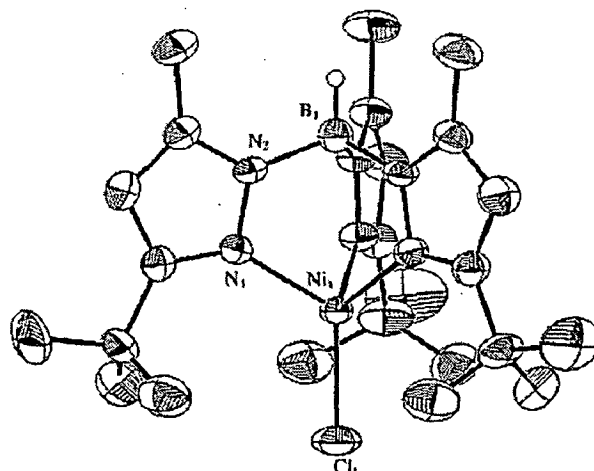


Fig. 1.3 Crystal structure of $[k^3N,N',N''\text{-Tp}^{t\text{-Bu,Me}}\text{NiCl}]$

Sun et al. presented the syntheses, crystal structure and properties of a new half-sandwich mononuclear nickel(II) complex containing a single hydrotris(3,5-dimethylpyrazolyl)borate (TpU) ligand and nitrito and methanol co-ligands, $[\text{TpUNiII}(\eta^2\text{-O}_2\text{N})(\text{CH}_3\text{OH})]$. The complex crystallizes in the triclinic system, space group (No. 2), with $a=10.0669(11)\text{ \AA}$, $b=10.1132(11)\text{ \AA}$, $c=11.8420(12)\text{ \AA}$, $\alpha=76.895(2)^\circ$, $\beta=73.234(2)^\circ$, $\gamma=62.470(2)^\circ$, $Z=2$, $R_1=0.0458$, $wR_2=0.1187$. The Ni(II) ion in the complex is coordinated to three pyrazolyl nitrogen atoms, two oxygen atoms of NO_2^- and one oxygen atom of CH_3OH to form a distorted octahedron. The NO_2^- was coordinated in an asymmetric nitrito-O,O'-bidentate coordination mode with an $\text{O}(1)\text{-Ni-O}(2)$ angle of $57.71(11)^\circ$ and Ni-O bond lengths of 2.1882 and 2.1222 \AA [52].

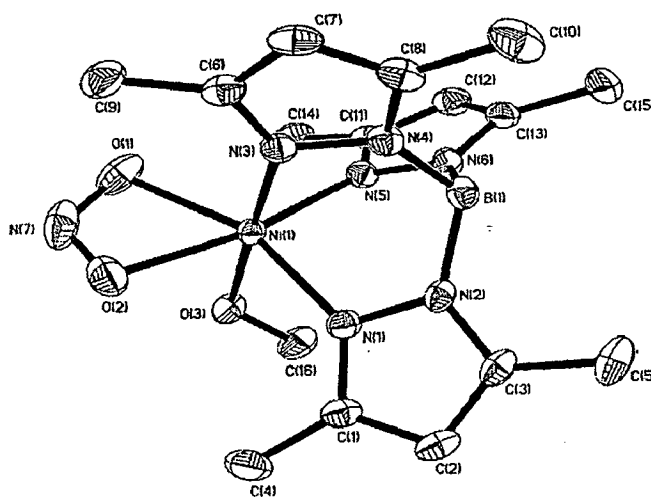


Fig. 1.4 Crystal structure of $[\text{TpNi}^{\text{II}}(\eta^2\text{-O}_2\text{N})(\text{CH}_3\text{OH})]$

Kitano et al. reported the solvent extraction of first-series transition metal ions {Mn(II), Fe(II), Co(II), Ni(II), Cu(II) and Zn(II)} with $[B(3-iPrpz)_4]^-$ (iPrpz = isopropylpyrazolyl) is reported. Although the previously reported tetrakis (pyrazolyl)borates, $[B(pz)_4]^-$ and $[B(3-Mepz)_4]^-$, quantitatively extracted all the studied transition metal ions, $[B(3-iPrpz)_4]^-$ extracted only Cu(II) and Zn(II). In order to elucidate the origin of the selectivity, the structures of the extracted species, $[B(3-iPrpz)_4]_2Zn$ (1) and $[B(3-iPrpz)_4]Cu(OCOCH_3)$ (2), were determined by single-crystal X-ray diffraction. Complex 1 has a tetrahedral geometry with each ligand having bidentate coordination. Complex 2 has a distorted square pyramidal geometry with $[B(3-iPrpz)_4]^-$ having tridentate coordination and the acetate anion having asymmetric bidentate coordination. These structures of the extracted species are different from those of the previously studied tetrakis(pyrazolyl)borates, which are octahedral A_2M with each ligand having tridentate coordination (A^- = tetrakis(pyrazolyl) borate, M^{2+} = first-series transition metal ion). Because the bulky isopropyl groups at the 3-position of the pyrazolyl ring prevent octahedral geometry, the other metal ions cannot form stable and extractable complexes with $[B(3-iPrpz)_4]^-$ [54].

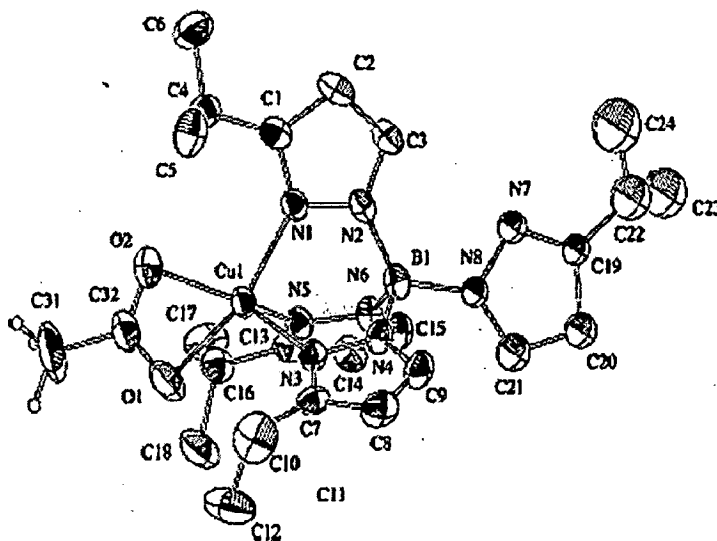


Fig. 1.5 Crystal structure of $[B(3-iPrpz)_4]Cu(OCOCH_3)$

Yakovenko et al. synthesized Ni(II), Co(II) and Mn(II) tris(pyrazolyl)borate complexes with 2,6-di-tert-butyl-4-carboxy-phenol and characterized crystallographically (Ni and Co complexes), spectroscopically and electrochemically. It was found that oxidation of Ni and Co complexes resulted in the formation of coordinated phenoxyl radical and

diphenoquinone, whereas only quinone formed in the case of Mn complex and free 2,6-di-tert-butyl-4-carboxy-phenol [55].

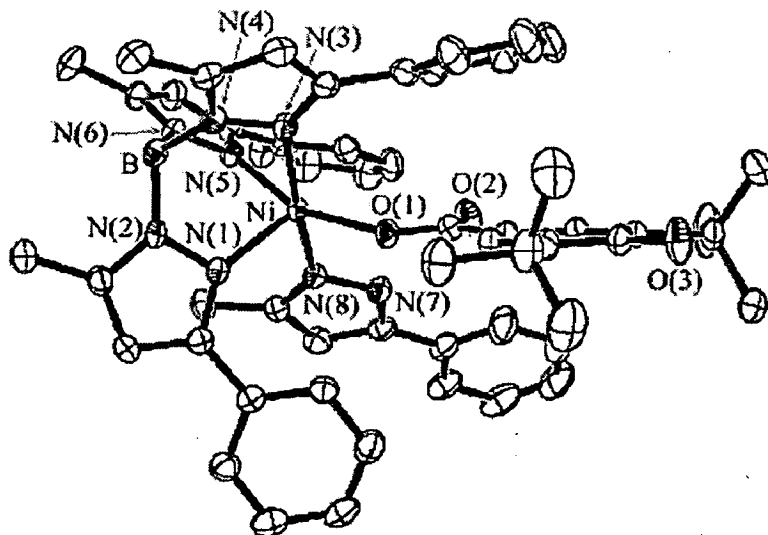


Fig. 1.6 Crystal structure of $[\text{Tp}^{\text{Ph,Me}}\text{NiL.Hpz}^{\text{Ph,Me}}]$

Matsunaga et al. worked out to obtain the structural and spectroscopic insight for the first-row transition metal(II) substituted complexes of Cu(II) (1) Mn(II) (2), Fe(II) (3), Co(II) (4), Ni(II) (5), and Zn(II) (6). These model complexes have a distorted tetrahedral geometry arising from the tripodal ligand L. The *d* value, which is defined by the distance from the N₂S basal plane to the metal(II) ion, and the bond angles such as N-M-N and S-M-N are good indicators of these structural distortions. The obtained complexes were characterized by UV-vis absorption, EPR, NMR, far-IR, and FT-Raman spectroscopies and electrochemical and magnetic properties. In UV-vis absorption spectra, the sulfur-to-metal(II) CT bands and the d-d transition bands are observed for 1 and 3-5. The CT energies of the Fe(II) (3), Co(II) (4), and Ni(II) (5) complexes are shifted to higher energy (308 and 355 nm for 3, 311 and 340 nm for 4, 357 and 434 nm for 5) and are almost the same as the corresponding Co(II)- and Ni(II)-substituted blue copper proteins. In the far-IR spectra, three far-IR absorption bands for 2-6 at ca. 400, ca. 350, and ca. 310 cm^{-1} are also observed similar to those for 1. Other properties are consistent with their distorted tetrahedral geometries [56].

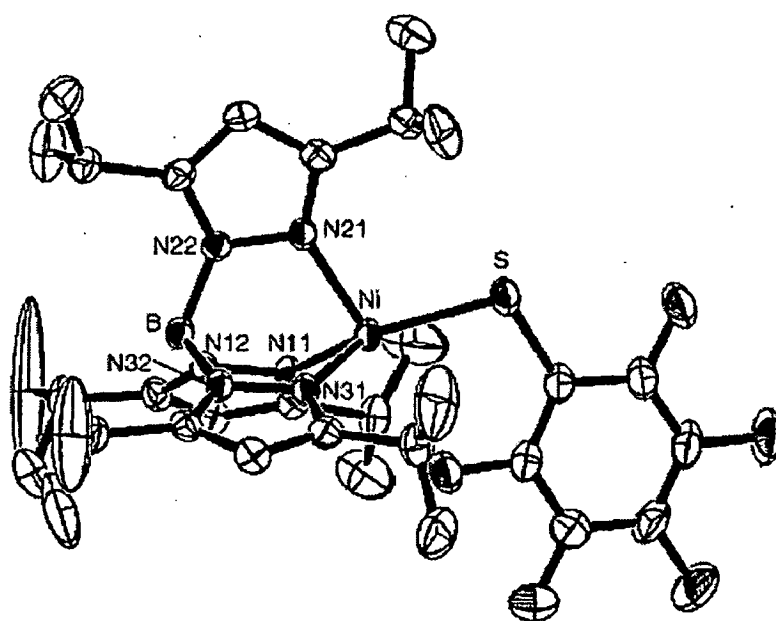


Fig. 1.7 Crystal structure of $[\text{Ni}(\text{HB}(3,5\text{-Me}_2\text{pz})_3)(\text{SC}_6\text{F}_5)]$

Harding et al. studied the addition of KTpPh_2 to a solution of NiX_2 ($\text{X} = \text{Cl}, \text{Br}, \text{NO}_3, \text{OAc}$ and acac) or $\text{NiBr}(\text{NO})(\text{PPh}_3)_2$ in THF yields the structurally characterized series $[\text{NiCl}(\text{HpzPh}_2)\text{TpPh}_2]$ 1 and $[\text{NiXTpPh}_2]$ ($\text{X} = \text{Br}$ 2, NO 3, NO_3 4, OAc 5 and acac 6) including the first example of a tris(pyrazolyl)borate nickel nitrosyl complex. IR spectroscopy confirmed that all the Tp^{Ph_2} ligands are k^3 coordinated and that the NO ligand in 3 is linearly bound. Electronic spectra are consistent with four- or five coordinate species in solution. NMR spectroscopic studies indicated that the complexes are paramagnetic, with the exception of 3. This is confirmed by magnetic susceptibility studies, which suggested that complexes 1, 2 and 4-6 are paramagnetic with two unpaired electrons. X-ray crystallographic studies of 5 reveal a distorted trigonal bipyramidal nickel centre with a symmetrically coordinated acetate ligand [57].

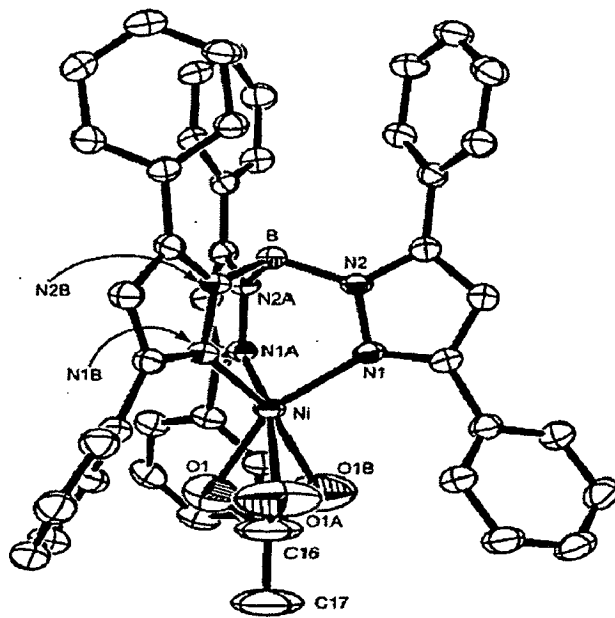


Fig 1.8 Crystal Structure of $[\text{Ni}(\text{OAc})\text{Tp}^{\text{Ph}_2}]$

c

Chapter-2

EXPERIMENTAL

Reagents Used:

S.No.	Reagents	Company Name	Grade	Mol. Wt.
1	Nickel Chloride ($\text{NiCl}_2 \cdot 6\text{H}_2\text{O}$)	Thomas Baker & Co.	AR	237.71
2	Potassium Cyanide (KCN)	Amrut Industrial Peoduct	LR	66.01
3	Sod. Benzoate ($\text{C}_7\text{H}_6\text{O}_2\text{Na}$)	Loba Chemie Pvt. Ltd.	AR	144.11
4	Benzylacetone ($\text{C}_{10}\text{H}_{10}\text{O}_2$)	Fluka	AR	162.19
5	Hydrazine Hydrate ($\text{N}_2\text{H}_4 \cdot \text{H}_2\text{O}$)	Rankem	AR	50.02
6	4-Methoxy Benzoic Acid	Merck	AR	152.13
7	4-Chloro Benzoic Acid	SRL	AR	156.57
8	4-Hydroxy Benzoic Acid	Merck	AR	138.12
9	4-Cyano Benzoic Acid	Aldrich	AR	147.27
10	4-Carboxybenzaldehyde	Aldrich	AR	150.37
11	4-Amino Benzoic Acid	Reidel-de Haën	AR	137.14
12	4-Fluoro Benzoic Acid	Spectro chem.	LR	140.12
13	4-Methoxy Benzoic Acid	Merck	LR	152.15
14	Thio Phenol	Merck	AR	110.23

2.2 Make and Model of the Instruments

IR spectra were recorded on a NEXUS FT-IR (THERMONICOLET). Solid samples were recorded as KBr wafers and liquid samples as film between NaCl plates. Element Analysis were recorded at Vario EL elementar. All the UV-Vis spectra were recorded by Perkin Elmer Lambda 35 spectrometer. The room temperature magnetic measurements were performed on Princeton applied research vibrating sample magnetometer Model 155. Thermal analysis were recorded by Perkin Elmer Pyris Diamond. The crystal structures were recorded by Bruker Kappa Apex Single Crystal Diffractometer.

2.2 Synthesis:

2.2.1a. Synthesis of 3-phenyl-5-methyl pyrazole [$\text{pz}^{\text{Ph,Me}}$] (1a)

25 g Benzoyl acetone was taken in a beaker and transfers it into two necked round bottom flask (one for condenser and other for dropping funnel). Add ~150 ml absolute ethanol by dropping funnel and stirred for 20 min. In separate beaker weighted 13 ml hydrazine and transferred it through dropping funnel drop by drop in 40 min of time span. Removed the ice bath, stirred it for 30 min at room temp. and refluxed it in oil bath at $110\text{ }^{\circ}\text{C}$ – $140\text{ }^{\circ}\text{C}$ for 10 h. After 10 h refluxing the mixture was allowed to cool at room temperature. The resultant white solid was washed with water 3 – 4 times and finally with hexane. Dried the compound under vacuum (Yield 73%). Anal. Calcd for $\text{C}_{10}\text{H}_{10}\text{N}_2$; C, 75.95; H, 6.33; N, 17.72; Found: C, 76.83; H, 7.12; N, 16.53.

2.2.1b. Synthesis of potassium hydrotris(3-phenyl- 5-methyl-pyrazoly)borate [$\text{KTp}^{\text{Ph,Me}}$] (1b)

3-phenyl-5-methyl pyrazole (10.39 g) and KBH_4 (1.17 g), were placed in 250 ml round bottom flask. The mixture was warmed gradually while monitoring hydrogen evolution. The temperature was elevated to $260\text{ }^{\circ}\text{C}$ and heating continued until no hydrogen evolution was observed. The solution was allowed to cool at room temperature, the solid mass dissolved in dichloro methane and filtered over celite. The solvent was evaporated under vacuum and the

resultant solid was carefully recrystallized from acetonitrile, affording potassium hydrotris(3-phenyl-5-methyl-pyrazolyl)borate [KTP^{Ph, Me}] as a white crystalline solid. Anal. Calcd for C₃₀H₂₇N₆BK; C, 68.83; H, 5.16; N, 16.06; Found: C, 69.12; H, 5.78; N, 15.58.

2.2.2. Synthesis of [Ni(Tp^{Ph, Me})(pz^{Ph, Me})Cl] (2)

(0.47 g, 1.99 mmol) NiCl₂·6H₂O, (0.32 g, 1.99 mmol) pz^{Ph, Me} and (1.04 g, 1.99 mmol) Tp^{Ph, Me} were stirred in 25 ml CH₂Cl₂ + 5 ml CH₃OH for 6 h. The mixture was filtered over celite and solvent was evaporated to dryness under vacuum. The compound was dissolved in 5 ml toluene and yellow crystals were obtained at -20 °C. (84.76% yield). Anal. Calcd for C₄₀H₃₈N₈BClNi: C, 65.26; H, 5.17; N, 15.2. Found: C, 66.10; H, 5.98; N, 16.12. IR (KBr pellet, v/cm⁻¹): 2532 (BH). UV-Vis (toluene, λ_{max}, nm, ε/M⁻¹cm⁻¹) 286 (832), 484 (272).

2.2.3. Synthesis of [Ni(Tp^{Ph, Me})(pz^{Ph, Me})(OBz)] (3)

In a schlenk tube, (0.36 g, 0.64 mmol) of **2**, (0.09 g, 0.64 mmol) of sodium benzoate and (0.09 g, 0.64 mmol) of pz^{Ph, Me} were reacted in a mixture of 15 ml acetonitrile and 15 ml toluene for 10 h. After filtration, the filtrate was dried under vacuum, yielding a green compound (73.2% yield). This coloured compound was recrystallized from toluene at -20 °C. Anal. Calcd for C₄₇H₄₃N₈O₂BNi: C, 68.69; H, 5.24; N, 13.64. Found: C, 69.13; H, 5.28; N, 13.12. IR (KBr pellet, v/cm⁻¹): ν(BH) 2534, ν_{as}(COO) 1552, ν_s(COO) 1420. UV-Vis (toluene, λ_{max}, nm, ε/M⁻¹cm⁻¹) 285 (842), 418 (287).

2.2.4. Synthesis of [Ni(Tp^{Ph, Me})(pz^{Ph, Me})(p-Cl-OBz)] (4)

The complexes **4-12** were obtained in similar manner applied to **3**. The samples used for elemental analysis were evacuated under vacuum extensively (yield 68.3%). Anal. Calcd for C₄₇H₄₂N₈O₂BClNi: C, 65.92; H, 4.91; N, 13.09. Found: C, 66.53; H, 4.88; N, 13.19. IR (KBr pellet, v/cm⁻¹): ν(BH) 2513, ν_{as}(COO) 1546, ν_s(COO) 1496. UV-Vis (toluene, λ_{max}, nm, ε/M⁻¹cm⁻¹) 282 (856), 402 (407).

2.2.5. Synthesis of $[\text{Ni}(\text{Tp}^{\text{Ph,Me}})(\text{pz}^{\text{Ph,Me}})(p\text{-F-OBz})]$ (5)

Yield 63.47%. Anal. Calcd for $\text{C}_{47}\text{H}_{42}\text{N}_8\text{O}_2\text{BFNi}$: C, 67.22; H, 5.00; N, 13.35. Found: C, 67.53; H, 4.88; N, 13.46. IR (KBr pellet, v/cm^{-1}): $\nu(\text{BH})$ 2534, $\nu_{\text{as}}(\text{COO})$ 1549, $\nu_{\text{s}}(\text{COO})$ 1497. UV-Vis (toluene, λ_{max} , nm, $\epsilon/\text{M}^{-1}\text{cm}^{-1}$) 289 (739), 416 (340).

2.2.6. Synthesis of $[\text{Ni}(\text{Tp}^{\text{Ph,Me}})(\text{pz}^{\text{Ph,Me}})(p\text{-NO}_2\text{-OBz})]$ (6)

Yield 67.32%. Anal. Calcd for $\text{C}_{47}\text{H}_{42}\text{N}_9\text{O}_4\text{BNi}$: C, 65.13; H, 4.85; N, 14.55. Found: C, 65.33; H, 4.78; N, 14.29. IR (KBr pellet, v/cm^{-1}): $\nu(\text{BH})$ 2520, $\nu_{\text{as}}(\text{COO})$ 1567, $\nu_{\text{s}}(\text{COO})$ 1412, $\nu(\text{NO}_2)$ 1342. UV-Vis (Dichloro methane, λ_{max} , nm, $\epsilon/\text{M}^{-1}\text{cm}^{-1}$) 286 (684), 419 (124).

2.2.7. Synthesis of $[\text{Ni}(\text{Tp}^{\text{Ph,Me}})(\text{pz}^{\text{Ph,Me}})(p\text{-Me-OBz})]$ (7)

Yield 71.13%. Anal. Calcd for $\text{C}_{48}\text{H}_{45}\text{N}_8\text{O}_2\text{BNi}$: C, 68.98; H, 5.39; N, 13.41. Found: C, 69.13; H, 5.28; N, 13.12. IR (KBr pellet, v/cm^{-1}): $\nu(\text{BH})$ 2540, $\nu_{\text{as}}(\text{COO})$ 1543, $\nu_{\text{s}}(\text{COO})$ 1501. UV-Vis (toluene, λ_{max} , nm, $\epsilon/\text{M}^{-1}\text{cm}^{-1}$) 285 (556), 414 (251)

2.2.8. Synthesis of $[\text{Ni}(\text{Tp}^{\text{Ph,Me}})(\text{pz}^{\text{Ph,Me}})(p\text{-MeO-OBz})]$ (8)

Yield 74.81%. Anal. Calcd for $\text{C}_{48}\text{H}_{45}\text{N}_8\text{O}_3\text{BNi}$: C, 68.69; H, 5.29; N, 13.16. Found: C, 69.57; H, 5.39; N, 13.28. IR (KBr pellet, v/cm^{-1}): $\nu(\text{BH})$ 2531, $\nu_{\text{as}}(\text{COO})$ 1552, $\nu_{\text{s}}(\text{COO})$ 1423. UV-Vis (toluene, λ_{max} , nm, $\epsilon/\text{M}^{-1}\text{cm}^{-1}$) 284 (871), 417 (412).

2.2.9. Synthesis of $[\text{Ni}(\text{Tp}^{\text{Ph,Me}})(\text{pz}^{\text{Ph,Me}})(p\text{-NH}_2\text{-OBz})]$ (9)

Yield 72.35%. Anal. Calcd for $\text{C}_{47}\text{H}_{44}\text{N}_9\text{O}_2\text{BNi}$: C, 67.46; H, 5.26; N, 15.07. Found: C, 67.59; H, 5.38; N, 14.92. IR (KBr pellet, v/cm^{-1}): $\nu(\text{BH})$ 2544, $\nu_{\text{as}}(\text{COO})$ 1548, $\nu_{\text{s}}(\text{COO})$ 1437, $\nu(\text{NH})$ 3132. UV-Vis (toluene, λ_{max} , nm, $\epsilon/\text{M}^{-1}\text{cm}^{-1}$) 283 (932), 419 (365).

2.2.10. Synthesis of $[\text{Ni}(\text{Tp}^{\text{Ph,Me}})(\text{pz}^{\text{Ph,Me}})(\text{p-HO-OBz})]$ (10)

Yield 70.65%. Anal. Calcd for $\text{C}_{47}\text{H}_{43}\text{N}_8\text{O}_3\text{BNi}$: C, 67.38; H, 5.14; N, 13.38. Found: C, 67.56; H, 5.26; N, 13.12. IR (KBr pellet, v/cm^{-1}): $\nu(\text{BH})$ 2539, $\nu_{\text{as}}(\text{COO})$ 1548, $\nu_{\text{s}}(\text{COO})$ 1416, $\nu(\text{OH})$ 3421. UV-Vis (acetonitrile, λ_{max} , nm, $\epsilon/\text{M}^{-1}\text{cm}^{-1}$) 283 (421), 489 (158).

2.2.11. Synthesis of $[\text{Ni}(\text{Tp}^{\text{Ph,Me}})(\text{pz}^{\text{Ph,Me}})(\text{p-CHO-OBz})]$ (11)

Yield 68.94%. Anal. Calcd for $\text{C}_{47}\text{H}_{43}\text{N}_8\text{O}_3\text{BNi}$: C, 67.38; H, 5.14; N, 13.38. Found: C, 67.56; H, 5.26; N, 13.12. IR (KBr pellet, v/cm^{-1}): $\nu(\text{BH})$ 2542, $\nu_{\text{as}}(\text{COO})$ 1542, $\nu_{\text{s}}(\text{COO})$ 1431, $\nu(\text{CO})$ 1698. UV-Vis (toluene, λ_{max} , nm, $\epsilon/\text{M}^{-1}\text{cm}^{-1}$) 285 (1514), 413 (265).

2.2.12. Synthesis of $[\text{Ni}(\text{Tp}^{\text{Ph,Me}})(\text{pz}^{\text{Ph,Me}})(\text{p-CN-OBz})]$ (12)

Yield 73.78%. Anal. Calcd for $\text{C}_{47}\text{H}_{43}\text{N}_8\text{O}_3\text{BNi}$: C, 67.38; H, 5.14; N, 13.38. Found: C, 67.56; H, 5.26; N, 13.12. IR (KBr pellet, v/cm^{-1}): $\nu(\text{BH})$ 2539, $\nu_{\text{as}}(\text{COO})$ 1543, $\nu_{\text{s}}(\text{COO})$ 1430, $\nu(\text{CN})$ 2267. UV-Vis (toluene, λ_{max} , nm, $\epsilon/\text{M}^{-1}\text{cm}^{-1}$) 286 (824), 413 (231).

2.2.13. Synthesis of $[\text{Ni}(\text{Tp}^{\text{Ph,Me}})_2]$ (13)

(0.20 g, .85 mmol) $\text{NiCl}_2 \cdot 6\text{H}_2\text{O}$ and (1.76 g, 1.70 mmol) $\text{KTp}^{\text{Ph,Me}}$ were stirred in 25 ml CH_2Cl_2 + 5 ml CH_3OH for 6 h. The mixture was filtered over celite and solvent was evaporated to dryness under vacuum. The compound was dissolved in 5 ml toluene and yellow crystals were obtained at -20°C . (67.56% yield). Anal. Calcd for $\text{C}_{60}\text{H}_{56}\text{N}_{12}\text{B}_2\text{Ni}$: C, 70.24; H, 5.46; N, 16.39. Found: C, 70.38; H, 5.57; N, 16.12. IR (KBr pellet, v/cm^{-1}): 2546 (BH). UV-Vis (dichloromethane, λ_{max} , nm, $\epsilon/\text{M}^{-1}\text{cm}^{-1}$) 287 (1048), 600 (373).

2.2.14. Synthesis of $[\text{Ni}(\text{Tp}^{\text{Ph,Me}})(\text{pz}^{\text{Ph,Me}})(\text{N}_3)]$ (14)

(0.17 g, 0.30 mmol) of compound 2 and (0.02 g, 0.30 mmol) of sodium azide were reacted in a mixture of 5 ml methanol and 10 ml toluene for 1 h. After filtration over celite, the filtrate was dried under vacuum, yielding a green compound (74.81% yield). This

coloured compound was kept for recrystallization in toluene at $-20\text{ }^{\circ}\text{C}$. Anal. Calcd for $\text{C}_{40}\text{H}_{38}\text{N}_{11}\text{BNi}$: C, 68.69; H, 5.29; N, 13.16. Found: C, 69.57; H, 5.39; N, 13.28. IR (KBr pellet, v/cm^{-1}): $\nu(\text{BH})$ 2524, $\nu(\text{N}_3)$ 2066. UV-Vis (acetonitrile, λ_{max} , nm, $\epsilon/\text{M}^{-1}\text{cm}^{-1}$) 394 (375), 644 (194).

2.2.15. Synthesis of $[\text{Ni}(\text{Tp}^{\text{Ph,Me}})(\text{pz}^{\text{Ph,Me}})(\text{NCS})]$ (15)

The complexes **15** and **16** were obtained in similar manner applied to **13**. The samples used for elemental analysis were evacuated under vacuum extensively (yield 71.69%). Anal. Calcd for $\text{C}_{41}\text{H}_{38}\text{N}_9\text{SBNi}$: C, 68.69; H, 5.29; N, 13.16. Found: C, 69.57; H, 5.39; N, 13.28. IR (KBr pellet, v/cm^{-1}): $\nu(\text{BH})$ 2529, $\nu(\text{SCN})$ 2058. UV-Vis (acetonitrile, λ_{max} , nm, $\epsilon/\text{M}^{-1}\text{cm}^{-1}$), 488 (136).

2.2.16. Synthesis of $[\text{Ni}(\text{Tp}^{\text{Ph,Me}})(\text{pz}^{\text{Ph,Me}})(\text{CN})]$ (16)

Yield 69.73%. Anal. Calcd for $\text{C}_{41}\text{H}_{38}\text{N}_9\text{BNi}$: C, 67.38; H, 5.14; N, 13.38. Found: C, 67.56; H, 5.26; N, 13.12. IR (KBr pellet, v/cm^{-1}): $\nu(\text{BH})$ 2532, $\nu(\text{CN})$ 2282. UV-Vis (acetonitrile, λ_{max} , nm, $\epsilon/\text{M}^{-1}\text{cm}^{-1}$) 368 (651), 493 (193).

Chapter-3

**RESULTS
AND
DISCUSSION**

The complex **2** was synthesised by the reaction of $\text{NiCl}_2 \cdot 6\text{H}_2\text{O}$, $[\text{KTp}^{\text{Ph, Me}}]$ and $\text{pz}^{\text{Ph, Me}}$ whereas the compounds **3-12** were synthesized by the reaction of **2** with sodium *p*-X-benzoate ($X = \text{H, Cl, F, NO}_2, \text{Me, OMe, NH}_2, \text{OH, CHO, CN}$). In all these complexes (**3-12**), three nitrogen atoms from $\text{Tp}^{\text{Ph, Me}}$ ligand, one nitrogen atom from $\text{pz}^{\text{Ph, Me}}\text{H}$ and one oxygen atom from benzoate group are coordinated to a nickel metal center and resulted the formation of five coordinated system. Complex **13** was synthesized by the reaction of Ni(II) chloride and $[\text{KTp}^{\text{Ph, Me}}]$ in 1 : 2 ratio, where two hydrotris(3-phenyl-5-methyl-pyrazolyl)borate ligands are coordinated to nickel center in octahedron fashion. The complexes **14-16** were prepared by the reaction of **2** with sodium azide, potassium thiocyanate and potassium cyanide respectively. In complexes **14-16**, nickel center is penta coordinated, three nitrogen atoms from $\text{Tp}^{\text{Ph, Me}}$ ligand, one nitrogen atom from $\text{pz}^{\text{Ph, Me}}\text{H}$ and one nitrogen atom from terminal azide and thiocyanate groups respectively whereas in complex **16** fifth site is occupied by carbon atom of cyanide group. All of these complexes were characterized by elemental analysis, infrared, UV-Visible spectra, magnetic susceptibility, thermogravimetry and single crystal X-ray crystallography.

Infrared spectra

The complexes **2-16** show B-H stretching vibration in their spectra in the range of $2513\text{-}2546\text{ cm}^{-1}$. The IR bands of **3-11** are in the range of $1567\text{-}1542\text{ cm}^{-1}$ and $1412\text{-}1437\text{ cm}^{-1}$ have been assigned to asymmetric (ν_{as}) and symmetric (ν_{s}) stretching vibrations of carboxylate group respectively. The position of these asymmetric and symmetric bands are very similar in these complexes indicating that the coordination behaviours of the different benzoate groups are same in all these complexes, ie. monodentate. In complex **14**, the presence of $\nu(\text{N}=\text{N})$ band at 2066 cm^{-1} suggested the coordination of azide in terminal mode which is in the usual range of terminal N-bonded azide anions. The C=N stretching frequency of thiocyanates are generally lower in the N-bonded complexes (near and below 2050 cm^{-1}), than the S-bonded complexes (near 2110 cm^{-1}). A single very strong band in **15** at 2058 cm^{-1} has been assigned as $\nu(\text{C}=\text{N})$ of thiocyanate suggested the bonding through nitrogen where as in complex **16**, the presence of $\nu(\text{C}\equiv\text{N})$ band at 2282 cm^{-1} indicated the coordination of cyanide through carbon atom.

Electronic spectra

Electronic spectra of complexes **2-5**, **7-9**, **11** and **12** were recorded in toluene and two prominent bands at 289-282 nm and 489-407 nm were observed. The bands at 289-282 nm may arise from the intraligand transition in $\text{Tp}^{\text{Ph, Me}}$ and bands at 489-407 nm due to the d-d transitions [57, 59]. The electronic spectra of complexes **6** and **13** in dichloromethane showed two bands at 286 nm, 287 nm and 419 nm, 600 nm respectively. The electronic spectra of **10** and **14-16** in acetonitrile and also shows two bands.

Table 3.1: Electronic Spectrum data for complexes 3-16.

S.No.	Complexes	Electronic Bands, nm ($M^{-1}cm^{-1}$)
1	$[\text{Ni}(\text{Tp}^{\text{Ph, Me}})(\text{pz}^{\text{Ph, Me}})\text{Cl}]$	286 (832), 484 (272)
2	$[\text{Ni}(\text{Tp}^{\text{Ph, Me}})(\text{pz}^{\text{Ph, Me}})(\text{oBz})]$	285 (842), 418 (287)
3	$[\text{Ni}(\text{Tp}^{\text{Ph, Me}})(\text{pz}^{\text{Ph, Me}})(\text{p-Cl-oBz})]$	282 (856), 402 (407)
4	$[\text{Ni}(\text{Tp}^{\text{Ph, Me}})(\text{pz}^{\text{Ph, Me}})(\text{p-F-oBz})]$	289 (739), 416 (340)
5	$[\text{Ni}(\text{Tp}^{\text{Ph, Me}})(\text{pz}^{\text{Ph, Me}})(\text{p-NO}_2\text{-OBz})]$	286 (684), 419 (124)
6	$[\text{Ni}(\text{Tp}^{\text{Ph, Me}})(\text{pz}^{\text{Ph, Me}})(\text{p-Me-OBz})]$	285 (556), 414 (251)
7	$[\text{Ni}(\text{Tp}^{\text{Ph, Me}})(\text{pz}^{\text{Ph, Me}})(\text{p-MeO-OBz})]$	284 (871), 417 (412)
8	$[\text{Ni}(\text{Tp}^{\text{Ph, Me}})(\text{pz}^{\text{Ph, Me}})(\text{p-NH}_2\text{-OBz})]$	283 (932), 419 (365)
9	$[\text{Ni}(\text{Tp}^{\text{Ph, Me}})(\text{pz}^{\text{Ph, Me}})(\text{p-HO-OBz})]$	283 (421), 489 (158)
10	$[\text{Ni}(\text{Tp}^{\text{Ph, Me}})(\text{pz}^{\text{Ph, Me}})(\text{p-CHO-OBz})]$	285 (1514), 413 (265)
11	$[\text{Ni}(\text{Tp}^{\text{Ph, Me}})(\text{pz}^{\text{Ph, Me}})(\text{p-CN-OBz})]$	286 (824), 413 (231)
12	$[\text{Ni}(\text{Tp}^{\text{Ph, Me}})_2]$	287 (1048), 600 (373)
13	$[\text{Ni}(\text{Tp}^{\text{Ph, Me}})(\text{pz}^{\text{Ph, Me}})(\text{N}_3)]$	394 (375), 644 (194)
14	$[\text{Ni}(\text{Tp}^{\text{Ph, Me}})(\text{pz}^{\text{Ph, Me}})(\text{NCS})]$	488 (136)
15	$[\text{Ni}(\text{Tp}^{\text{Ph, Me}})(\text{pz}^{\text{Ph, Me}})(\text{CN})]$	368 (651), 493 (193)

Magnetic Measurement

$$\mu_{\text{eff}} = 2.84 [(\mu_2 - \mu_1)MT / (w_2 - w_1)H]^{1/2}$$

Where

$$T = 25 + 273 = 298 \text{ K}$$

$$H = 5000 \text{ Gauss}$$

M = molecular weight of the complex

Table 3.2 Magnetic susceptibility data of complexes

S.No.	Compounds	μ of Empty holder (emu) * 10^{-2}	Wt. Of holder (gm)		μ of Filled holder (emu) * 10^{-2}	Wt. of sample (gm)	μ of sample (emu)
			Empty	Filled			
1	[Ni(Tp ^{Ph,Me})(pz ^{Ph,Me})Cl]	-0.044	1.03626	1.0639	0.018	0.02764	0.062
2	[Ni(Tp ^{Ph,Me})(pz ^{Ph,Me})(oBz)]	-0.067	1.07832	1.10271	-0.031	0.02439	0.036
3	[Ni(Tp ^{Ph,Me})(pz ^{Ph,Me})(p-Cl-oBz)]	-0.088	1.05169	1.07835	-0.056	0.02666	0.032
4	[Ni(Tp ^{Ph,Me})(pz ^{Ph,Me})(p-F-oBz)]	-0.063	0.93477	0.95466	-0.025	0.01989	0.038
5	[Ni(Tp ^{Ph,Me})(pz ^{Ph,Me})(p-NO ₂ -OBz)]	-0.084	0.93992	0.96331	-0.047	0.02339	0.037
6	[Ni(Tp ^{Ph,Me})(pz ^{Ph,Me})(p-Me-OBz)]	-0.073	0.91342	0.93776	-0.038	0.02434	0.035
7	[Ni(Tp ^{Ph,Me})(pz ^{Ph,Me})(p-MeO-OBz)]	-0.087	1.12072	1.09334	-0.046	0.02738	0.041
8	[Ni(Tp ^{Ph,Me})(pz ^{Ph,Me})(p-NH ₂ -OBz)]	-0.071	0.98373	1.01272	-0.032	0.02899	0.039
9	[Ni(Tp ^{Ph,Me})(pz ^{Ph,Me})(p-HO-OBz)]	-0.068	0.97218	0.99347	-0.037	0.02129	0.031
10	[Ni(Tp ^{Ph,Me})(pz ^{Ph,Me})(p-CHO-OBz)]	-0.031	0.99631	1.0208	0.011	0.02449	0.042
11	[Ni(Tp ^{Ph,Me})(pz ^{Ph,Me})(p-CN-OBz)]	-0.063	0.91435	0.94541	-0.012	0.03106	0.051
12	[Ni(Tp ^{Ph,Me}) ₂]	-0.057	1.03868	1.00681	-0.018	0.03187	0.039
13	[Ni(Tp ^{Ph,Me})(pz ^{Ph,Me})(N ₃)]	-0.092	1.08592	1.09322	-0.073	0.00730	0.019
14	[Ni(Tp ^{Ph,Me})(pz ^{Ph,Me})(NCS)]	-0.045	1.0619	1.0772	0.008	0.0153	0.053
15	[Ni(Tp ^{Ph,Me})(pz ^{Ph,Me})(CN)]	-0.072	0.94531	0.95968	-0.026	0.01437	0.046

Table 3.3 Magnetic susceptibility calculated for complexes

S.No.	Compound	Molecular Weight	μ_{eff} (B.M.)
1	$[\text{Ni}(\text{Tp}^{\text{Ph,Me}})(\text{pz}^{\text{Ph,Me}})\text{Cl}]$	576.5	2.49
2	$[\text{Ni}(\text{Tp}^{\text{Ph,Me}})(\text{pz}^{\text{Ph,Me}})(\text{oBz})]$	821.0	2.41
3	$[\text{Ni}(\text{Tp}^{\text{Ph,Me}})(\text{pz}^{\text{Ph,Me}})(p\text{-Cl-oBz})]$	855.5	2.22
4	$[\text{Ni}(\text{Tp}^{\text{Ph,Me}})(\text{pz}^{\text{Ph,Me}})(p\text{-F-oBz})]$	839.0	2.78
5	$[\text{Ni}(\text{Tp}^{\text{Ph,Me}})(\text{pz}^{\text{Ph,Me}})(p\text{-NO}_2\text{-OBz})]$	866.0	2.57
6	$[\text{Ni}(\text{Tp}^{\text{Ph,Me}})(\text{pz}^{\text{Ph,Me}})(p\text{-Me-OBz})]$	835.0	2.40
7	$[\text{Ni}(\text{Tp}^{\text{Ph,Me}})(\text{pz}^{\text{Ph,Me}})(p\text{-MeO-OBz})]$	851.0	2.48
8	$[\text{Ni}(\text{Tp}^{\text{Ph,Me}})(\text{pz}^{\text{Ph,Me}})(p\text{-NH}_2\text{-OBz})]$	836.0	2.33
9	$[\text{Ni}(\text{Tp}^{\text{Ph,Me}})(\text{pz}^{\text{Ph,Me}})(p\text{-HO-OBz})]$	837.0	2.42
10	$[\text{Ni}(\text{Tp}^{\text{Ph,Me}})(\text{pz}^{\text{Ph,Me}})(p\text{-CHO-OBz})]$	849.0	2.64
11	$[\text{Ni}(\text{Tp}^{\text{Ph,Me}})(\text{pz}^{\text{Ph,Me}})(p\text{-CN-OBz})]$	846.0	2.58
12	$[\text{Ni}(\text{Tp}^{\text{Ph,Me}})_2]$	1025	2.46
13	$[\text{Ni}(\text{Tp}^{\text{Ph,Me}})(\text{pz}^{\text{Ph,Me}})(\text{N}_3)]$	742.0	3.23
14	$[\text{Ni}(\text{Tp}^{\text{Ph,Me}})(\text{pz}^{\text{Ph,Me}})(\text{NCS})]$	758.0	3.55
15	$[\text{Ni}(\text{Tp}^{\text{Ph,Me}})(\text{pz}^{\text{Ph,Me}})(\text{CN})]$	726.0	3.34

Description of crystal structures:

Molecular structure of $[\text{Ni}(\text{Tp}^{\text{Ph,Me}})(\text{pz}^{\text{Ph,Me}})\text{Cl}]$ (2)

The single crystal X-ray diffraction studies confirm the formulation of **2** as $[\text{Ni}(\text{Tp}^{\text{Ph,Me}})(\text{pz}^{\text{Ph,Me}})\text{Cl}]$. The bond lengths and bond angles are listed in table 3.6 and the molecular structure is given in Fig. 3.15 with thermal ellipsoidal representation at 30% probability level. As shown in Fig. 3.15, the unit cell consist of one crystallographically independent molecule. In this molecule nickel ion is in five-coordination environment, as three nitrogen atoms from hydrotris(3-phenyl-5-methyl-pyrazolyl)borate ligand, one nitrogen atom from 3-phenyl-5-methyl-pyrazole and one with chlorine atom coordinated to the metal centre. The nickel-nitrogen bond distances are found in between 2.047(2) - 2.145(2) Å and are well within the range reported in the literature for nickel complexes [59]. The nickel-chlorine bond distance is 2.3057(8) Å showing its covalent character.

Molecular structure of $[\text{Ni}(\text{Tp}^{\text{Ph,Me}})(\text{pz}^{\text{Ph,Me}})(\text{OBz})]$ (3)

The complex **3** crystallizes in triclinic space group $P\bar{1}$. The molecular structure of complex is shown in Fig. 3.16 with thermal ellipsoidal representation at 50% probability level. The selected bond lengths and bond angles are listed in table 3.7. The nickel centre is five coordinated with three nitrogen from hydrotris(3-phenyl-5-methyl-pyrazolyl)borate ligand, one nitrogen atom from 3-phenyl-5-methyl-pyrazole and one oxygen from benzoate ligand. Like complex **2**, in this complex **3**, Ni-N bond distances of coordinated ligands are in the range of 2.0430(15) - 2.1053(14) Å. The average Ni-N bond distance (2.066 Å) in complex **2** is shorter than the average Ni-N bond distances in other reported Ni (II) complexes with Tp ligands [57]. The Ni-O bond distance is 1.9925(12) Å shows the monodentate binding behaviour of benzoate with Ni(II) ion [56, 57].

Molecular structure of $[\text{Ni}(\text{Tp}^{\text{Ph,Me}})(\text{pz}^{\text{Ph,Me}})(p\text{-Cl-OBz})]$ (4)

The single crystal X-ray studies revealed that the complex **4** crystallizes in triclinic space group $P\bar{1}$ ($Z = 2$). Thermal ellipsoidal representation at 30% probability level of complex **4** is shown in Fig. 3.17. The selected bond lengths and bond angles are listed in

table 3.8. The crystal structure of **4** contains a mononuclear metal center in which nickel is in five-coordination environment and coordination sites are same as for complex **3**. The difference between complex **3** and **4** is that **4** contain *p*-chlorobenzoate in place of benzoate. The nickel-nitrogen bond distances are in the range of 2.027(3) - 2.112(3) Å. The Ni-O bond distance is 1.983(2) Å which is shorter as compare to Ni-O bond distance to complex **3** which reflects the Ni-O bond from coordinated chlorobenzoate group in complex **4** is stronger than in complex **3**. The strengthening of Ni-O bond in complex **4** may be due to the presence of chlorine atom which provides lone pair of electrons for conjugation.

Molecular structure of [Ni(Tp^{Ph,Me})(pz^{Ph,Me})(*p*-F-OBz)] (**5**)

The complex **5** crystallizes in triclinic space group $P\bar{1}$ ($Z = 2$). The molecular structure of complex is shown in Fig. 3.18 with thermal ellipsoidal representation at 30% probability level. The selected bond lengths and bond angles are listed in table 3.9. The crystal structure of **5** also contains a mononuclear metal center in which nickel is five coordinated by four nitrogen atoms and one oxygen atom. This complex is also similar to **3** but it contain *p*-fluorobenzoate in place of benzoate. The nickel-nitrogen bond distances are in the range of 2.043(2) - 2.098(2) Å. The Ni-O bond distance is 2.0014 Å which is longer as compared to Ni-O bond distance to complex **3** and **4** which reflects that Ni-O bond from coordinated fluorobenzoate group in complex **5** is weaker than in complex **3** and **4**. The weakening of Ni-O bond in complex **5** is due to the presence of electronegative atom fluorine on benzene ring in comparison to hydrogen atom in complex **3** and chlorine atom in compound **4**.

Molecular structure of [Ni(Tp^{Ph,Me})(pz^{Ph,Me})(*p*-Me-OBz)] (**7**)

The complex **7** crystallizes in triclinic space group $P\bar{1}$. The molecular structure of complex is shown in Fig. 3.19 with thermal ellipsoidal representation at 50% probability level. The selected bond lengths and bond angles are listed in table 3.10. The nickel centre is five coordinated with three nitrogen from hydrotris(3-phenyl-5-methyl-pyrazolyl)borate ligand, one nitrogen atom from 3-phenyl-5-methyl-pyrazole and one oxygen from *p*-methylbenzoate ligand. Like complex **2**, in this complex **7**, Ni-N bond distances of

coordinated ligands are in the range of 2.039(5) - 2.094(5) Å. The average Ni-N bond distance (2.057 Å) in complex **7** is shorter than the average Ni-N bond distances in other reported Ni (II) complexes with Tp ligands [57]. The Ni-O bond distance is 2.024(5) Å shows the monodentate binding behaviour of benzoate with Ni(II) ion.

Molecular structure of [Ni(Tp^{Ph,Me})₂] (13)

The single crystal X-ray diffraction studies confirmed the formulation of complex **13** as being [Ni(Tp^{Ph,Me})₂]. The molecular structure of complex is shown in Fig. 3.20. The selected bond lengths and bond angles are listed in table 3.11. The crystal structure of **13** contains a mononuclear metal centre where nickel is in six-fold coordination with six nitrogen from two hydrotris(3-phenyl-5-methyl-pyrazolyl)borate ligand. The nickel-nitrogen bond distances are in the range of 2.130(6) - 2.276(5) Å.

Molecular structure of [Ni(Tp^{Ph,Me})(pz^{Ph,Me})(N₃)] (14)

The single crystal X-ray diffraction studies confirmed the formulation of complex **14** as being [Ni(Tp^{Ph,Me})(pz^{Ph,Me})(N₃)]. The molecular structure of complex is shown in Fig. 3.21 with thermal ellipsoidal representation at 30% probability level. The selected bond lengths and bond angles are listed in table 3.12. The crystal structure of **14** contains a mononuclear metal center in which nickel center is five coordinated with three nitrogen from hydrotris(3-phenyl-5-methyl-pyrazolyl)borate ligand, one nitrogen from 3-phenyl-5-methyl-pyrazole and one nitrogen atom from terminal azide ion. The nickel-nitrogen bond distances are in the range of 2.005(4) - 2.114(4) Å. The Ni-N bond distance is 2.005 Å in Ni- azide coordination which is shorter as compared to Ni-N bond distance in bridging azide complexes [57].

Molecular structure of [Ni(Tp^{Ph,Me})(pz^{Ph,Me})(NCS)] (15)

The complex **15** crystallizes in the triclinic space group P $\bar{1}$ (Z = 2). Fig. 3.22 shows the molecular structure of the complex with thermal ellipsoidal representation at 30% probability level. Selected bond lengths and bond angles are listed in table 3.13. From crystal structure, it is clear that nickel is five coordinated, bonding of three nitrogen atoms from hydrotris(3-

phenyl-5-methyl-pyrazolyl)borate ligand, one nitrogen from 3-phenyl-5-methyl-pyrazole and one nitrogen atom from monodentate thiocyanate group. The nickel-nitrogen bond distances are in the range of 2.007(13) - 2.122(8) Å. The Ni-N bond distance is 2.005 Å in Ni-thiocyanate coordination.

Thermal Properties:

The thermal stability of complexes in nitrogen atmosphere was examined by TG, DTG and DTA techniques in the temperature range of 27–800 °C at the heating rate of 10 °C min⁻¹ under nitrogen atmosphere. As shown in Fig. 3.23 (TG curve), thermal decomposition of complex **2**, can be divided in three stages. The first weight loss of 5.17% between 70–200 °C, corresponds to the release of one chloride. The second weight loss 69% was observed in the temperature range of 250–450 °C due to the removal of Tp^{Ph, Me} ligand and the final weight loss in the temperature range of 450–800 °C was due to the loss of pz^{Ph, Me} ligand. The thermo decomposition process indicates of complexes **3 – 16** are stable up to about 100 °C and at higher temperatures curves shows regular pattern until plateau reaches between 700–800 °C, due to the formation of thermally stable Ni. Also complexes **3 – 12** show the three stage decomposition processes. The first stage decomposition occurs at the range of about 300–450 °C, the second stage occurs in the range of about 450–600 °C and the third stage decomposition was found in the range of 600–800 °C. TG curve of complex **13** (Fig. 3.34) exhibited two well separated weight loss stages. The complex is stable up to 200 °C and the first stage weight loss of 47.12% occurred from 199–501 °C temperature due to the release of one Tp^{Ph, Me} ligand. The second weight loss of 51.11% between 501–795 °C corresponds to the loss of second Tp^{Ph, Me} ligand. TG curve of complexes **14 – 16** are stable up to 100 °C and exhibited two stage weight loss. Complex **14 - 16** also gives Ni as final decomposition product.

Superoxide dismutase activity studies:

The complexes **3-16** were tested for their SOD activity using xanthine-xanthine oxidase-nitro blue tetrazolium (NBT) methods [58, 59], The test was performed separately in duplicate for each compound in 3 ml of 50 mM potassium phosphate buffer (pH 7.4) at 25 °C in the absence of EDTA. The reaction mixture was prepared as follows:

50 μ M of NBT, 50 μ M xanthine, 1000 U/ml catalase and 0.04 U/ml xanthine oxidase were used to produce superoxide ions in solution. The formation of diformazan was monitored at 560 nm wavelength. The IC_{50} values in Fig. 3.1-3.14 means the concentration of the complex which exerts SOD activity equivalent to one unit of native SOD. Out of these tested complexes only complexes **6, 11** and **12** exhibited IC_{50} values at $\sim 15 \mu$ M concentration (Fig. 3.9), clearly indicating that this may be a suitable model for a SOD mimic. The SOD activity value for **6, 11** and **12** are much better than the previously reported SOD model complexes screened by the NBT method under the same conditions [60]. The better SOD activities of complex **6, 11** and **12** may be attributable to the very close structural similarities of this complex with the active site of native Ni-SOD and also due to the open active site for substrate binding [63]. As these complexes **6, 11** and **12** having substituted benzoate with electron withdrawing groups make the Ni-O bond weaker and open up the active site for substrate binding. The complexes with substituted benzoates having electron donating groups make the active site less available for substrate binding relative to the benzoate complexes with withdrawing groups; due to this these complexes have intermediate activity. As complex **11** do not have any proton donating groups also is in octahedral geometry having small cavity for substrate addition shows a very small activity for SOD and does not considered as mimic for Ni-SOD.

Table 3.5: IC₅₀ values for different compounds

S.No.	Complex No.	Complex	IC ₅₀ Value
1	3	[Ni(Tp ^{Ph,Me})(pz ^{Ph,Me})(OBz)]	18.50
2	4	[Ni(Tp ^{Ph,Me})(pz ^{Ph,Me})(<i>p</i> -Cl-OBz)]	19.03
3	5	[Ni(Tp ^{Ph,Me})(pz ^{Ph,Me})(<i>p</i> -F-OBz)]	20.20
4	6	[Ni(Tp ^{Ph,Me})(pz ^{Ph,Me})(<i>p</i> -NO ₂ -OBz)]	16.32
5	7	[Ni(Tp ^{Ph,Me})(pz ^{Ph,Me})(<i>p</i> -Me-OBz)]	20.87
6	8	[Ni(Tp ^{Ph,Me})(pz ^{Ph,Me})(<i>p</i> -MeO-OBz)]	22.58
7	9	[Ni(Tp ^{Ph,Me})(pz ^{Ph,Me})(<i>p</i> -NH ₂ -OBz)]	19.92
8	10	[Ni(Tp ^{Ph,Me})(pz ^{Ph,Me})(<i>p</i> -HO-OBz)]	23.17
9	11	[Ni(Tp ^{Ph,Me})(pz ^{Ph,Me})(<i>p</i> -CHO-OBz)]	16.72
10	12	[Ni(Tp ^{Ph,Me})(pz ^{Ph,Me})(<i>p</i> -CN-OBz)]	16.82
11	13	[Ni(Tp ^{Ph,Me}) ₂]	48.73
12	14	[Ni(Tp ^{Ph,Me})(pz ^{Ph,Me})(N ₃)]	29.27
13	15	[Ni(Tp ^{Ph,Me})(pz ^{Ph,Me})(NCS)]	28.54
14	16	[Ni(Tp ^{Ph,Me})(pz ^{Ph,Me})(CN)]	30.12

Table 3.6 Crystal data and structure refinement parameters for the complex [Ni(Tp^{Ph,Me})(pz^{Ph,Me})Cl] (2)

Complex	(2)
Empirical Formula	C ₄₇ H ₄₆ N ₈ BcINi
Formula weight	827.87
Crystal system	Monoclinic
Space group	P2(1)/c
<i>Unit cell dimensions</i>	
<i>a</i> (Å)	16.1062(8)
<i>b</i> (Å)	11.9682(5)
<i>c</i> (Å)	22.3387(11)
<i>α</i> (°)	90.00
<i>β</i> (°)	98.195(2)
<i>γ</i> (°)	90.00
<i>V</i> (Å ³)	4262.1(3)
<i>Z</i>	4
<i>D</i> _{calc} (g/cm ³)	1.285
Data collection	
2θ _{max} (°)	52.72
Number of measured reflections	8285
Number of observed reflections	5817
Number of parameters refined	532
<i>R</i>	0.0447
<i>R</i> _w	0.1290

Selected interatomic bond lengths (Å) and angles (°) of the complex [Ni(Tp^{Ph,Me})(pz^{Ph,Me})Cl]

Ni1-N4	2.047(2)	N4-Ni1-N5	94.23(9)
Ni1-N5	2.051(2)	N4-Ni1-N7	90.63(9)
Ni1-N7	2.126(2)	N5-Ni1-N7	93.52(8)
Ni1-N1	2.145(2)	N4-Ni1-N1	90.37(9)
Ni1-Cl1	2.3057(8)	N5-Ni1-N1	84.76(8)
		N7-Ni1-N1	178.07(8)
		N4-Ni1-Cl1	119.73(7)
		N5-Ni1-Cl1	145.85(7)
		N7-Ni1-Cl1	89.90(6)
		N1-Ni1-Cl1	91.04(6)

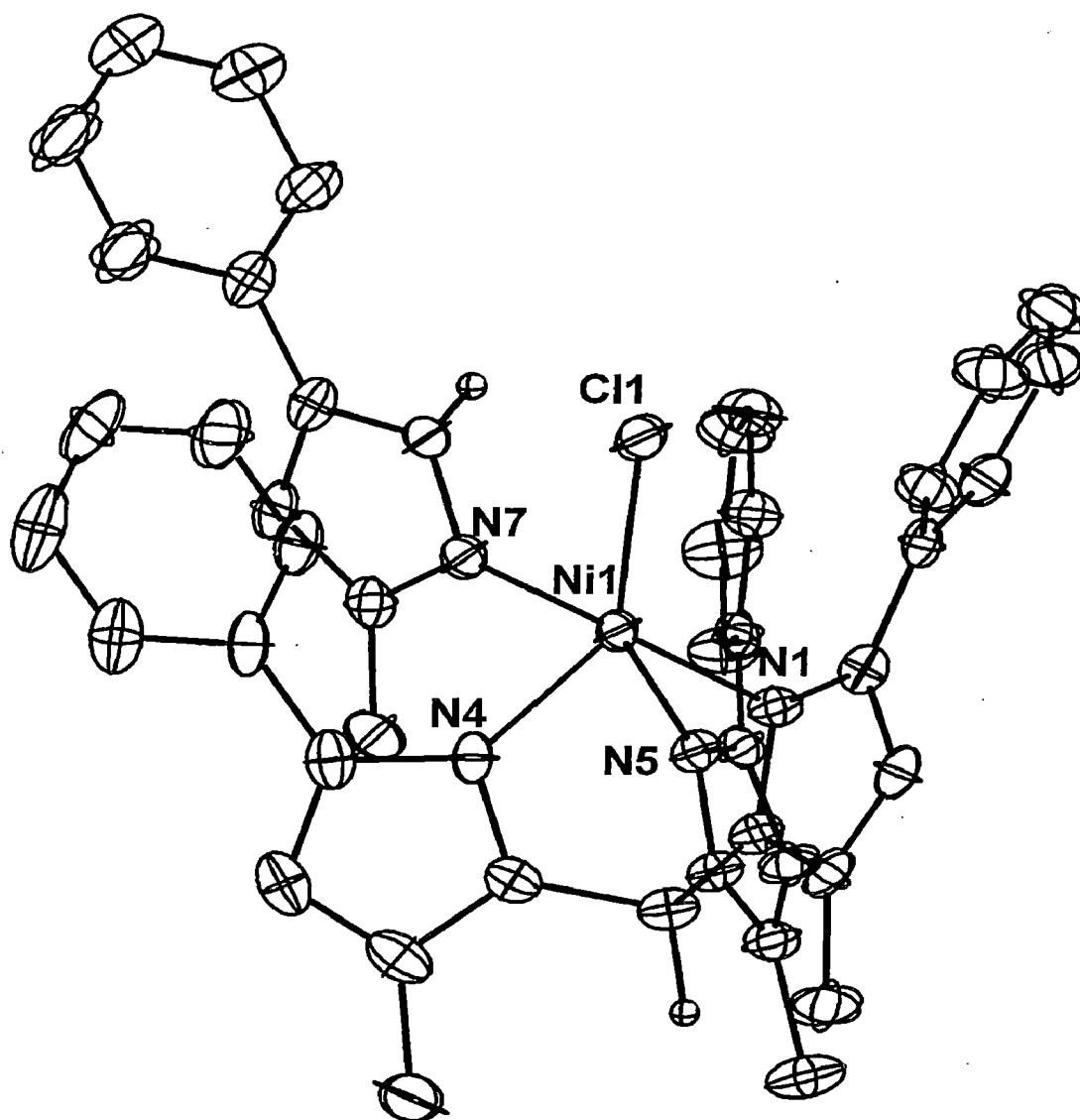


Fig. 3.15 Thermal ellipsoidal representation for $[\text{Ni}(\text{Tp}^{\text{Ph,Me}})(\text{pz}^{\text{Ph,Me}})\text{Cl}]$ drawn at 30% probability level (2)

Table 3.7 Crystal data and structure refinement parameters for the complex [Ni(Tp^{Ph,Me})(pz^{Ph,Me})(OBz)] (3)

Complex	(3)		
Empirical Formula	C ₅₈ H ₅₆ N ₈ O ₂ BNi		
Formula weight	966.61		
Crystal system	Triclinic		
Space group	<i>P</i> $\bar{1}$		
<i>Unit cell dimensions</i>			
<i>a</i> (Å)	12.4267(9)		
<i>b</i> (Å)	12.8452(10)		
<i>c</i> (Å)	16.1978(12)		
α (°)	76.512(2)		
β (°)	84.087(3)		
γ (°)	85.361(3)		
<i>V</i> (Å ³)	2486.5(3)		
<i>Z</i>	2		
<i>D</i> _{calc} (g/cm ³)	1.286		
Data collection			
2 θ _{max} (°)	71.34		
Number of measured reflections	23112		
Number of observed reflections	13962		
Number of parameters refined	645		
<i>R</i>	0.0571		
<i>R</i> _w	0.1483		
Selected interatomic bond lengths (Å) and angles (°) of the complex [Ni(Tp ^{Ph,Me})(pz ^{Ph,Me})(OBz)]			
Ni1-O1	1.9925(12)	N3-Ni1-N5	94.80(6)
Ni1-N3	2.0430(15)	N3-Ni1-N7	90.32(6)
Ni1-N5	2.0473(14)	N3-Ni1-N1	94.22(6)
Ni1-N7	2.1053(14)	N5-Ni1-N7	83.67(6)
Ni1-N1	2.0687(14)	N5-Ni1-N1	89.60(5)
		N7-Ni1-N1	172.19(6)
		O1-Ni1-N3	105.08(6)
		O1-Ni1-N5	158.68(6)
		O1-Ni1-N7	88.53(5)
		O1-Ni1-N1	96.41(5)

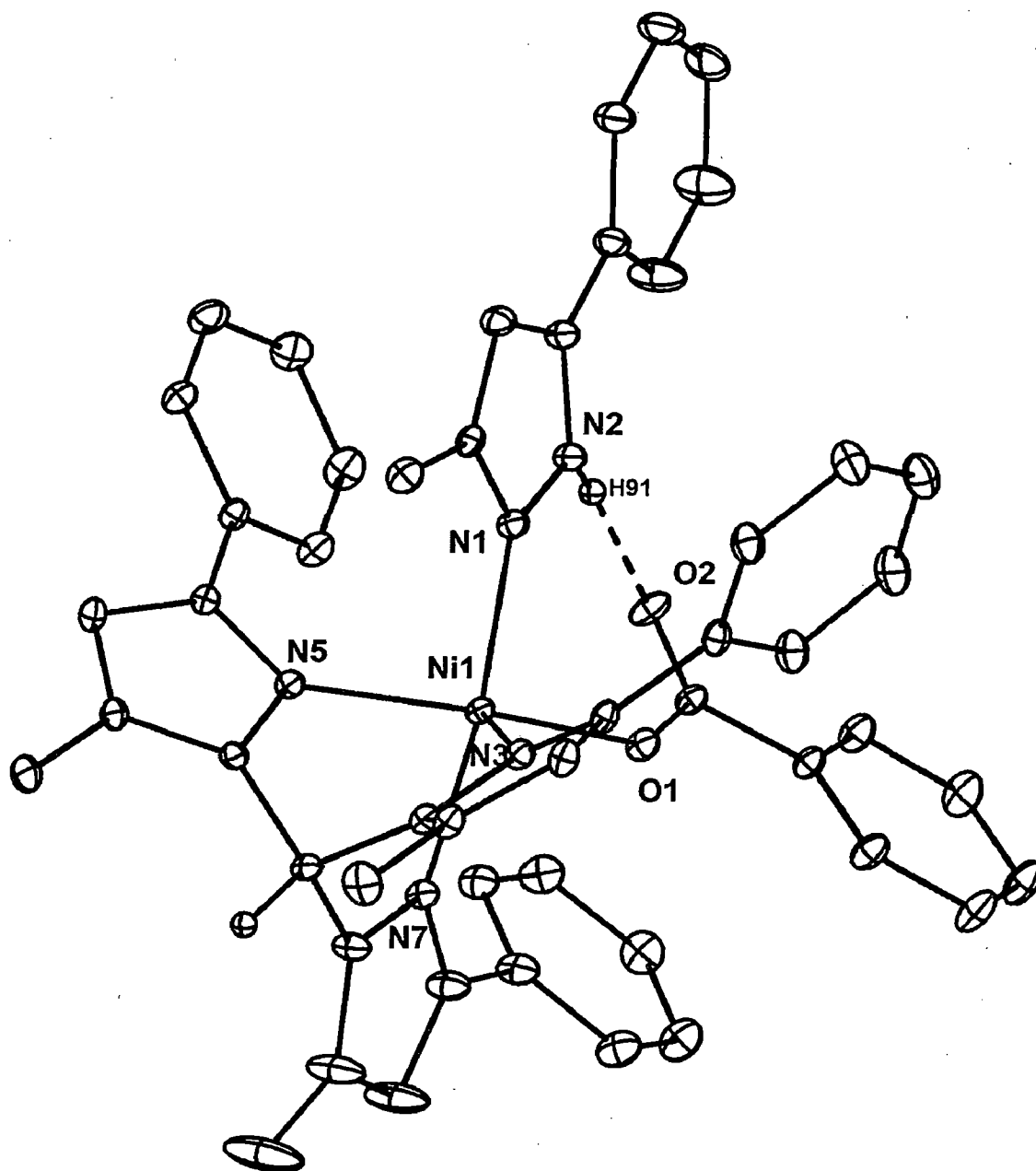


Fig. 3.16 Thermal ellipsoidal representation for $[\text{Ni}(\text{Tp}^{\text{Ph,Me}})(\text{pz}^{\text{Ph,Me}})(\text{OBz})]$ drawn at 50% probability level (3)

Table 3.8 Crystal data and structure refinement parameters for the complex [Ni(Tp^{Ph,Me})(pz^{Ph,Me})(p-Cl-OBz)] (4)

Complex	(4)
Empirical Formula	C ₅₄ H ₅₀ N ₈ O ₂ BClNi
Formula weight	947.97
Crystal system	Triclinic
Space group	<i>P</i> $\bar{1}$
<i>Unit cell dimensions</i>	
<i>a</i> (Å)	12.2449(9)
<i>b</i> (Å)	14.5984(11)
<i>c</i> (Å)	15.8697(13)
α (°)	116.012(3)
β (°)	94.100(4)
γ (°)	90.265(4)
<i>V</i> (Å ³)	2333.4 (3)
<i>Z</i>	2
<i>D</i> _{calc} (g/cm ³)	1.349
Data collection	
2 θ _{max} (°)	50.92
Number of measured reflections	8408
Number of observed reflections	5948
Number of parameters refined	617
<i>R</i>	0.0530
<i>R</i> _w	0.1382

Selected interatomic bond lengths (Å) and angles (°) of the complex [Ni(Tp^{Ph,Me})(pz^{Ph,Me})(p-Cl-OBz)]

Ni1-O1	1.983(2)	N3-Ni1-N5	94.67(12)
Ni1-N3	2.027(3)	N3-Ni1-N7	94.58(12)
Ni1-N5	2.045(3)	N3-Ni1-N1	91.57(12)
Ni1-N7	2.063(3)	N5-Ni1-N7	91.31(12)
Ni1-N1	2.112(3)	N5-Ni1-N1	84.08(12)
		N7-Ni1-N1	172.60(12)
		O1-Ni1-N3	103.11(11)
		O1-Ni1-N5	160.84(11)
		O1-Ni1-N7	94.29(11)
		O1-Ni1-N1	88.32(11)

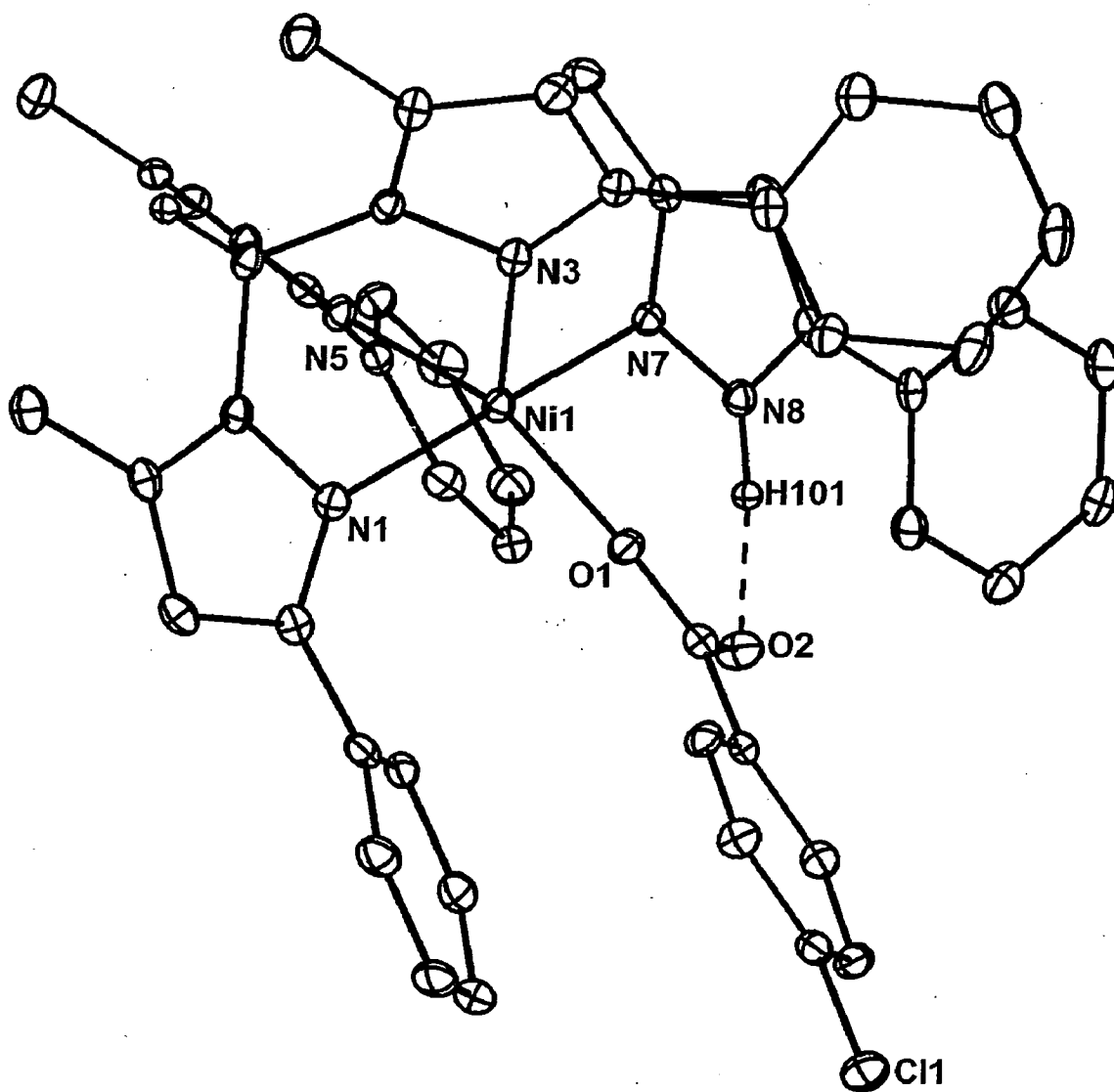


Fig. 3.17 Thermal ellipsoidal representation for $[\text{Ni}(\text{Tp}^{\text{Ph,Me}})(\text{pz}^{\text{Ph,Me}})(\text{p-Cl-OBz})]$
 drawn at 30% probability level (4)

Table 3.9 Crystal data and structure refinement parameters for the complex [Ni(Tp^{Ph,Me})(pz^{Ph,Me})(p-F-OBz)] (5)

Complex	(5)
Empirical Formula	C ₅₉ H ₅₅ N ₉ O ₂ FBNi
Formula weight	984.60
Crystal system	Triclinic
Space group	$P\bar{1}$
<i>Unit cell dimensions</i>	
<i>a</i> (Å)	12.4269(9)
<i>b</i> (Å)	12.8270(9)
<i>c</i> (Å)	16.3643(12)
<i>α</i> (°)	76.248(4)
<i>β</i> (°)	83.789(4)
<i>γ</i> (°)	90.910(5)
<i>V</i> (Å ³)	84.482(4)
<i>Z</i>	2
<i>D</i> _{calc} (g/cm ³)	1.302
Data collection	
2θ _{max} (°)	48.24
Number of measured reflections	8005
Number of observed reflections	6613
Number of parameters refined	654
R	0.0425
R _w	0.1271

Selected interatomic bond lengths (Å) and angles (°) of the complex [Ni(Tp^{Ph,Me})(pz^{Ph,Me})(p-F-OBz)]

Ni1-O1	2.0014	N1-Ni1-N7	88.83(9)
Ni1-N7	2.069(2)	N1-Ni1-N3	84.28(8)
Ni1-N5	2.043(2)	N5-Ni1-N1	95.10(8)
Ni1-N1	2.053(2)	N5-Ni1-N7	94.07(9)
Ni1-N3	2.098(2)	N5-Ni1-N3	90.28(9)
		N7-Ni1-N3	172.16(8)
		O1-Ni1-N5	105.03(8)
		O1-Ni1-N1	158.52(8)
		O1-Ni1-N7	97.00(8)
		O1-Ni1-N3	88.15(8)

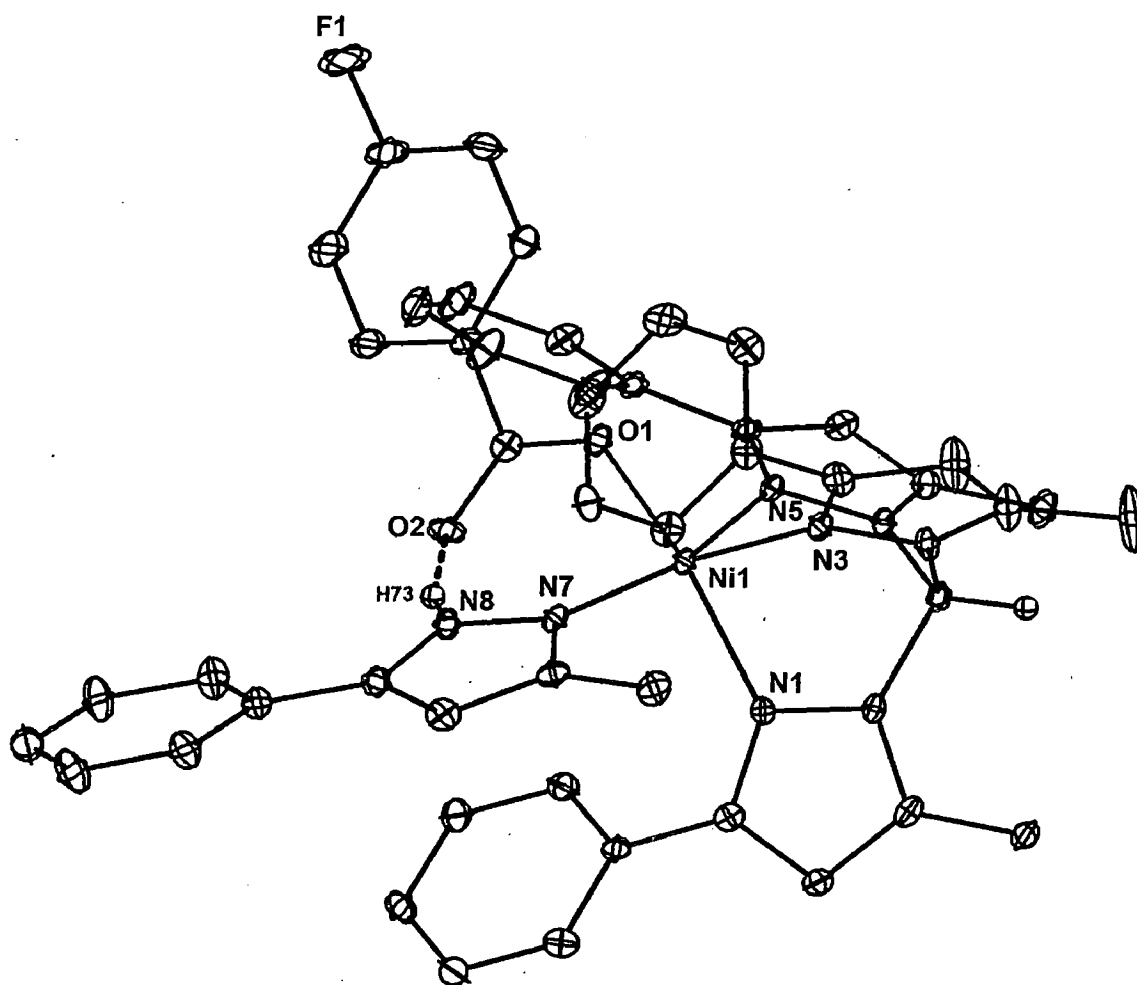


Fig. 3.18 Thermal ellipsoidal representation for $[\text{Ni}(\text{Tp}^{\text{Ph,Me}})(\text{pz}^{\text{Ph,Me}})(\text{p-F-OBz})]$
 drawn at 30% probability level (5)

Table 3.10 Crystal data and structure refinement parameters for the complex [Ni(Tp^{Ph,Me})(pz^{Ph,Me})(p-Me-OBz)] (7)

Complex	(7)
Empirical Formula	C ₄₉ H ₄₉ N ₈ O ₂ BNi
Formula weight	649.87
Crystal system	Triclinic
Space group	<i>P</i> $\bar{1}$
Unit cell dimensions	
a (Å)	12.4106(10)
b (Å)	15.2244(13)
c (Å)	15.5054(13)
α (°)	64.385(2)
β (°)	75.449(3)
γ (°)	75.849(3)
V (Å ³)	75.849(3)
Z	2
D _{calc} (g/cm ³)	2.368
Data collection	
2 θ max (°)	49.46
Number of measured reflections	8478
Number of observed reflections	6352
Number of parameters refined	595
R	0.0986
R _w	0.2971

Selected interatomic bond lengths (Å) and angles (°) of the complex [Ni(Tp ^{Ph,Me})(pz ^{Ph,Me})(p-Me-OBz)]			
Ni1-O1	2.024(5)	N1-Ni1-N7	93.7(2)
Ni1-N7	2.072(5)	N1-Ni1-N3	89.5(2)
Ni1-N5	2.056(5)	N5-Ni1-N1	94.2(2)
Ni1-N1	2.039(5)	N5-Ni1-N7	88.7(2)
Ni1-N3	2.094(5)	N5-Ni1-N3	84.2(2)
		N7-Ni1-N3	172.4(2)
		O1-Ni1-N5	157.4(2)
		O1-Ni1-N1	107.4(2)
		O1-Ni1-N7	96.3(2)
		O1-Ni1-N3	89.3(2)

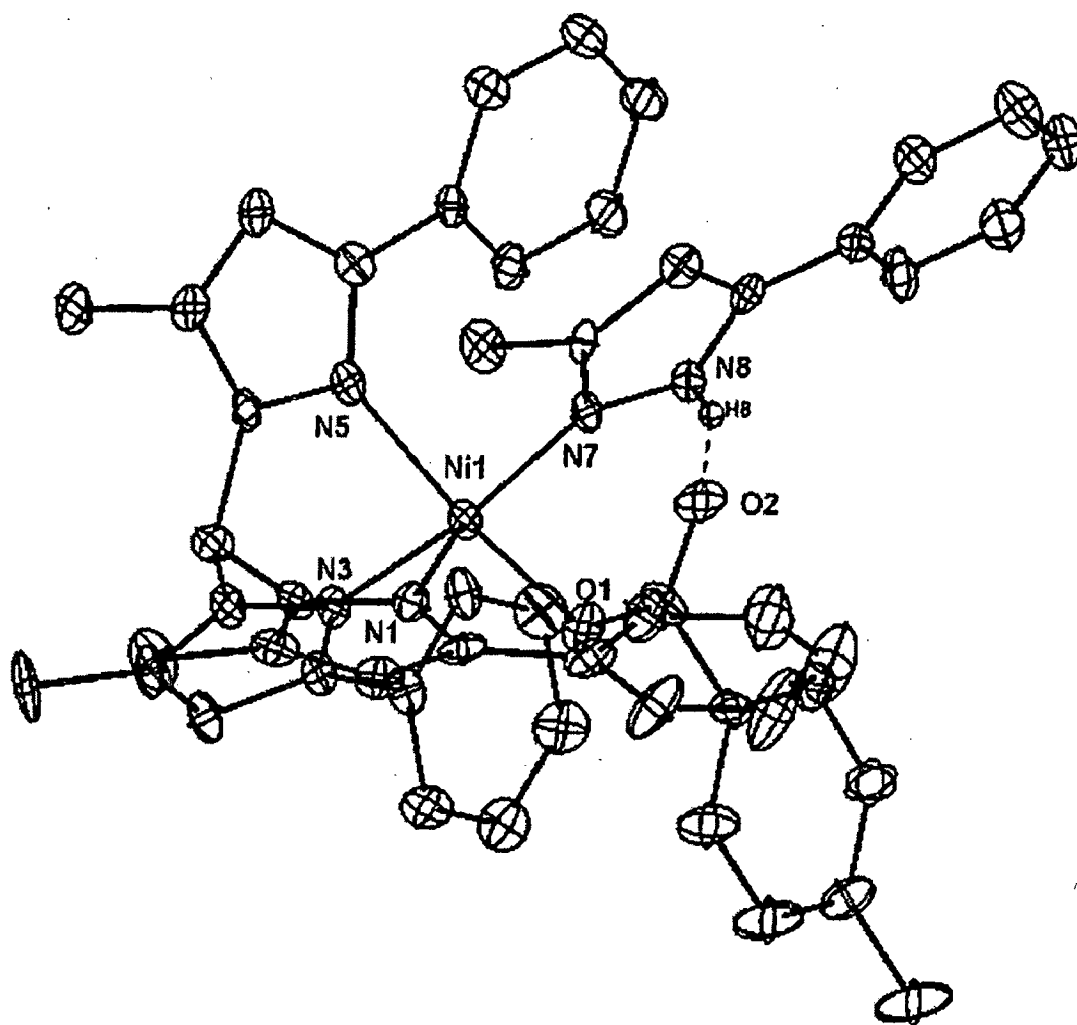


Fig. 3.19 Thermal ellipsoidal representation for $[\text{Ni}(\text{Tp}^{\text{Ph,Me}})(\text{pz}^{\text{Ph,Me}})(\text{p-Me-OBz})]$ drawn at 30% probability level (7)

Table 3.11 Crystal data and structure refinement parameters for the complex [Ni(Tp^{Ph,Me})₂] (13)

Complex	(13)
Empirical Formula	C ₆₀ H ₅₆ B ₂ N ₁₂ Ni
Formula weight	1025.48
Crystal system	Monoclinic
Space group	C -2yc
<i>Unit cell dimensions</i>	
<i>a</i> (Å)	17.9257(10)
<i>b</i> (Å)	13.7128(8)
<i>c</i> (Å)	21.9737(16)
<i>α</i> (°)	90.00
<i>β</i> (°)	80.76(2)
<i>γ</i> (°)	111.638(2)
<i>V</i> (Å ³)	90.00
<i>Z</i>	4
<i>D</i> _{calc} (g/cm ³)	1.936
<i>Data collection</i>	
2θ _{max} (°)	59.48
Number of measured reflections	12483
Number of observed reflections	10591
Number of parameters refined	690
<i>R</i>	0.0689
<i>R</i> _w	0.2262

Selected interatomic bond lengths (Å) and angles (°) of the complex [Ni(Tp^{Ph,Me})₂]

Ni1-N9	2.130(6)	N9-Ni1-N12	93.7(2)
Ni1-N12	2.134(5)	N9-Ni1-N5	96.59(11)
Ni1-N5	2.157(5)	N12-Ni1-N5	89.4(2)
Ni1-N4	2.170(6)	N9-Ni1-N4	92.1(2)
Ni1-N1	2.181(6)	N12-Ni1-N4	98.2(2)
Ni1-N8	2.276(5)	N5-Ni1-N4	84.1(2)
		N12-Ni1-N1	84.60(11)
		N5-Ni1-N1	170.13(19)
		N4-Ni1-N1	89.0(2)
		N9-Ni1-N8	80.98(19)
		N12-Ni1-N8	89.25(18)
		N5-Ni1-N8	91.34(19)
		N4-Ni1-N8	171.24(12)
		N1-Ni1-N8	96.39(18)

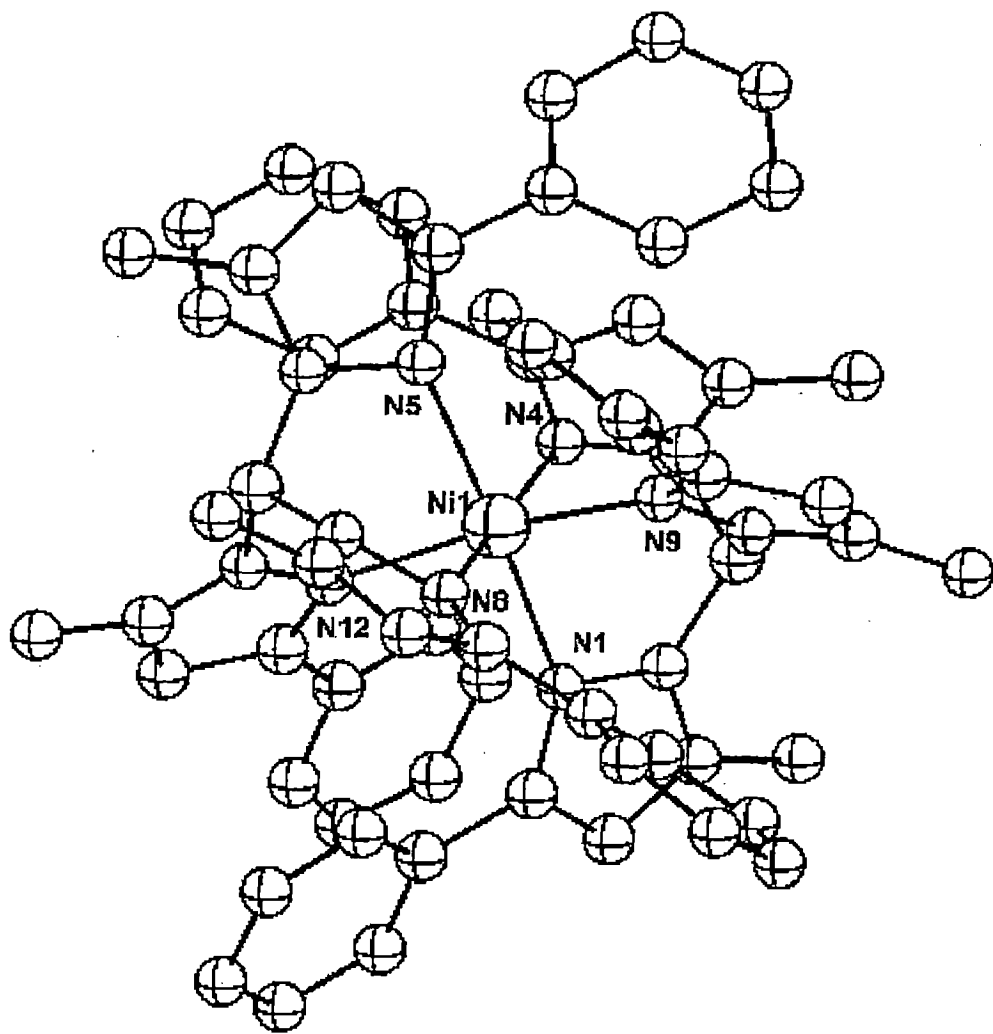


Fig. 3.20 Molecular structure of $[\text{Ni}(\text{Tp}^{\text{Ph,Me}})_2]$ (13)

Table 3.12 Crystal data and structure refinement parameters for the complex $[\text{Ni}(\text{Tp}^{\text{Ph,Me}})(\text{pz}^{\text{Ph,Me}})(\text{N}_3)]$ (14)

Complex	(14)		
Empirical Formula	$\text{C}_{84}\text{H}_{82}\text{N}_{23}\text{B}_2\text{Ni}_2$		
Formula weight	1552.73		
Crystal system	Triclinic		
Space group	$P\bar{1}$		
<i>Unit cell dimensions</i>			
<i>a</i> (Å)	11.3684(19)		
<i>b</i> (Å)	12.344(2)		
<i>c</i> (Å)	14.252(2)		
α (°)	86.878(10)		
β (°)	89.953(10)		
γ (°)	72.004(9)		
<i>V</i> (Å ³)	1899.1 (5)		
<i>Z</i>	1		
<i>D</i> _{calc} (g/cm ³)	1.358		
Data collection			
$2\theta_{\text{max}}$ (°)	55.60		
Number of measured reflections	8973		
Number of observed reflections	6509		
Number of parameters refined	515		
<i>R</i>	0.0828		
<i>R</i> _w	0.2307		
Selected interatomic bond lengths (Å) and angles (°) of the complex $[\text{Ni}(\text{Tp}^{\text{Ph,Me}})(\text{pz}^{\text{Ph,Me}})(\text{N}_3)]$			
Ni1-N9	2.005(4)	N3-Ni1-N5	95.30(16)
Ni1-N3	2.015(4)	N3-Ni1-N7	90.06(15)
Ni1-N5	2.039(4)	N3-Ni1-N1	90.78(16)
Ni1-N7	2.114(4)	N5-Ni1-N7	83.86(15)
Ni1-N1	2.084(4)	N5-Ni1-N1	90.45(16)
		N7-Ni1-N1	174.31(15)
		N9-Ni1-N3	116.54(17)
		N9-Ni1-N5	147.98(18)
		N9-Ni1-N7	98.62(16)
		N9-Ni1-N1	86.03(16)

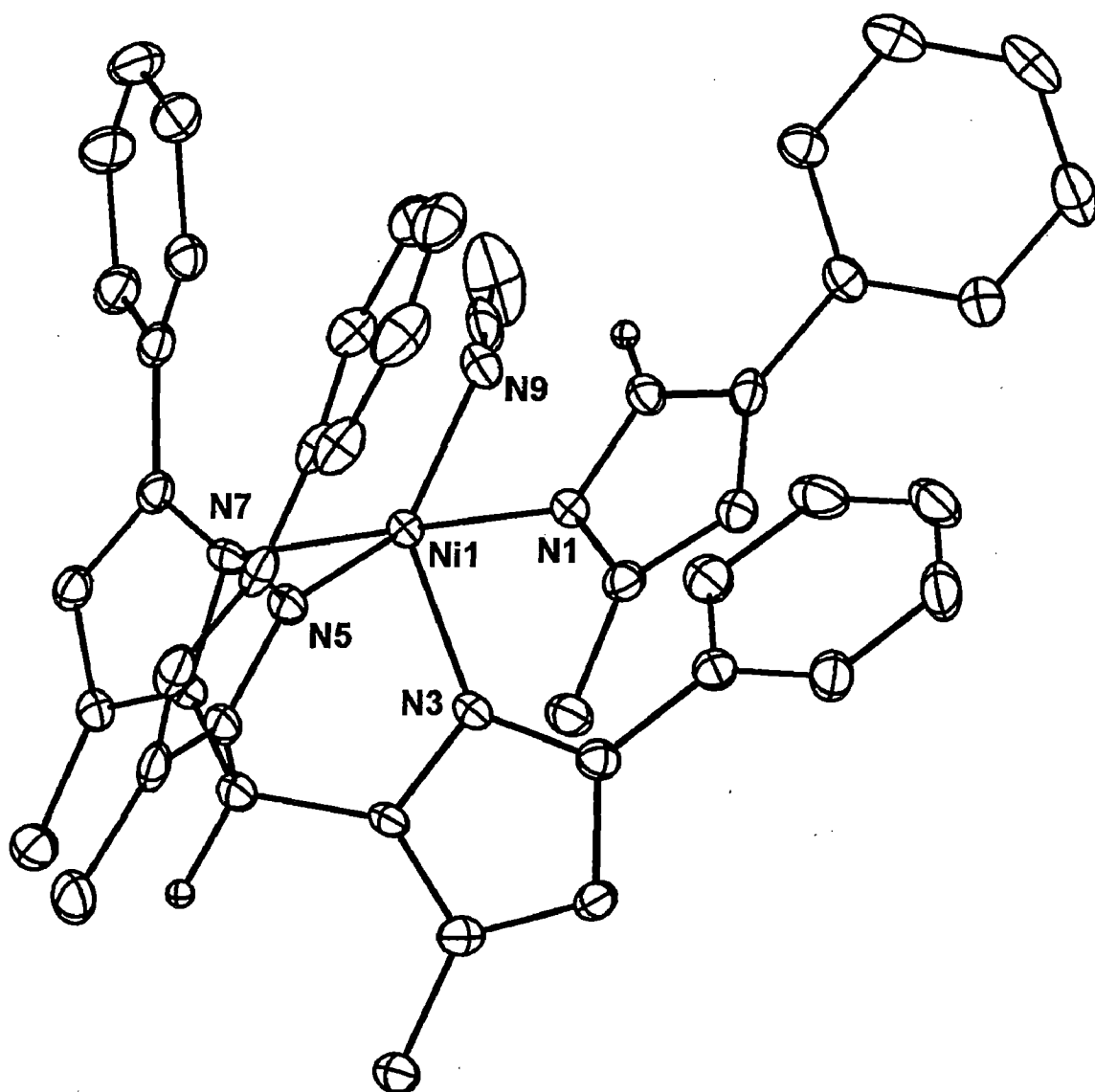


Fig. 3.21 Thermal ellipsoidal representation for $[\text{Ni}(\text{Tp}^{\text{Ph,Me}})(\text{pz}^{\text{Ph,Me}})(\text{N}_3)]$ drawn at 50% probability level (14)

Table 3.13 Crystal data and structure refinement parameters for the complex [Ni(Tp^{Ph,Me})(pz^{Ph,Me})(NCS)] (15)

Complex	(15)		
Empirical Formula	C ₄₁ H ₃₈ N ₉ BSNi		
Formula weight	758.37		
Crystal system	Triclinic		
Space group	<i>P</i> $\bar{1}$		
<i>Unit cell dimensions</i>			
<i>a</i> (Å)	11.707(4)		
<i>b</i> (Å)	11.806(4)		
<i>c</i> (Å)	15.481(6)		
<i>α</i> (°)	83.07(2)		
<i>β</i> (°)	80.76(2)		
<i>γ</i> (°)	64.931(19)		
<i>V</i> (Å ³)	1909.7(12)		
<i>Z</i>	2		
<i>D</i> _{calc} (g/cm ³)	1.319		
Data collection			
2θ _{max} (°)	38.38		
Number of measured reflections	3227		
Number of observed reflections	2046		
Number of parameters refined	490		
<i>R</i>	0.0758		
<i>R</i> _w	0.1793		
Selected interatomic bond lengths (Å) and angles (°) of the complex [Ni(Tp ^{Ph,Me})(pz ^{Ph,Me})(NCS)]			
Ni1-N11	2.007(13)	N3-Ni1-N5	95.8(4)
Ni1-N3	2.030(9)	N3-Ni1-N8	92.6(4)
Ni1-N5	2.032(9)	N3-Ni1-N1	89.4(3)
Ni1-N8	2.101(9)	N5-Ni1-N8	90.4(4)
Ni1-N1	2.122(8)	N5-Ni1-N1	87.0(4)
		N8-Ni1-N1	176.8(3)
		N11-Ni1-N3	118.4(5)
		N11-Ni1-N5	145.8(5)
		N11-Ni1-N8	89.2(4)
		N11-Ni1-N1	92.1(4)

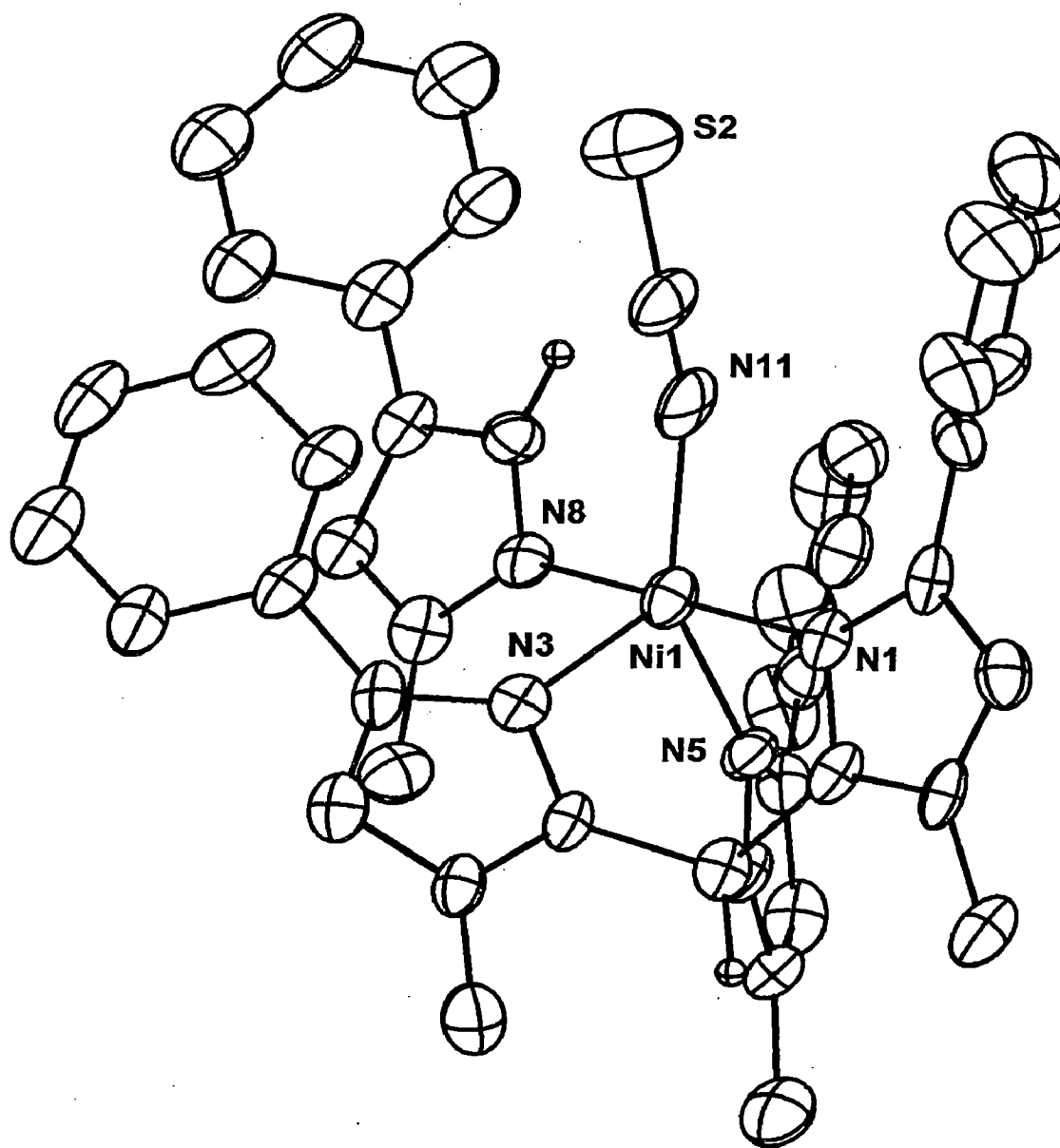


Fig. 3.22 Thermal ellipsoidal representation for $[\text{Ni}(\text{Tp}^{\text{Ph,Me}})(\text{pz}^{\text{Ph,Me}})(\text{NCS})]$ drawn at 30% probability level (15)

Chapter-4

CONCLUSIONS

Some interesting nickel complexes have been prepared with hydrotris(3-phenyl-5-methyl pyrazolyl)borate ligand [$\text{Tp}^{\text{Ph, Me}}$], 3-phenyl-5-methyl-pyrazole [$\text{pz}^{\text{Ph, MeH}}$] and different substituted benzoates. The result showed that the benzoate ligands have monodentate behaviour and second oxygen atom of that carboxylate group is showing hydrogen bonding with the N-H of 3-phenyl-5-methyl-pyrazole. Thus forming five coordinated distorted square pyramidal nickel complexes type $[\text{Ni}(\text{Tp}^{\text{Ph, Me}})(\text{pz}^{\text{Ph, Me}})(\text{X-OBz})]$ having coordination sites N4O. Also some nickel complexes with azide, thiocyanate and cyanide groups were synthesized to give different coordination environment to metal centre. All these complexes were characterized by IR, UV/Vis., TGA/DTG/DTA, magnetic susceptibility measurements and Single Crystal X-ray Diffractometer. SOD activities suggest that complexes **14**, **15** and **16** show less activity as the orientation of ligands ($-\text{N}_3$, $-\text{NCS}$, $-\text{CN}$) makes the active site less available for substrate binding while complex **13** show least activity towards superoxide inhibition because the approach of substrate is retarded by six coordination around the metal centre. The result showed that complexes with substituted benzoates having electron donating groups make the active site less available for substrate binding relative to the benzoate complexes with electron withdrawing groups so complex **6**, **11** and **12** having nitro, formyl and cyano benzoates show better SOD activity than other nickel complexes and can be considered as best model complexes for NiSOD among all the complexes synthesized in the present thesis.

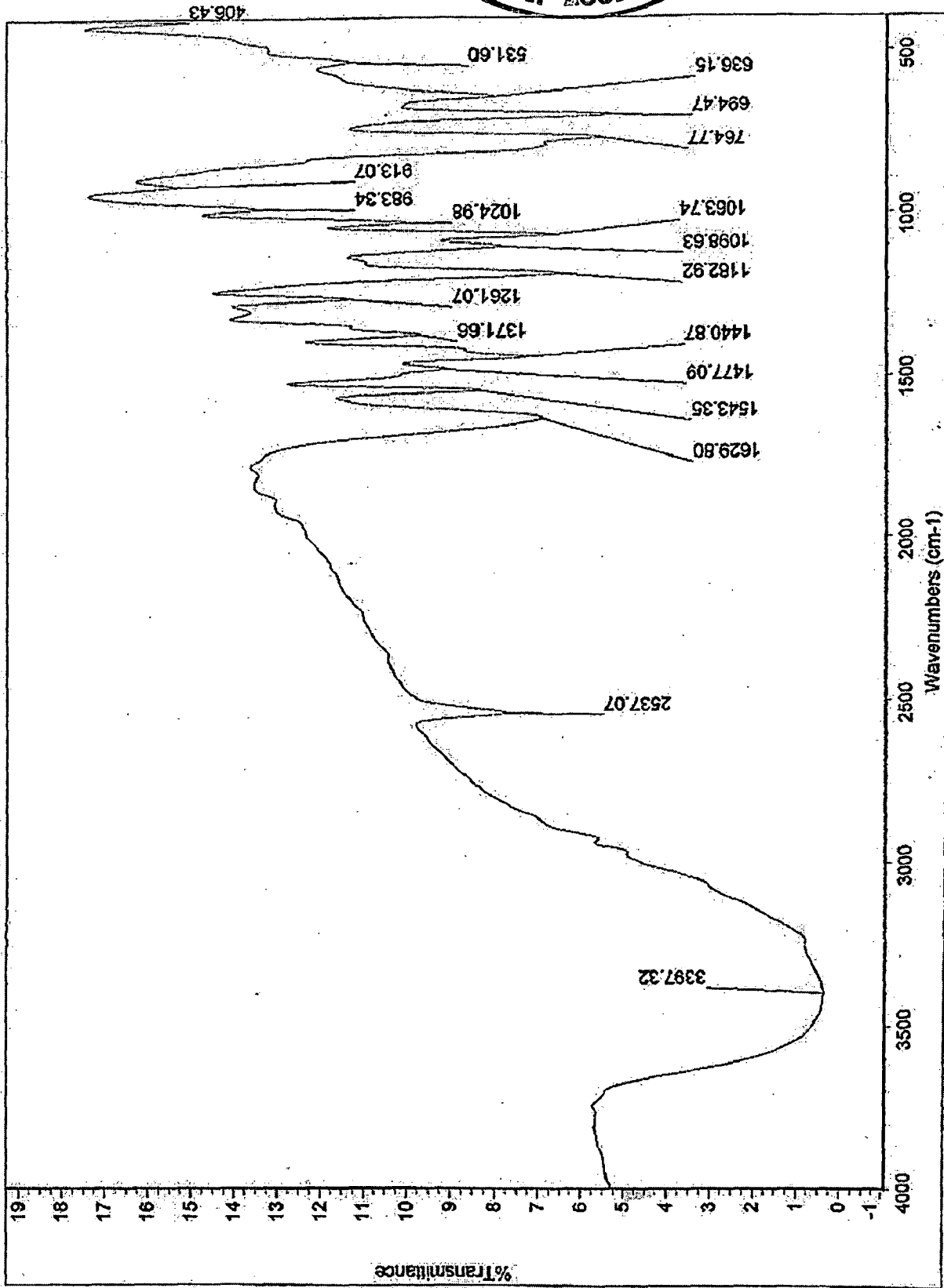


Fig. 5.1 IR spectrum of $[\text{Ni}(\text{Tp})^{\text{Ph}_4\text{Me}_6}(\text{pz}^{\text{Ph}_4\text{Me}_6})\text{Cl}]$ complex

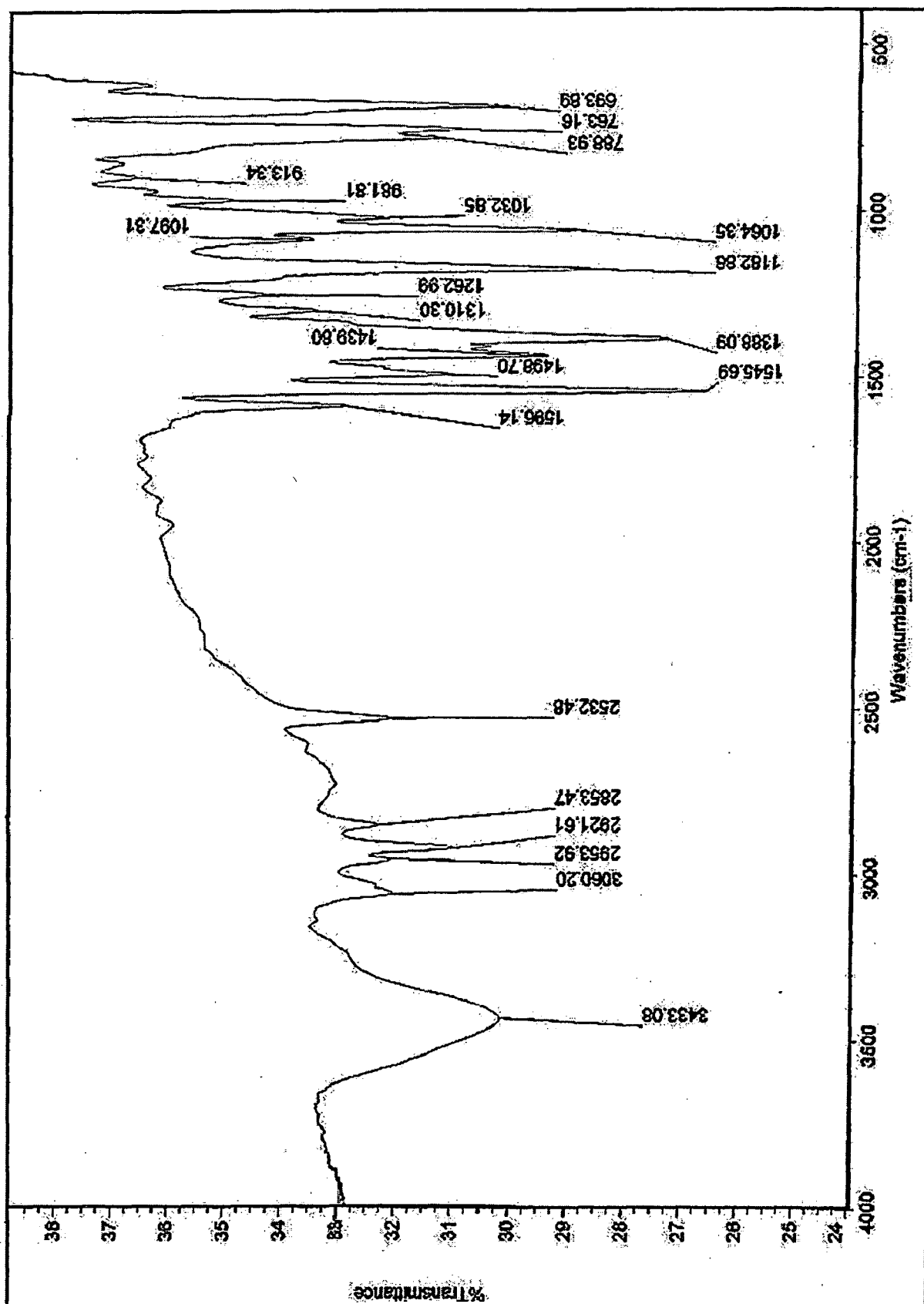


Fig. 5.2 IR spectrum of [Ni(Tp^{Ph,Me})(pz^{Ph,Me})(OBz)] complex

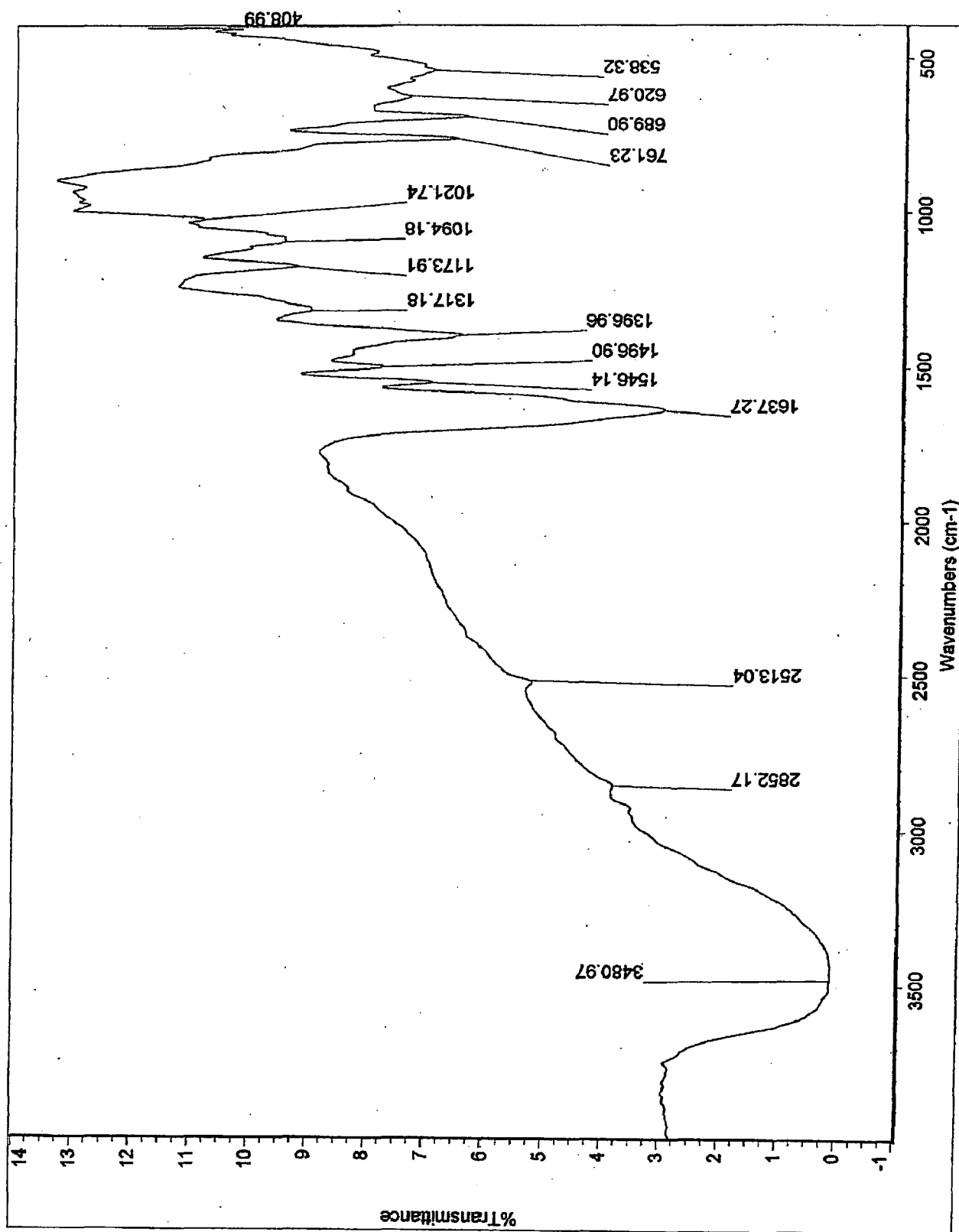


Fig. 5.3 IR spectrum of $[\text{Ni}(\text{Tp}^{\text{Ph,Me}})(\text{pz}^{\text{Ph,Me}})(p\text{-Cl-OBz})]$ complex

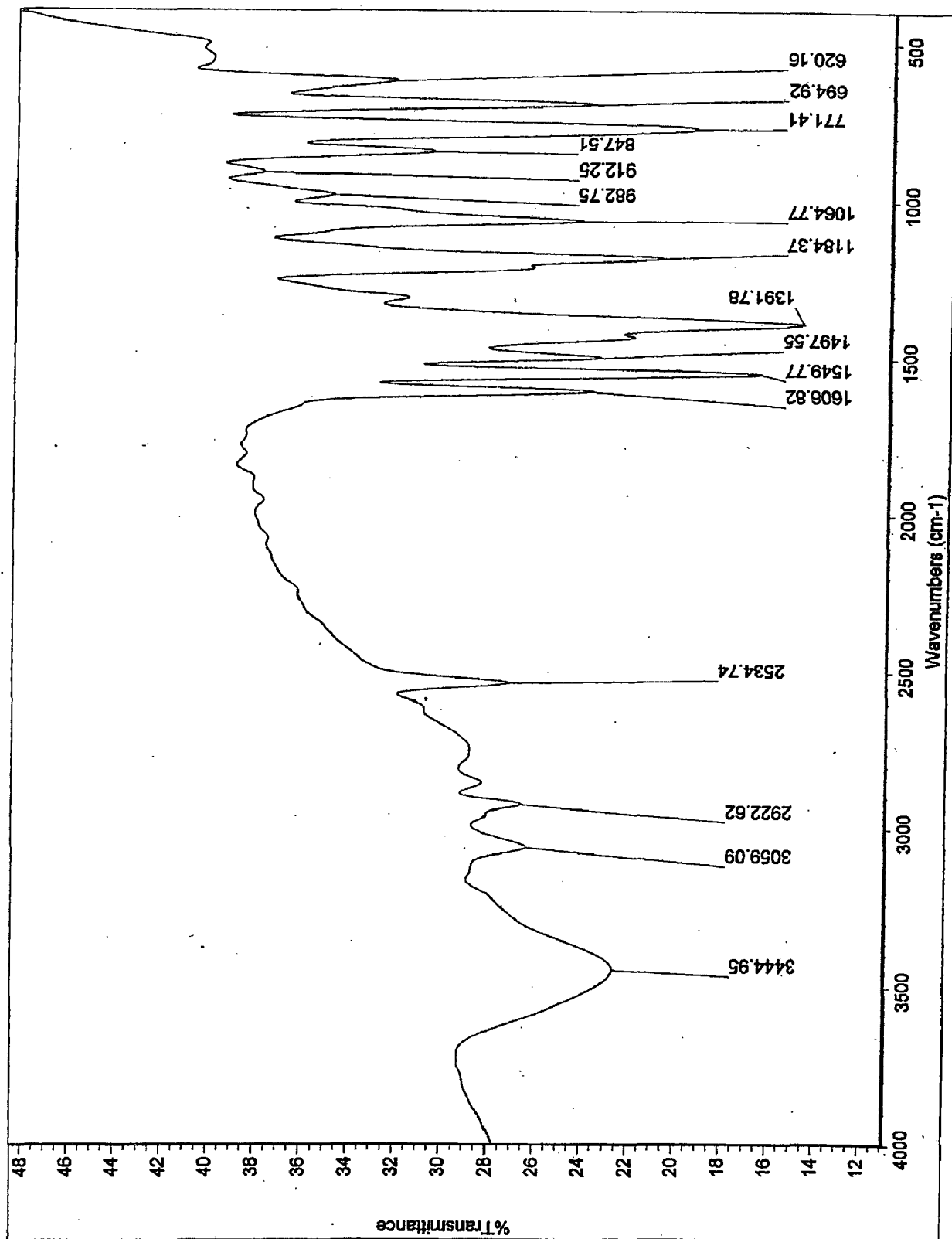


Fig. 5.4 IR spectrum of [Ni(Tp^{Ph,Me})(pz^{Ph,Me})(p-F-OBz)] complex

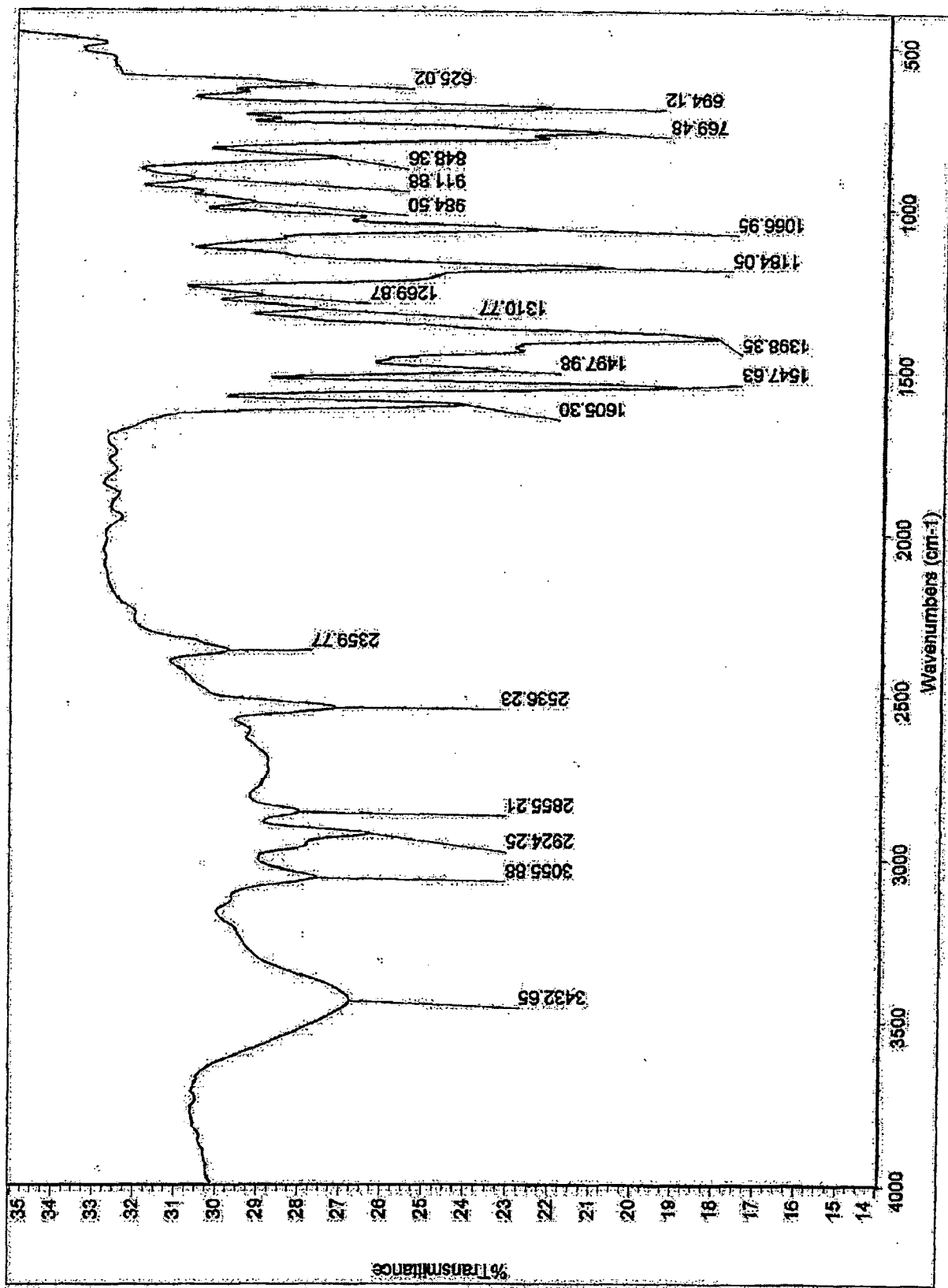


Fig. 5.5 IR spectrum of $[\text{Ni}(\text{Tp}^{\text{Ph,Me}})(\text{pz}^{\text{Ph,Me}})(p\text{-NO}_2\text{-OBz})]$ complex

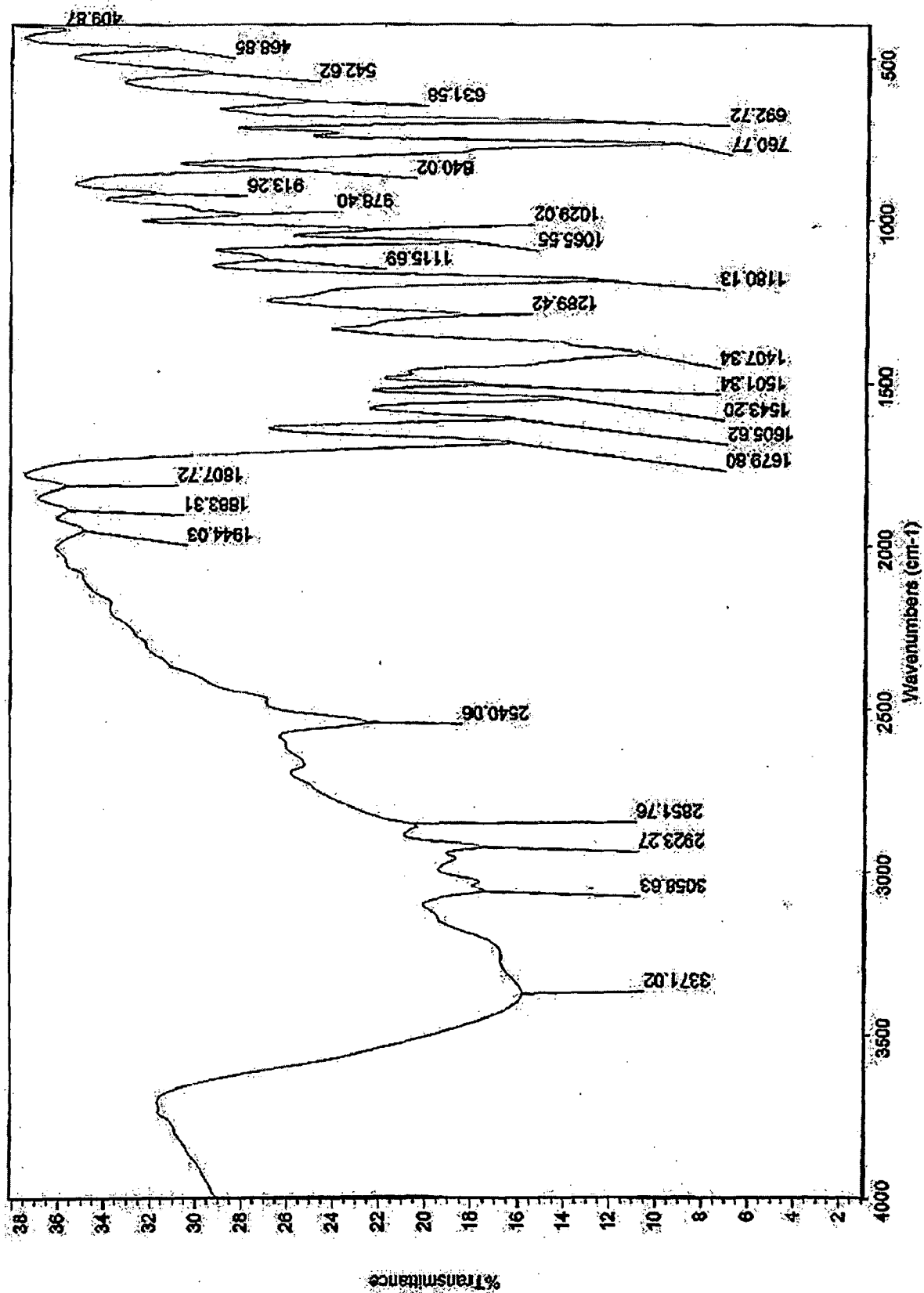


Fig. 5.6 IR spectrum of $[\text{Ni}(\text{Tp}^{\text{Ph,Me}})(\text{pz}^{\text{Ph,Me}})(p\text{-Me-OBz})]$ complex

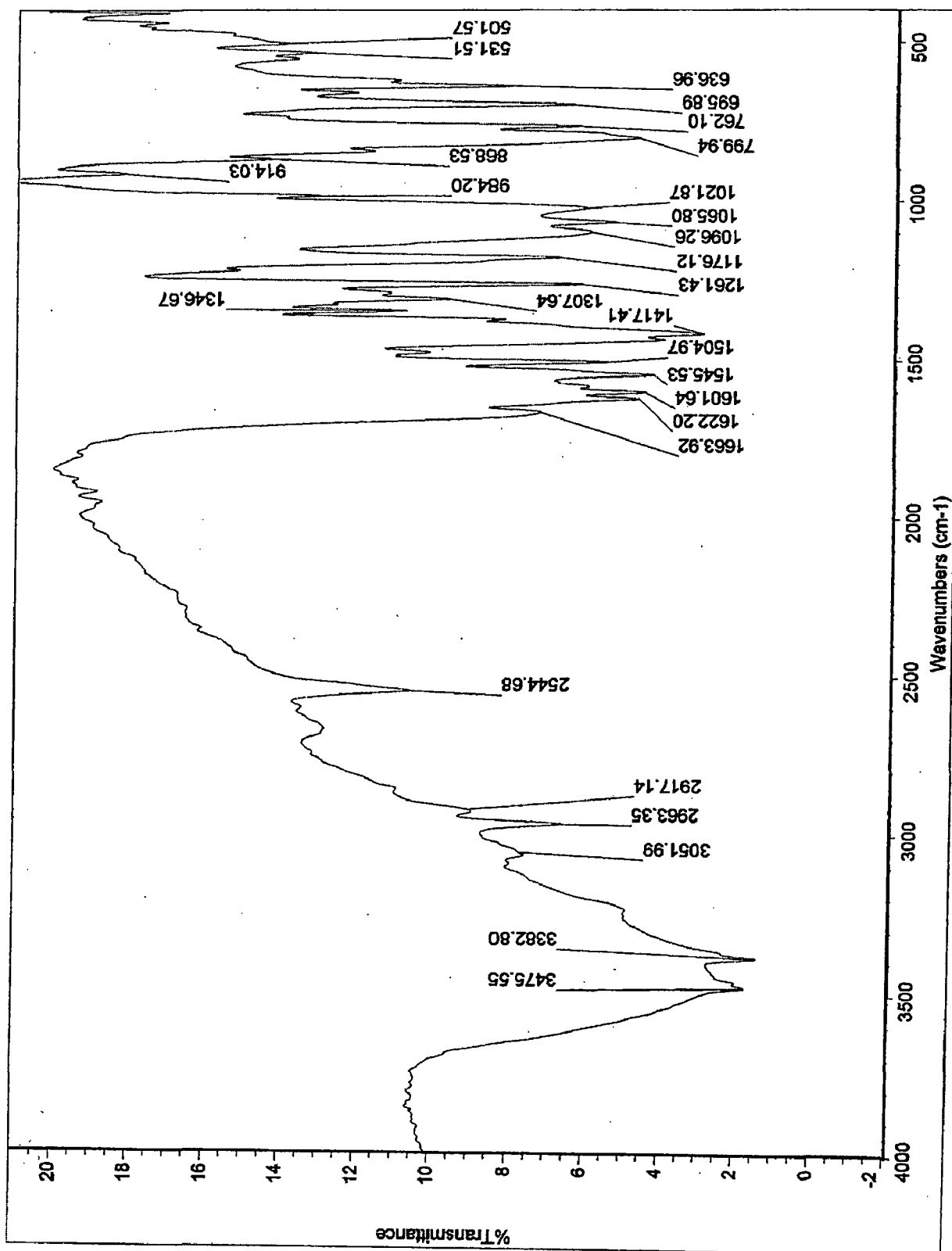


Fig. 5.7 IR spectrum of $[\text{Ni}(\text{T}^{\text{Ph,Mc}})(\text{pz}^{\text{Ph,Mc}})(\text{p-OH-OBz})]$ complex

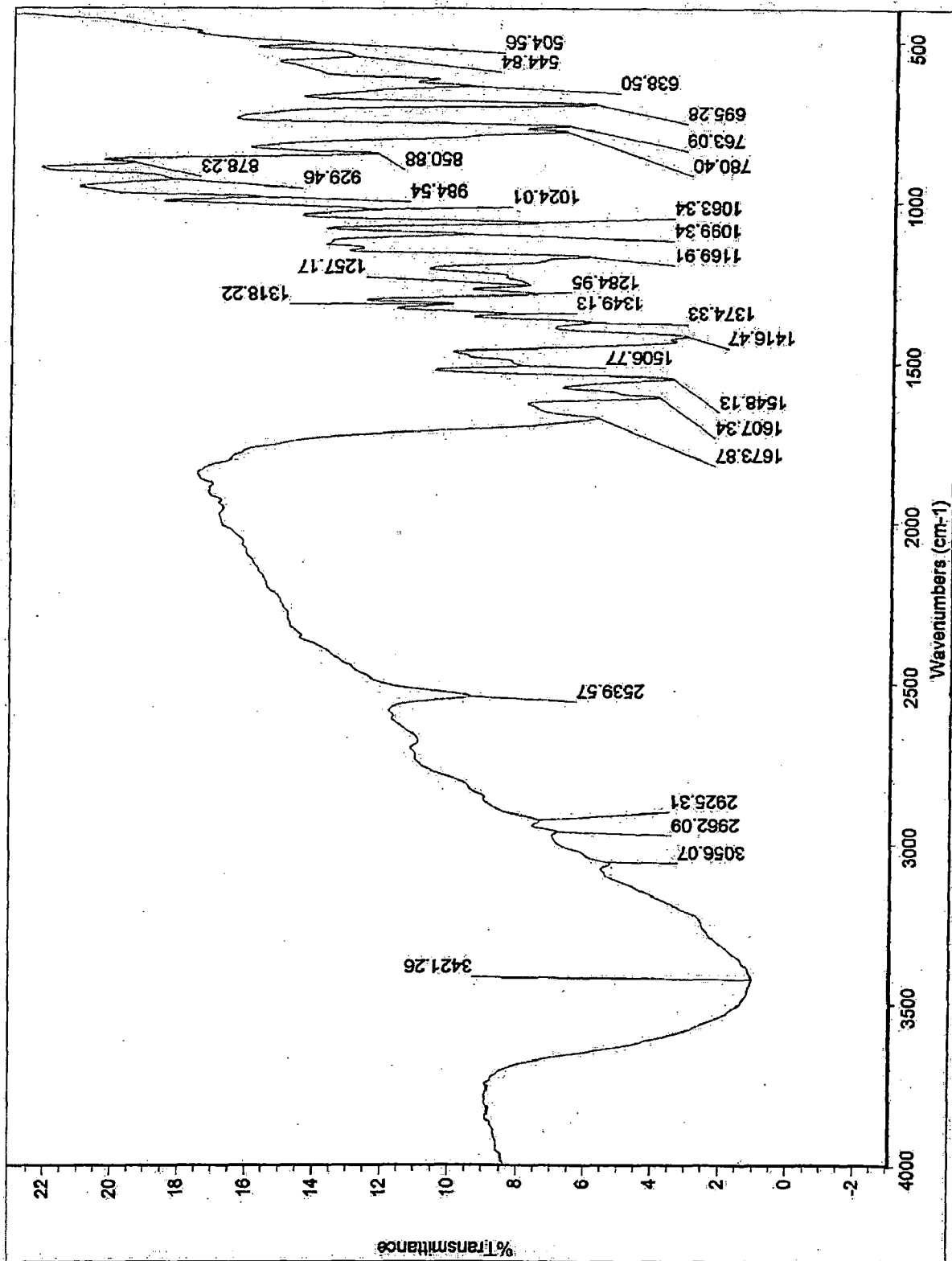


Fig. 5.8 IR spectrum of $[\text{Ni}(\text{Tp}^{\text{Ph},\text{M}^e})(\text{pz}^{\text{Ph},\text{M}^e})(p\text{-NH}_2\text{-OBz})]$ complex

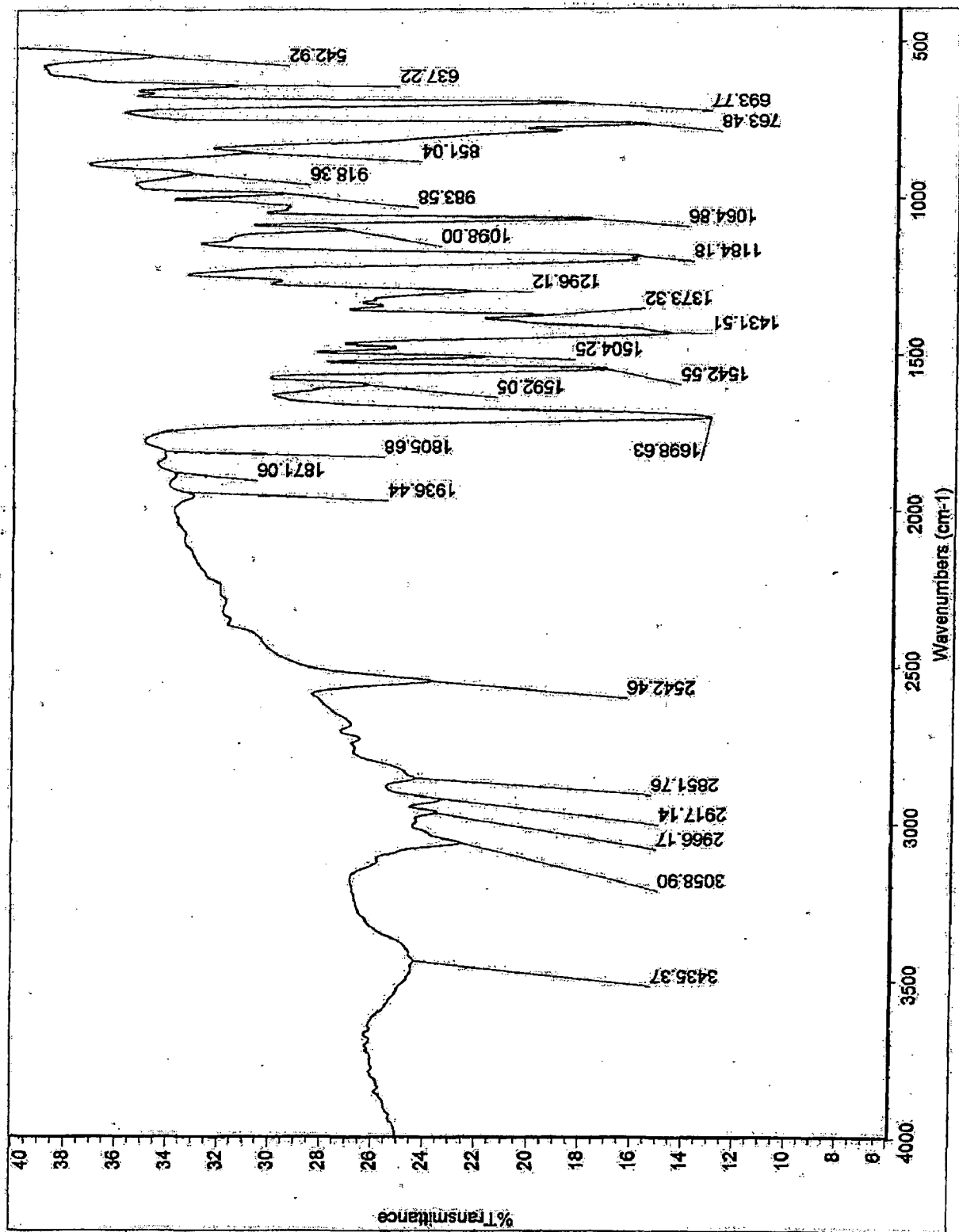


Fig. 5.9 IR spectrum of $[\text{Ni}(\text{T}^{\text{Ph,Me}})(\text{pz}^{\text{Ph,Me}})(p\text{-CHO-OBz})]$ complex

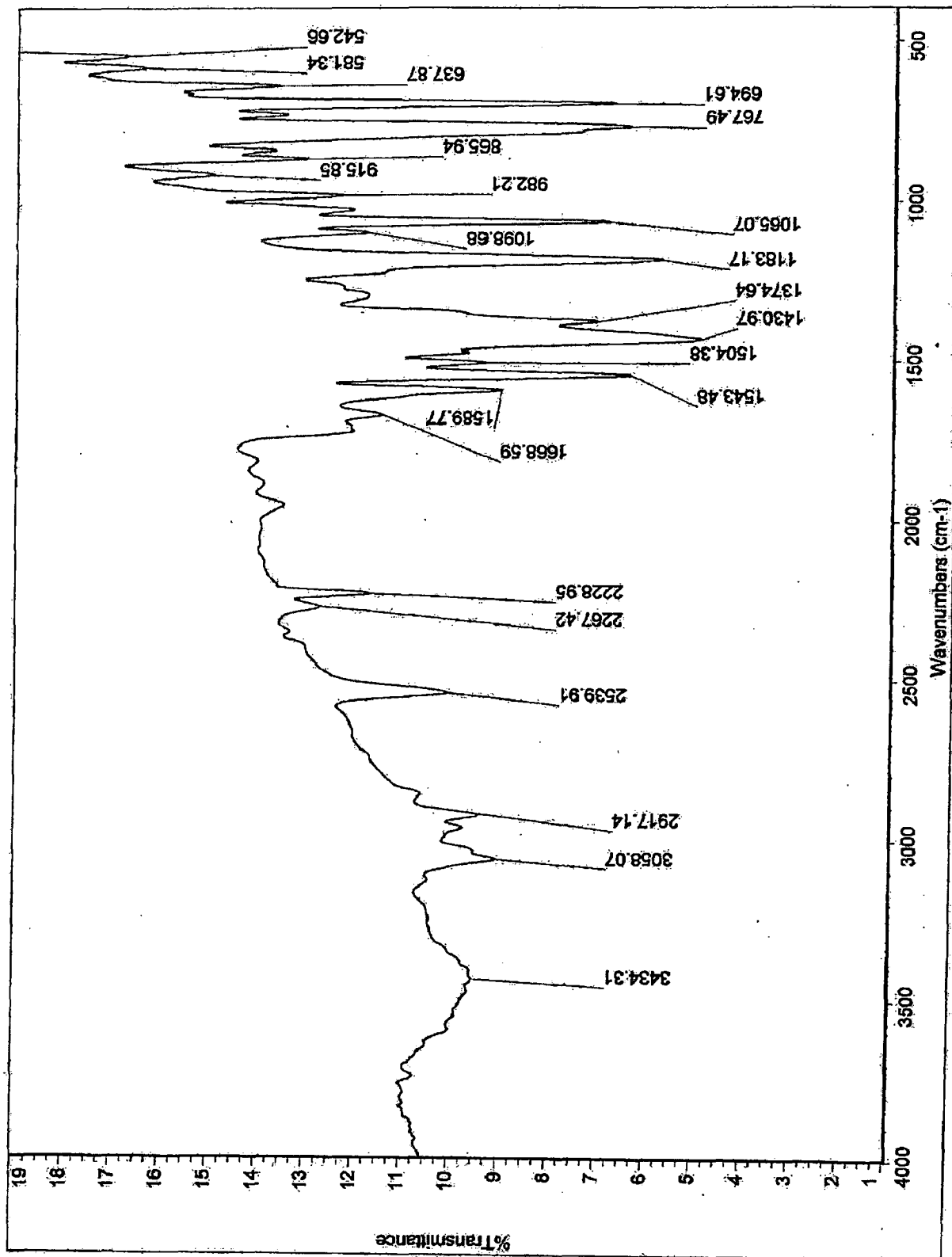


Fig. 5.10 IR spectrum of $[\text{Ni}(\text{Tp}^{\text{Ph,Me}})(\text{pz}^{\text{Ph,Me}})(p\text{-CN-OBz})]$ complex

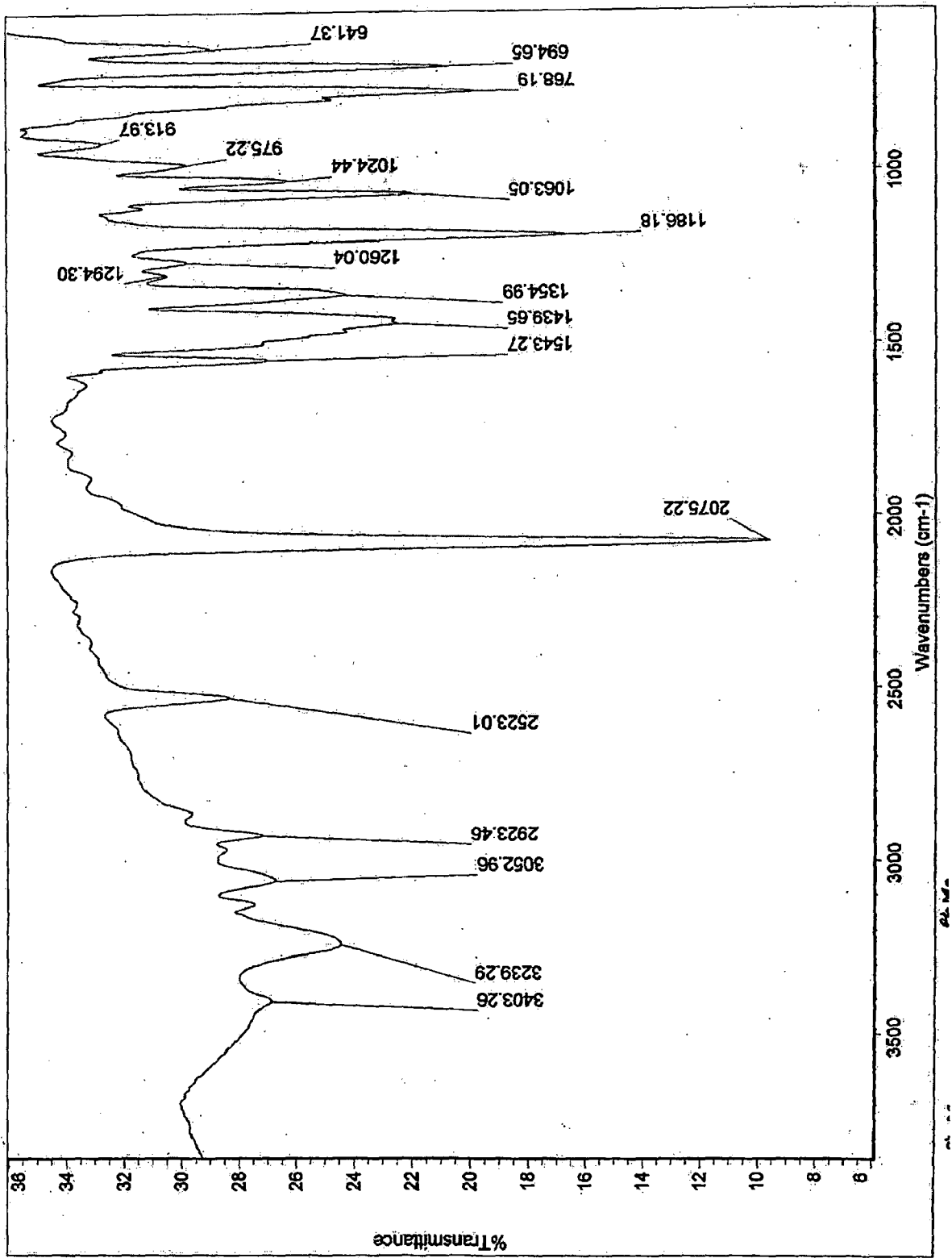


Fig. 5.11 IR spectrum of $[\text{Ni}(\text{Tp}^{\text{Ph,Mg}})(\text{pz}^{\text{Ph,Mg}})(\text{N}_3)]$ complex

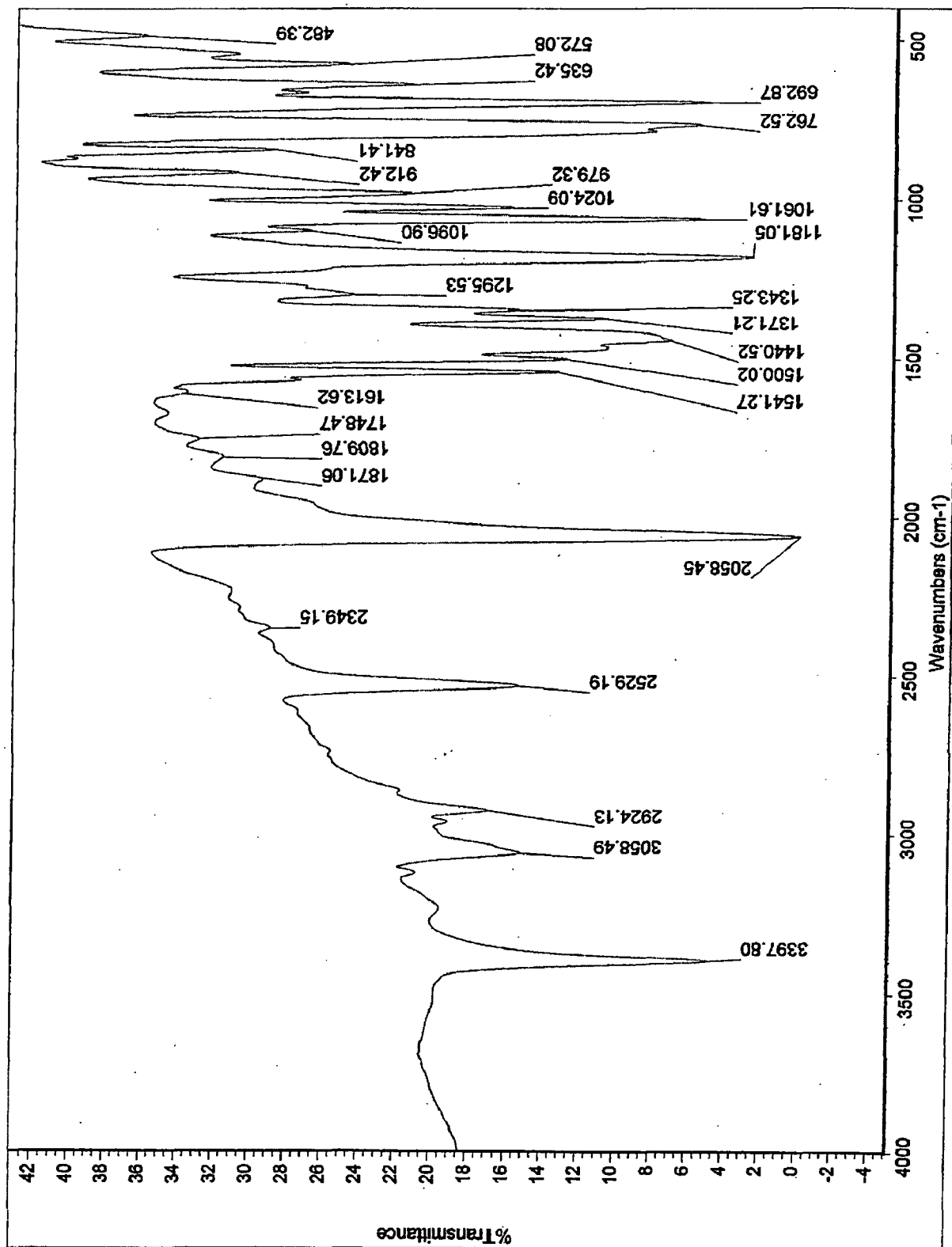


Fig. 5.12 IR spectra of $[\text{Ni}(\text{Tp}^{\text{Ph,Me}})(\text{pz}^{\text{Ph,Me}})(\text{NCS})]$ complex

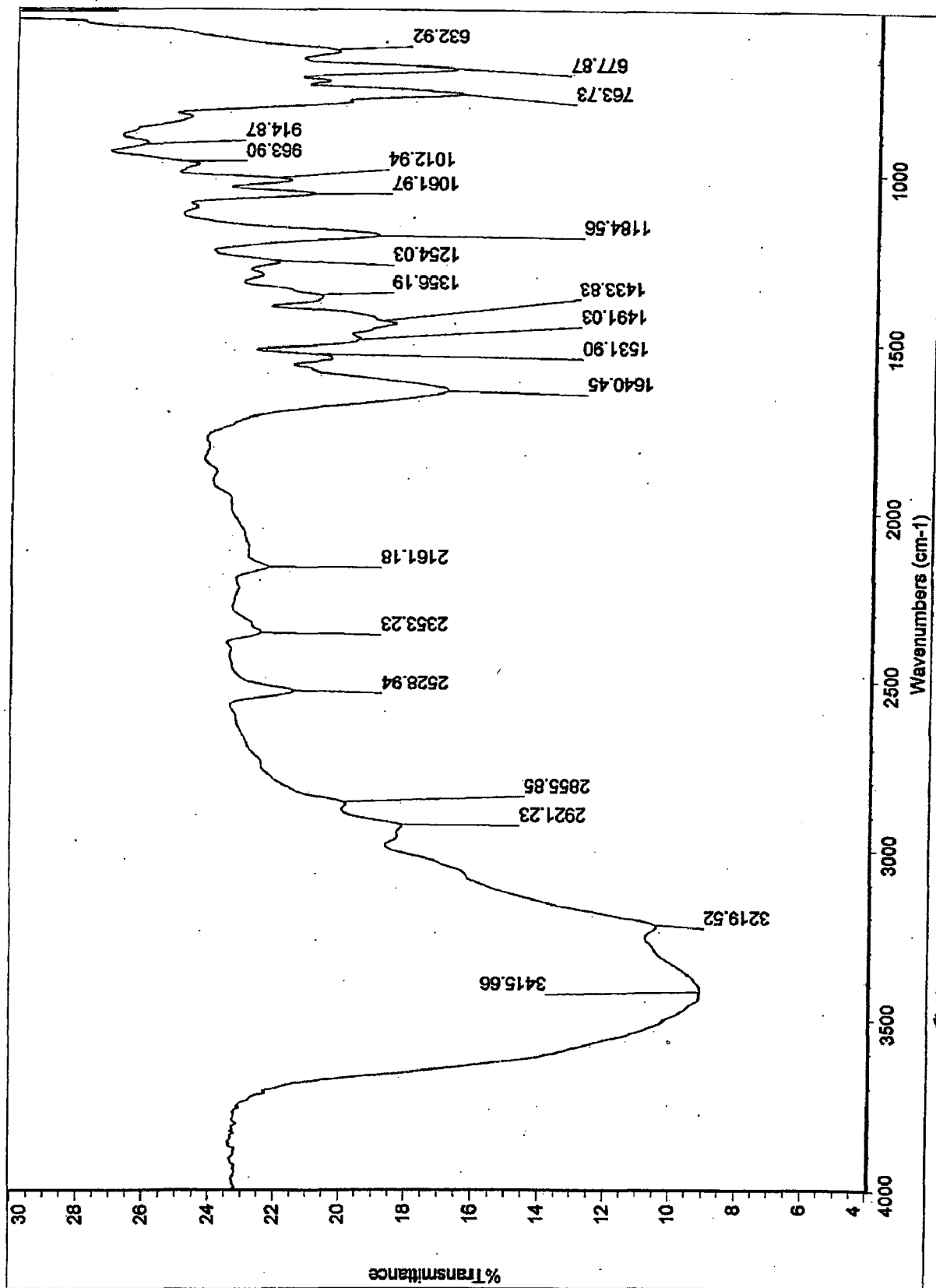


Fig. 5.13 IR spectrum of $[\text{Ni}(\text{Tp}^{\text{Ph,Mg}})(\text{pz}^{\text{Ph,Mg}})(\text{CN})]$ complex

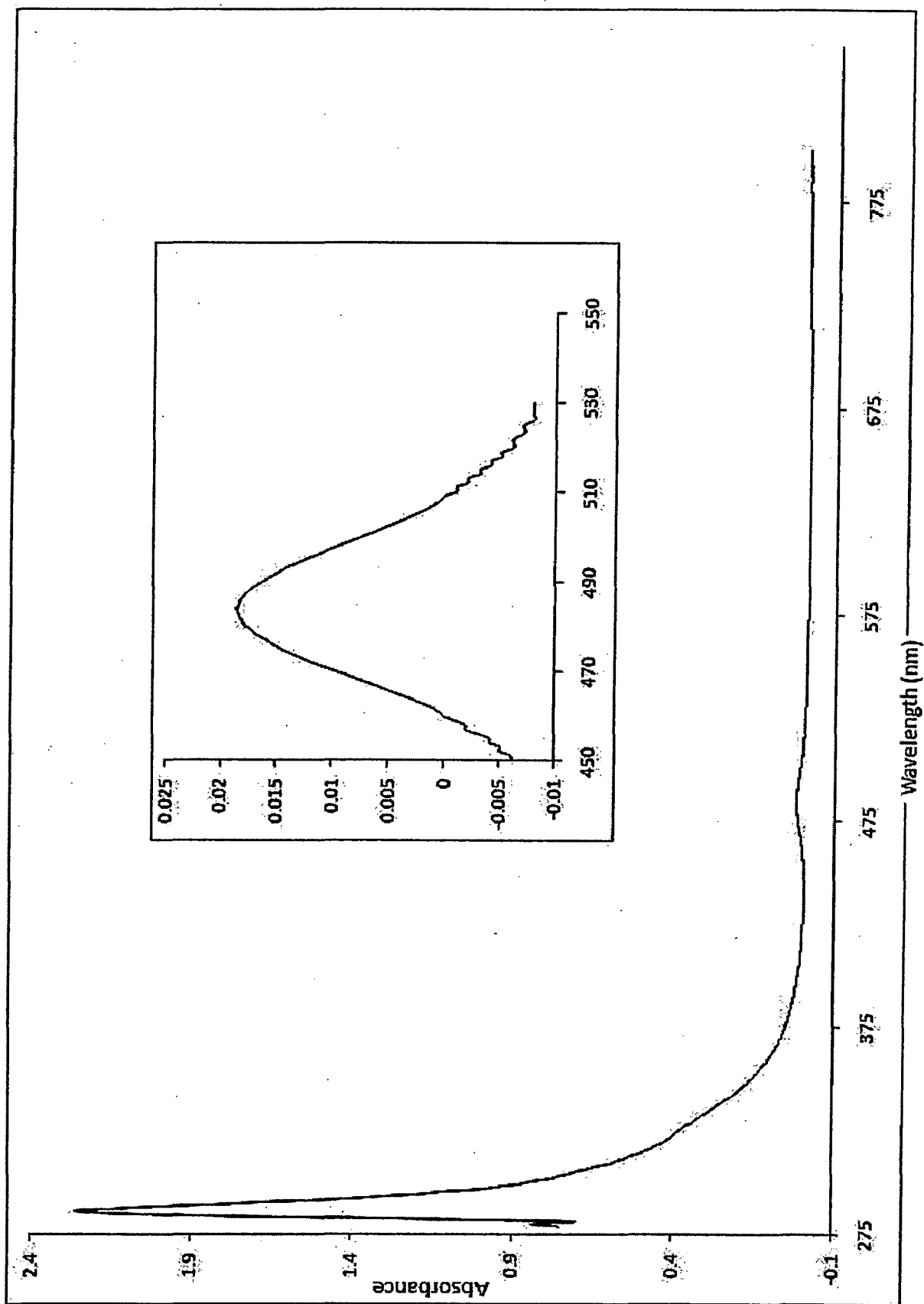


Fig. 5.14 Electronic spectrum of $[\text{Ni}(\text{Tp}^{\text{Ph},\text{M}^{\text{S}}})(\text{pz}^{\text{Ph},\text{M}^{\text{S}}})\text{Cl}]$ complex

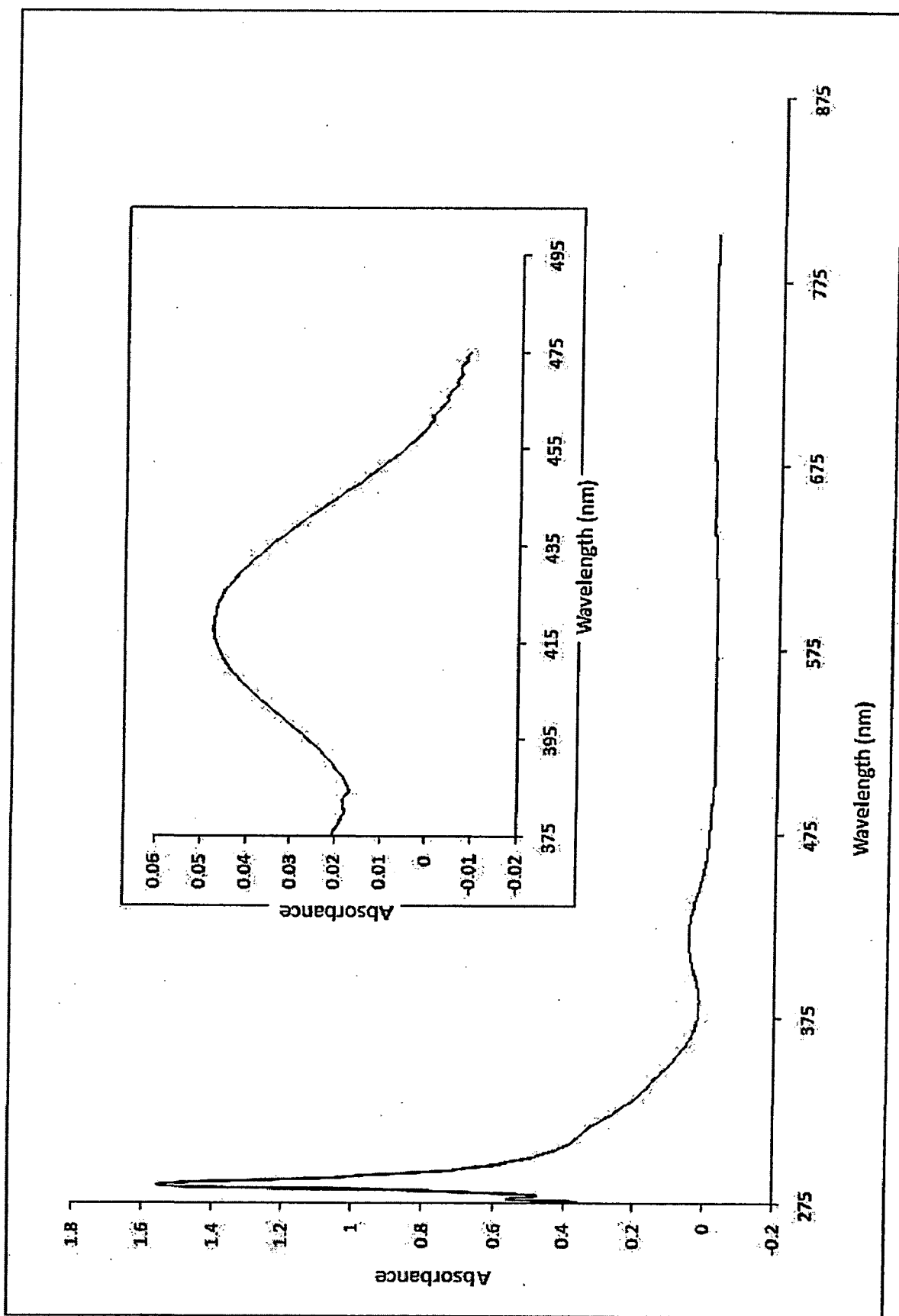


Fig. 5.15 Electronic spectrum of $[\text{Ni}(\text{Tp}^{\text{Ph},\text{M}^e})(\text{pz}^{\text{Ph},\text{M}^e})(\text{OBz})]$ complex

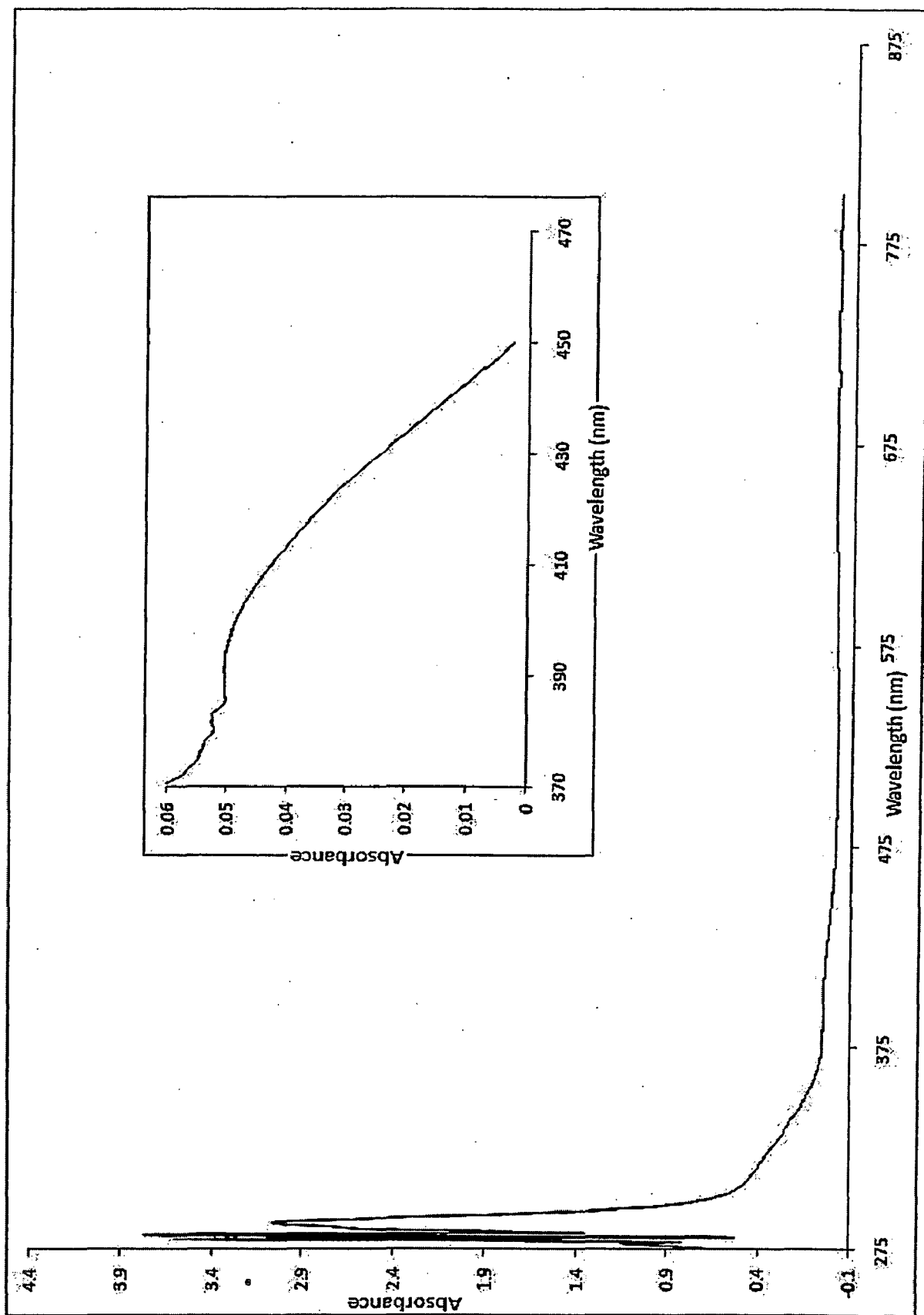


Fig. 5.16 Electronic spectrum of $[\text{Ni}(\text{Tp}^{\text{Ph},\text{M}^c})(\text{pz}^{\text{Ph},\text{M}^c})(p\text{-Cl-OBz})]$ complex

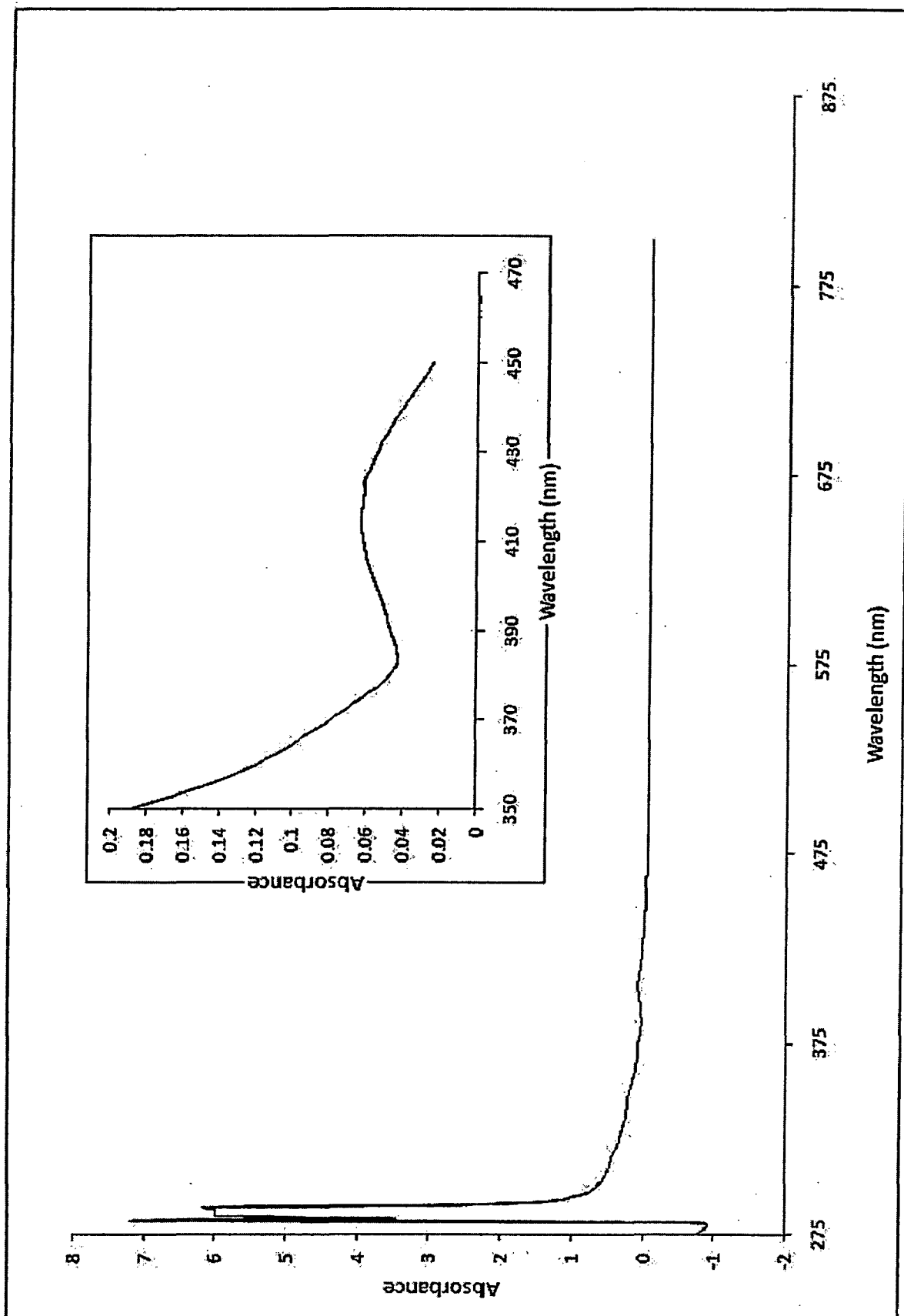


Fig. 5.17 Electronic spectrum of $[\text{Ni}(\text{Tp}^{\text{Ph},\text{M}^6})(\text{pz}^{\text{Ph},\text{M}^6})(p\text{-F-OBz})]$ complex

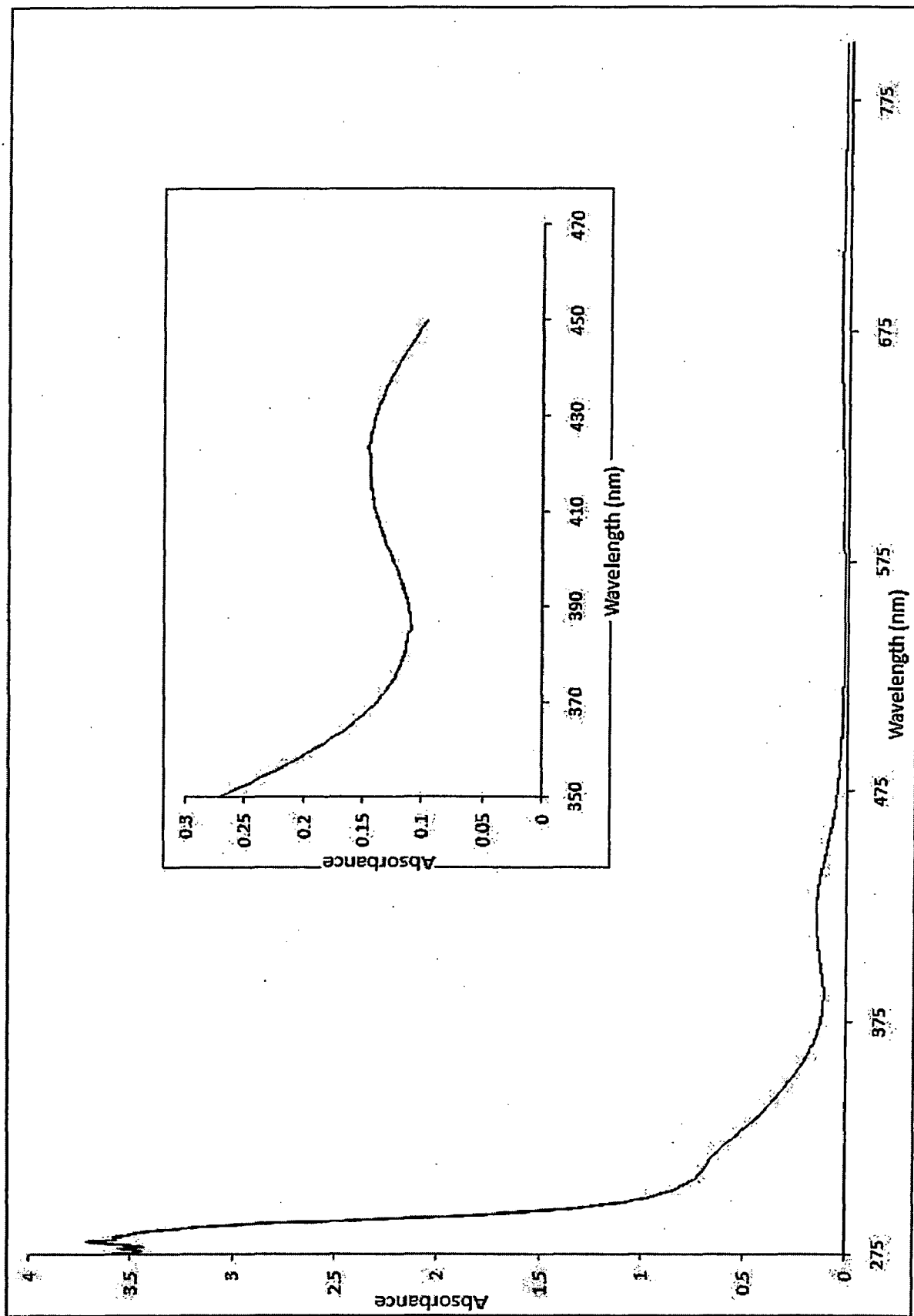


Fig. 5.18 Electronic spectrum of $[\text{Ni}(\text{Tp}^{\text{Ph,Me}})(\text{pz}^{\text{Ph,Me}})(\text{p-NO}_2\text{-OBz})]$ complex

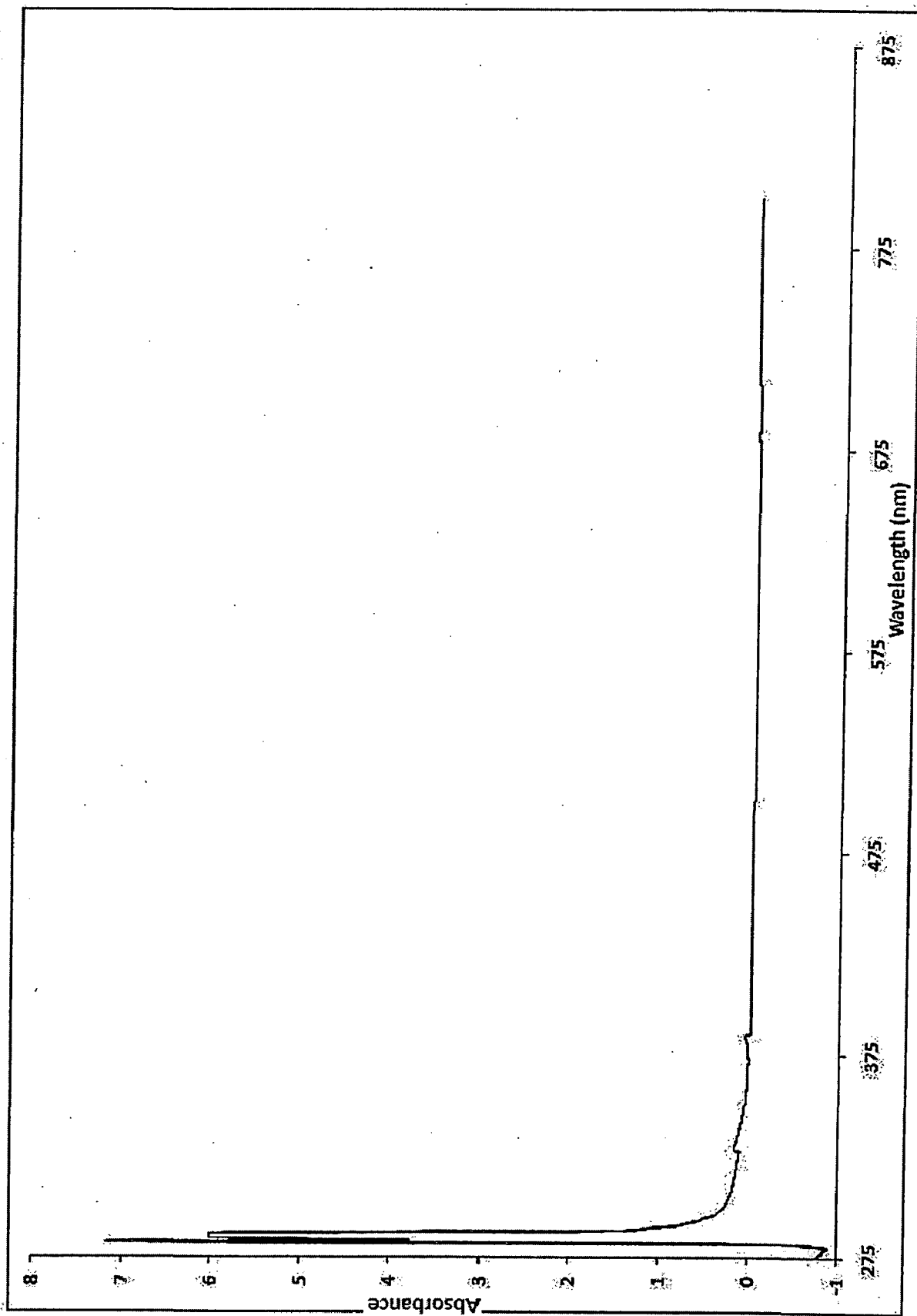


Fig. 5.19 Electronic spectrum of [Ni(Tp^{Ph,Me^c})(pz^{Ph,Me^c})(p-Me-OBz)] complex

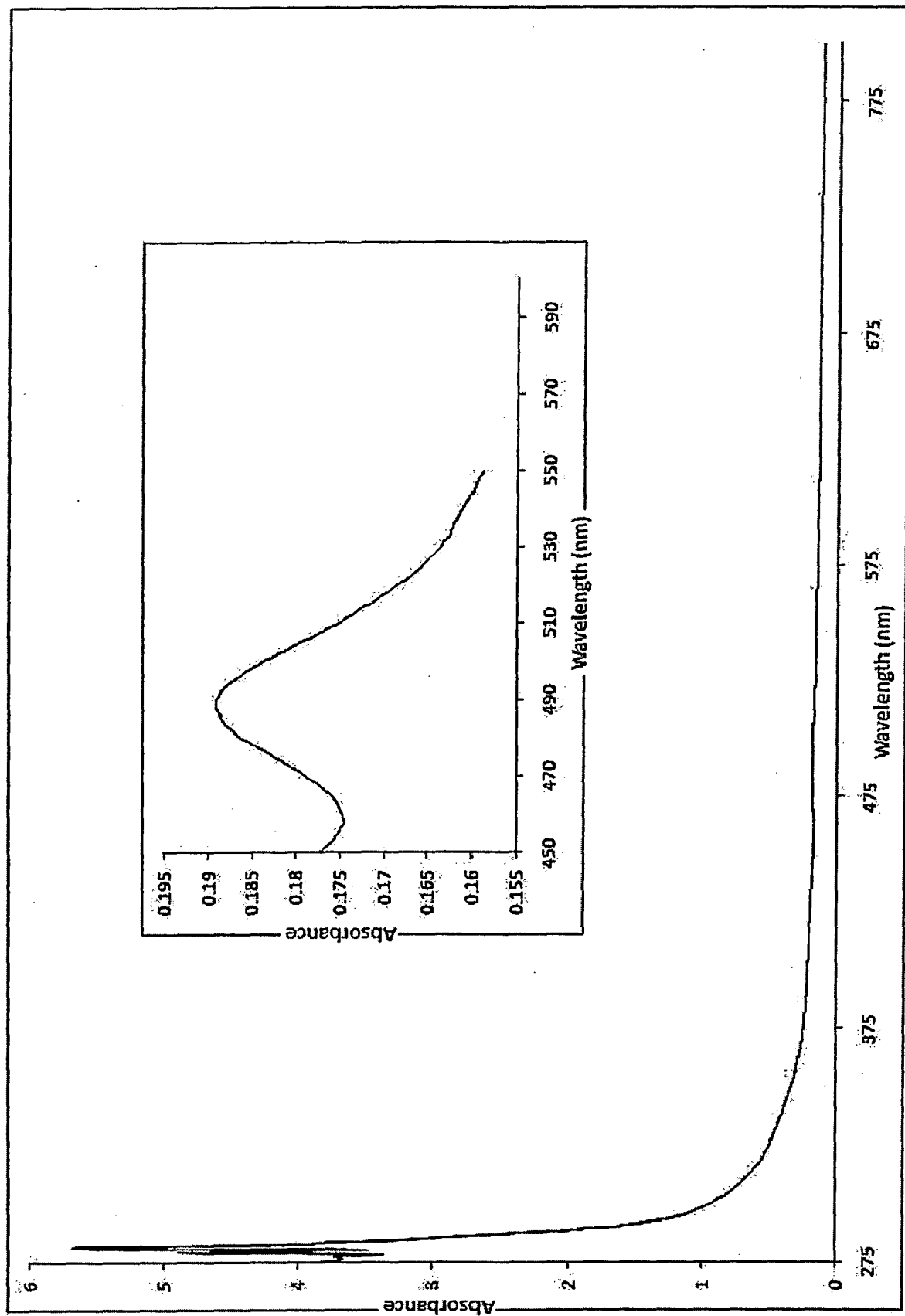


Fig. 5.20 Electronic spectrum of $[\text{Ni}(\text{Tp}^{\text{Ph,Me}})(\text{pz}^{\text{Ph,Me}})(\text{p-HO-OBz})]$ complex

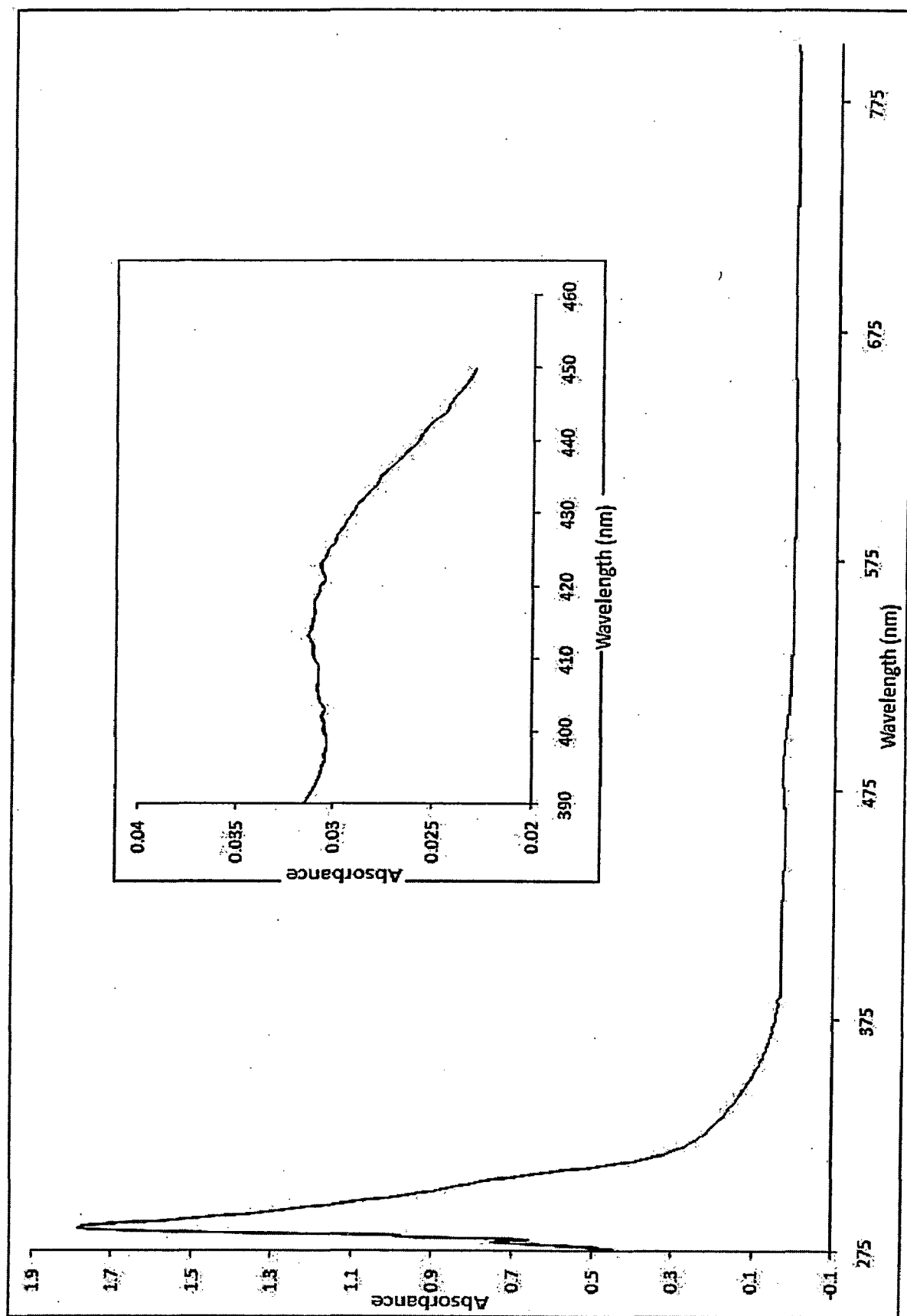


Fig. 5.21 Electronic spectrum of $[\text{Ni}(\text{Tp}^{\text{Ph,Me}})(\text{pz}^{\text{Ph,Me}})(\text{p-CHO-OBz})]$ complex

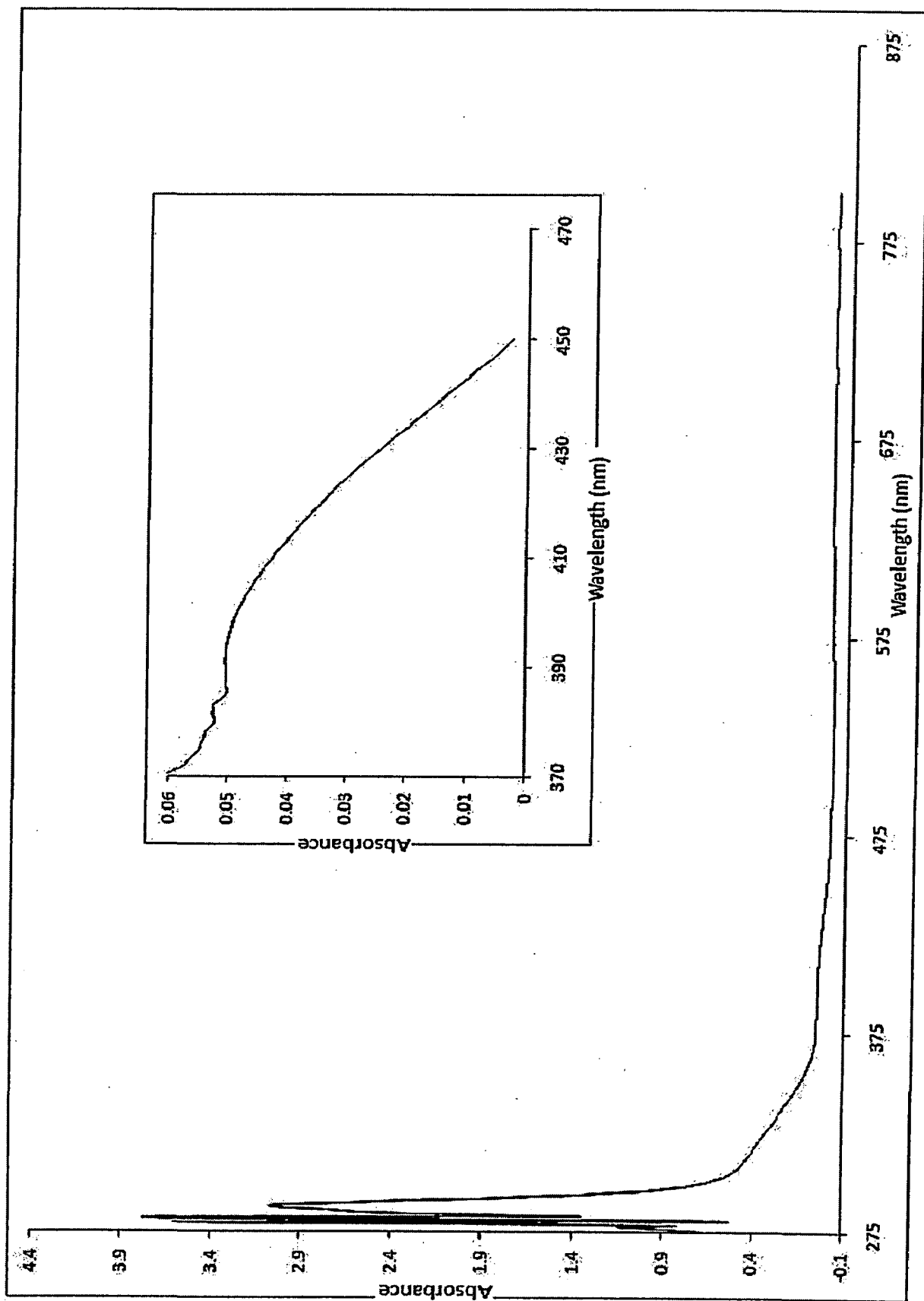


Fig. 5.22 Electronic spectrum of $[\text{Ni}(\text{Tp}^{\text{Ph},\text{M}^6})(\text{pz}^{\text{Ph},\text{M}^6})(\text{p-CN-OBz})]$ complex

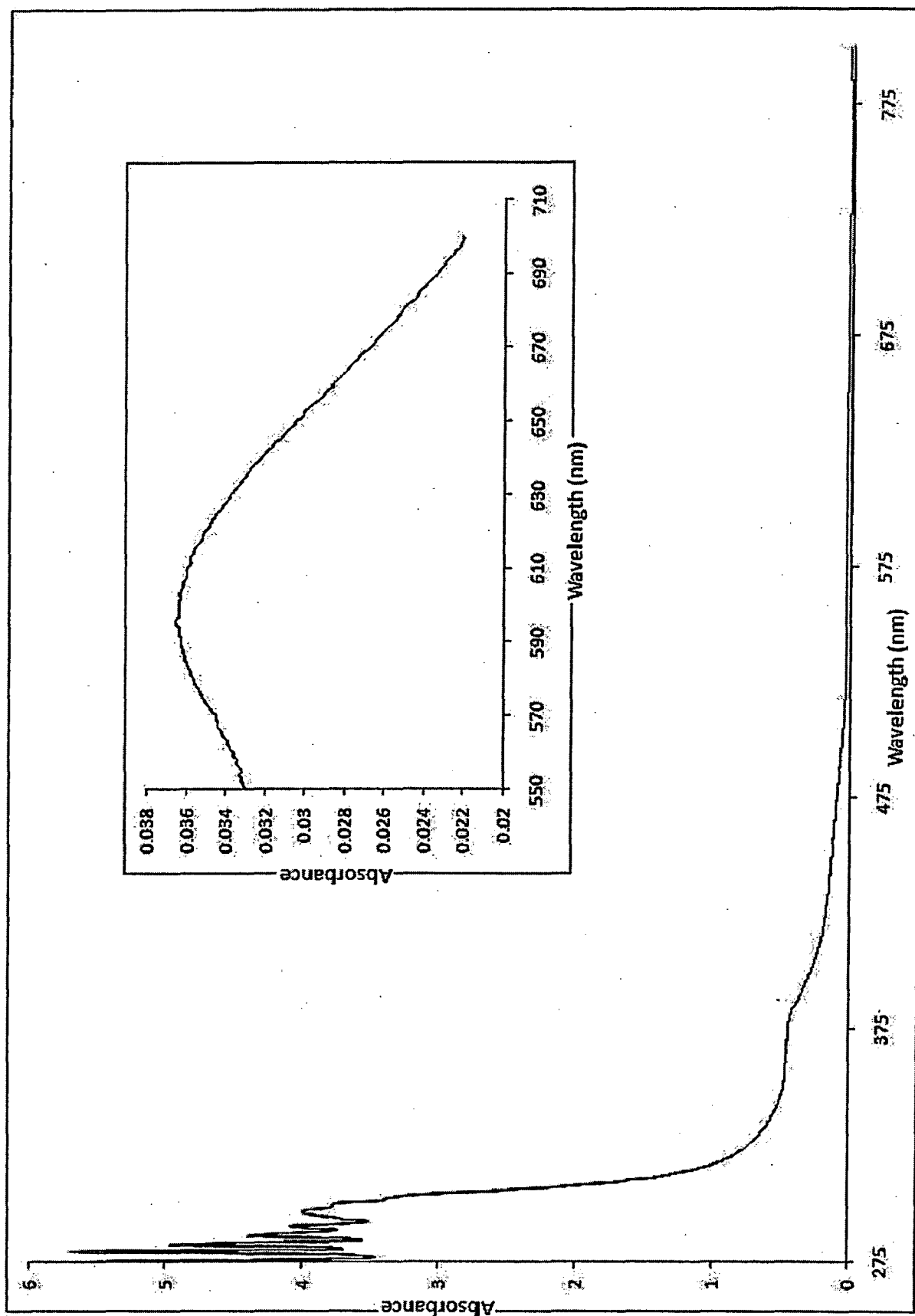


Fig. 5.23 Electronic spectrum of $[\text{Ni}(\text{Tp}^{\text{Ph}_3\text{Me}_6})_2]$ complex

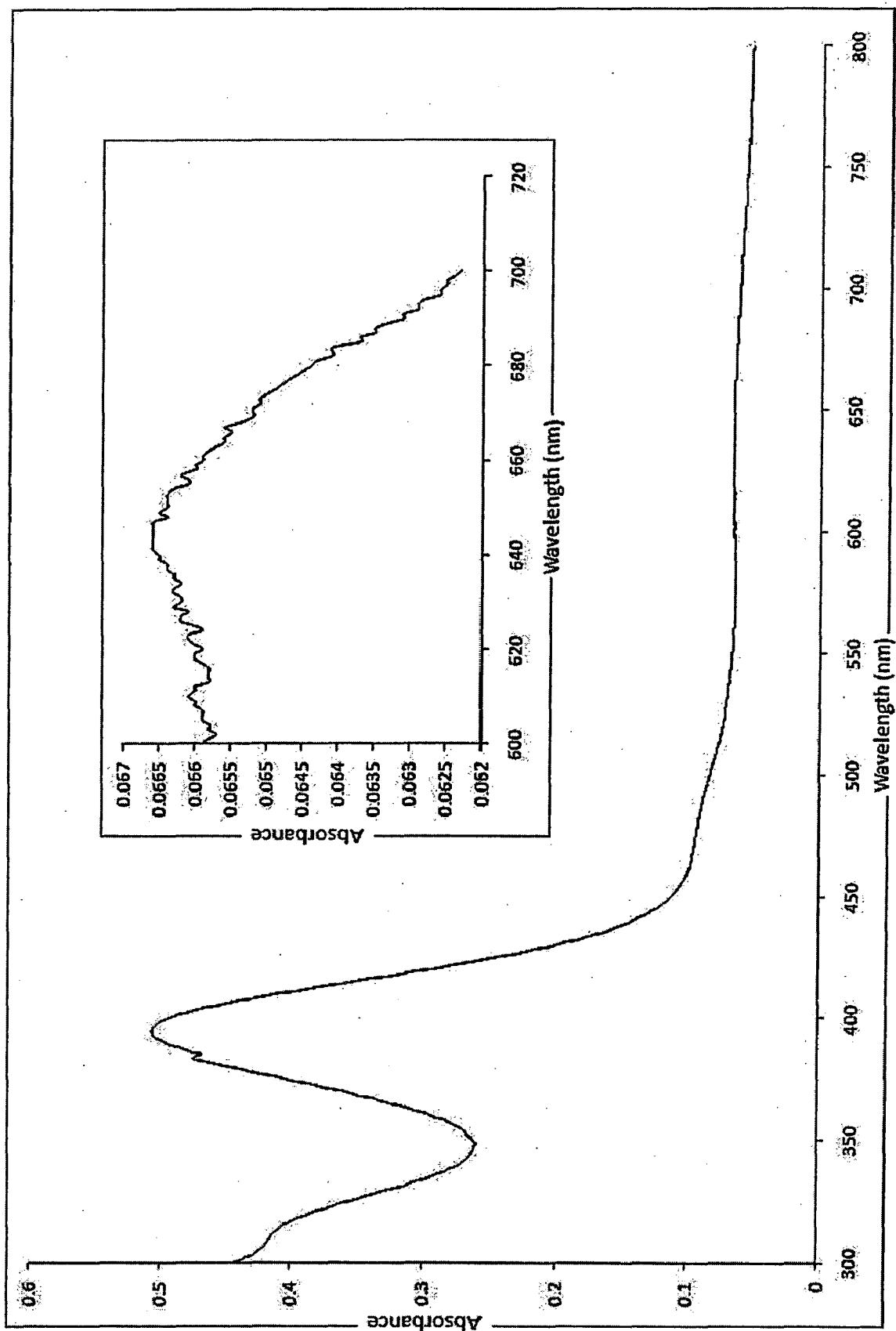


Fig. 5.24 Electronic spectrum of [Ni(Tp^{Ph,Me})(pZ^{Ph,Me})(N₃)] complex

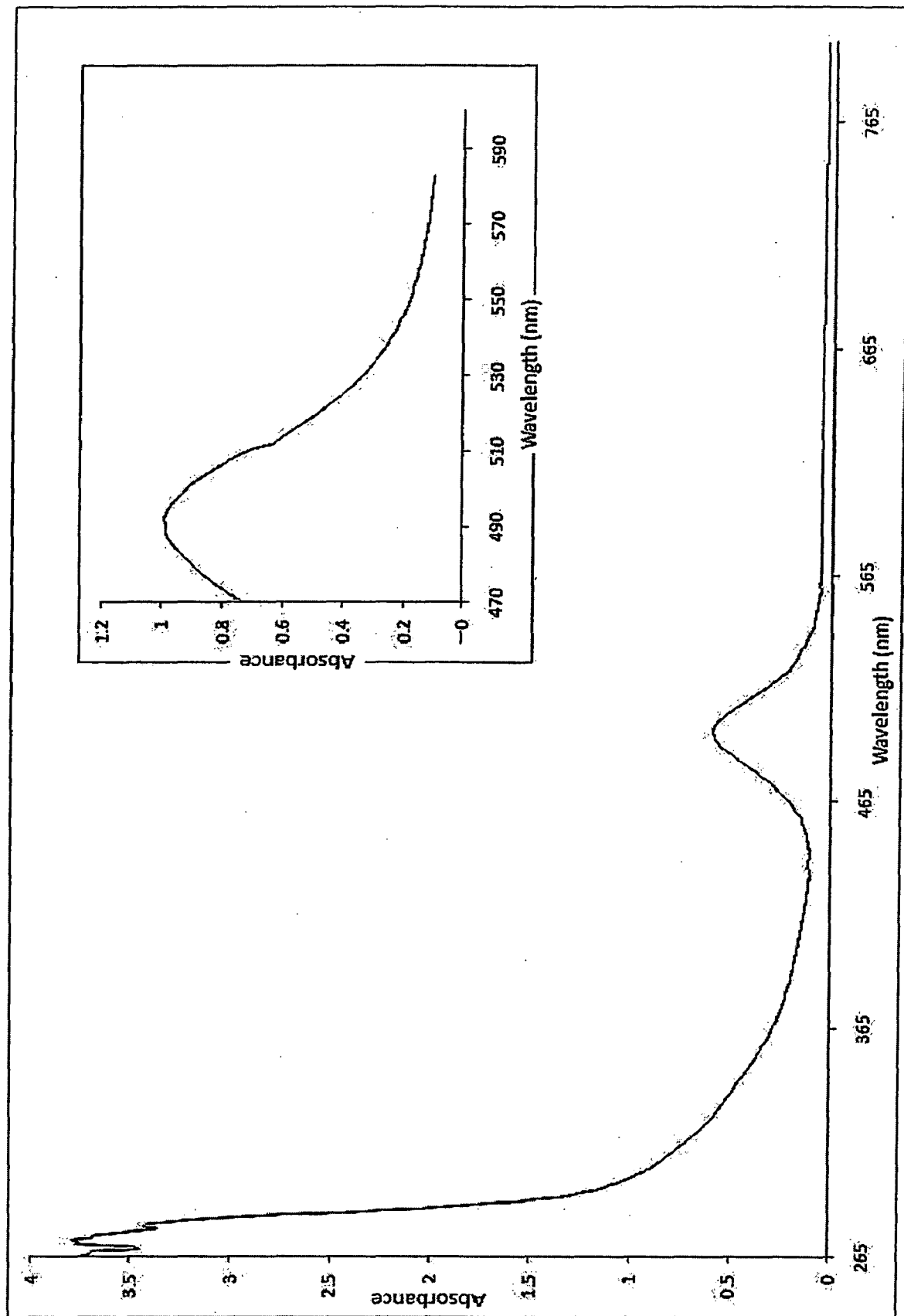


Fig. 5.25 Electronic spectrum of $[\text{Ni}(\text{Tp}^{\text{Ph,Me}^6})(\text{pz}^{\text{Ph,Me}^6})(\text{NCS})]$ complex

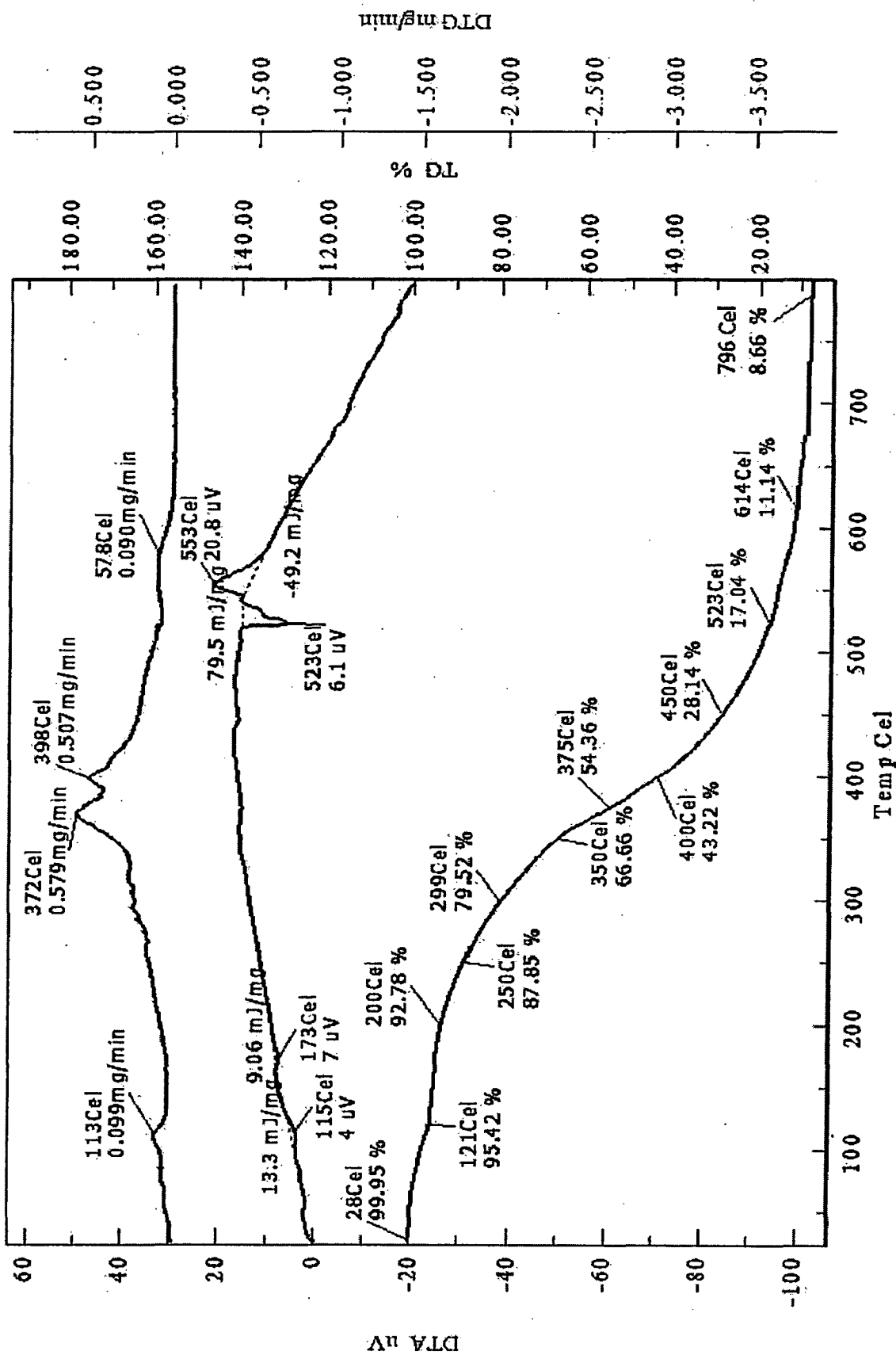


Fig. 5.26 Thermal decomposition data of $[\text{Ni}(\text{Tp}^{\text{Ph,Me}})(\text{pz}^{\text{Ph,Me}})\text{Cl}]$ complex

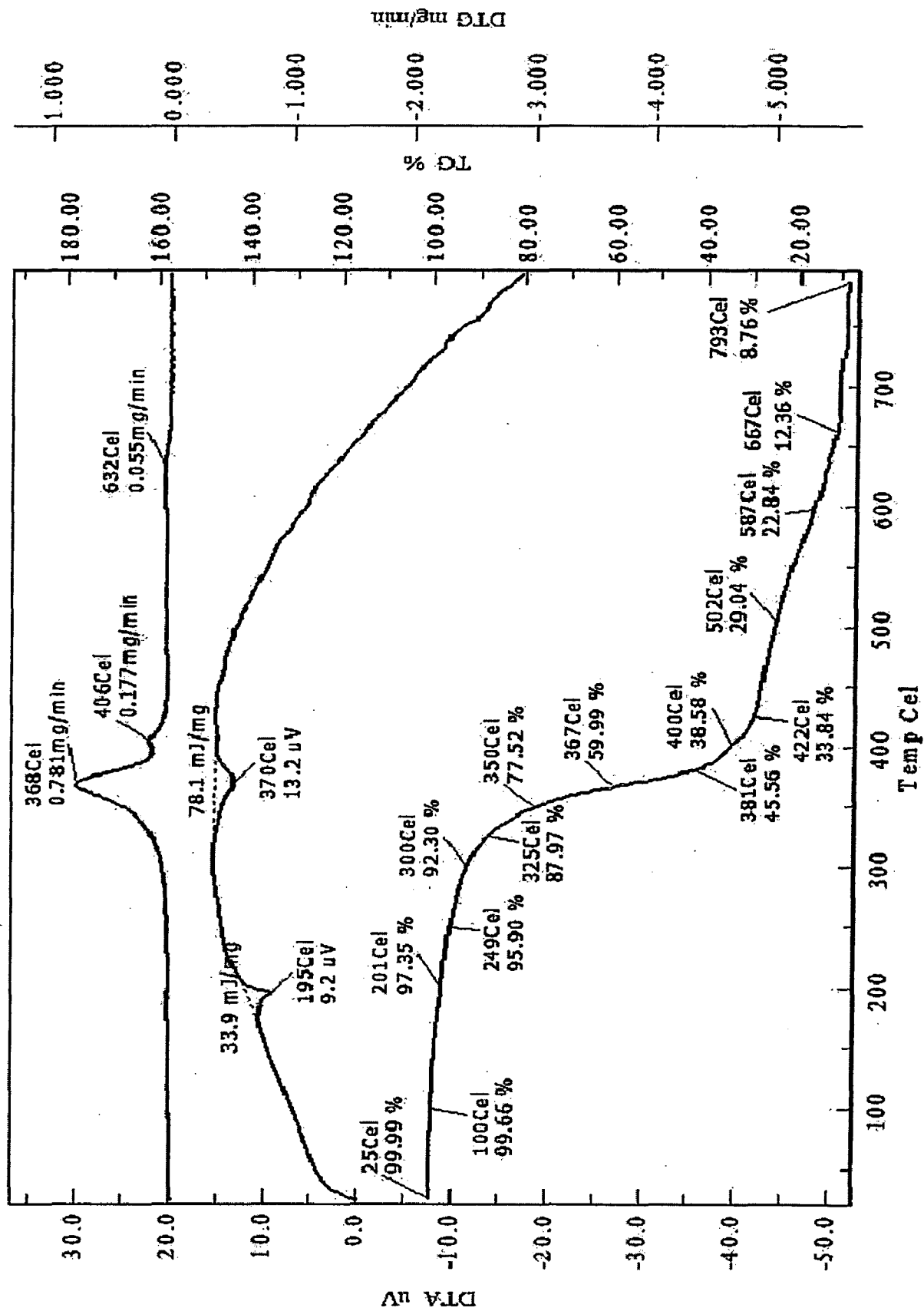


Fig. 5.27 Thermal decomposition data of $[\text{Ni}(\text{Tp}^{\text{Ph,Me}})(\text{pz}^{\text{Ph,Me}})(\text{OBz})]$ complex

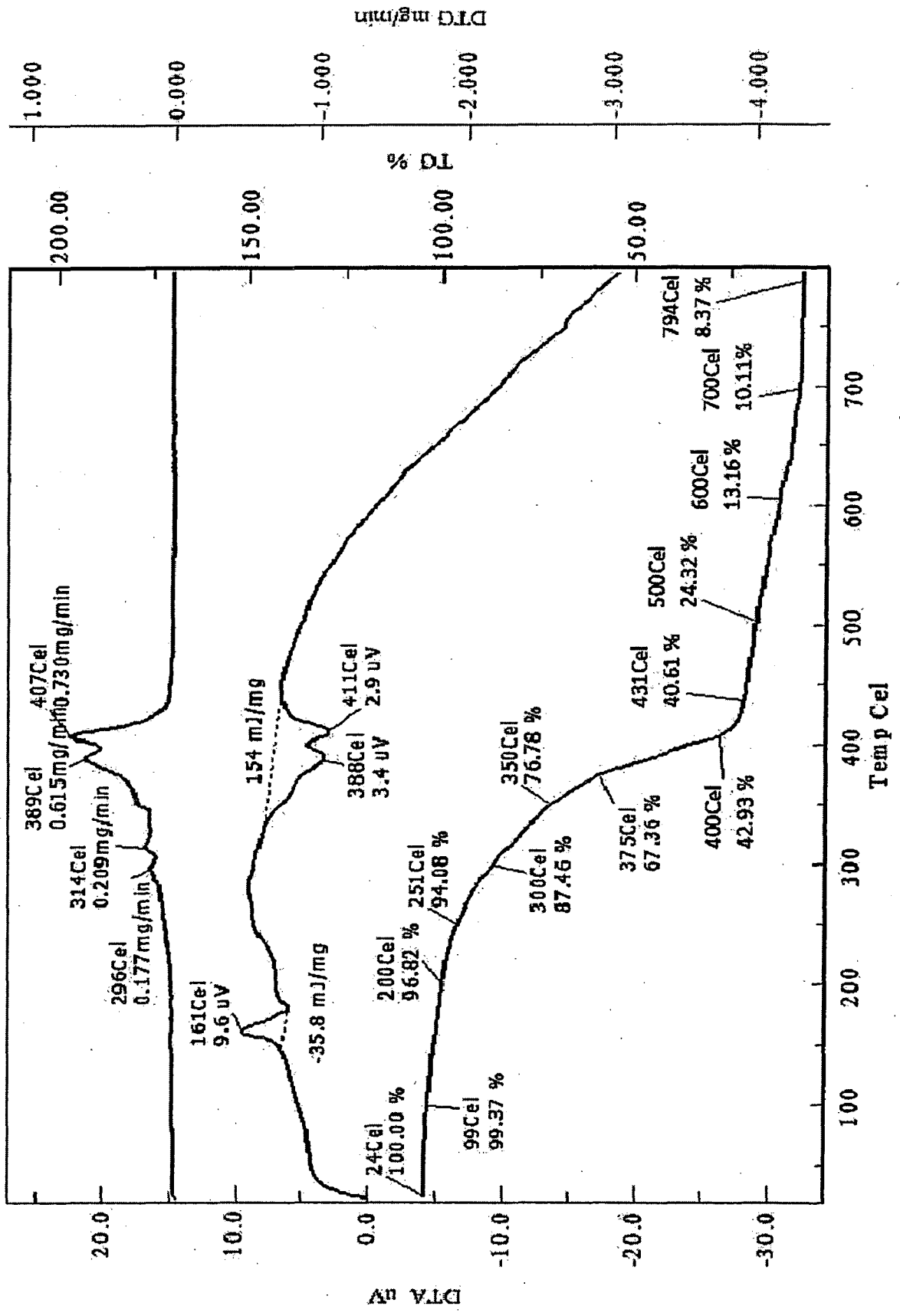


Fig. 5.28 Thermal decomposition data of $[\text{Ni}(\text{Tp}^{\text{Ph,Me}})(\text{pz}^{\text{Ph,Me}})(p\text{-Cl-OBz})]$ complex

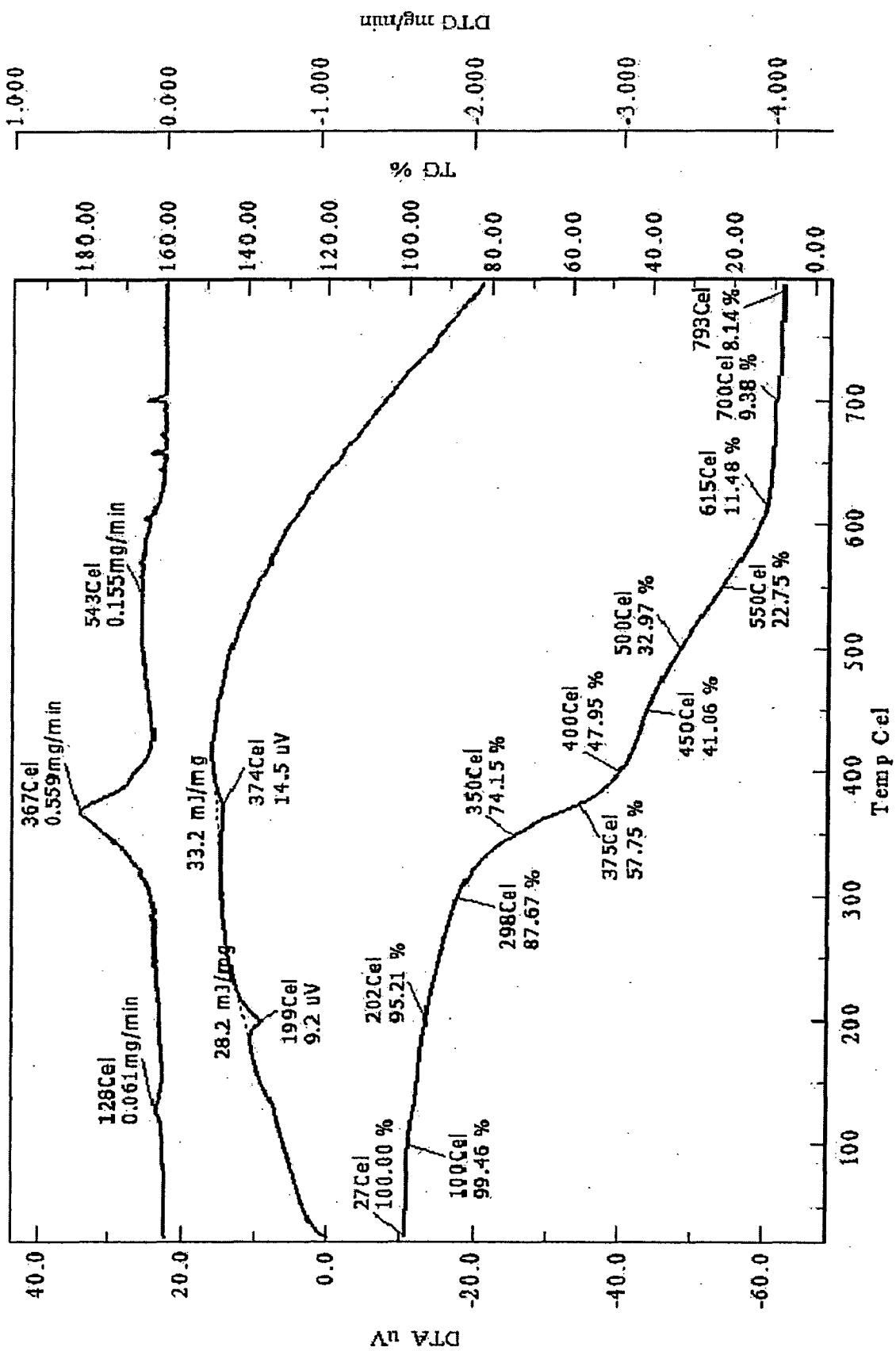


Fig. 5.29 Thermal decomposition data of $[\text{Ni}(\text{Tp}^{\text{Ph,Me}})(\text{pz}^{\text{Ph,Me}})(p\text{-F-OBz})]$ complex

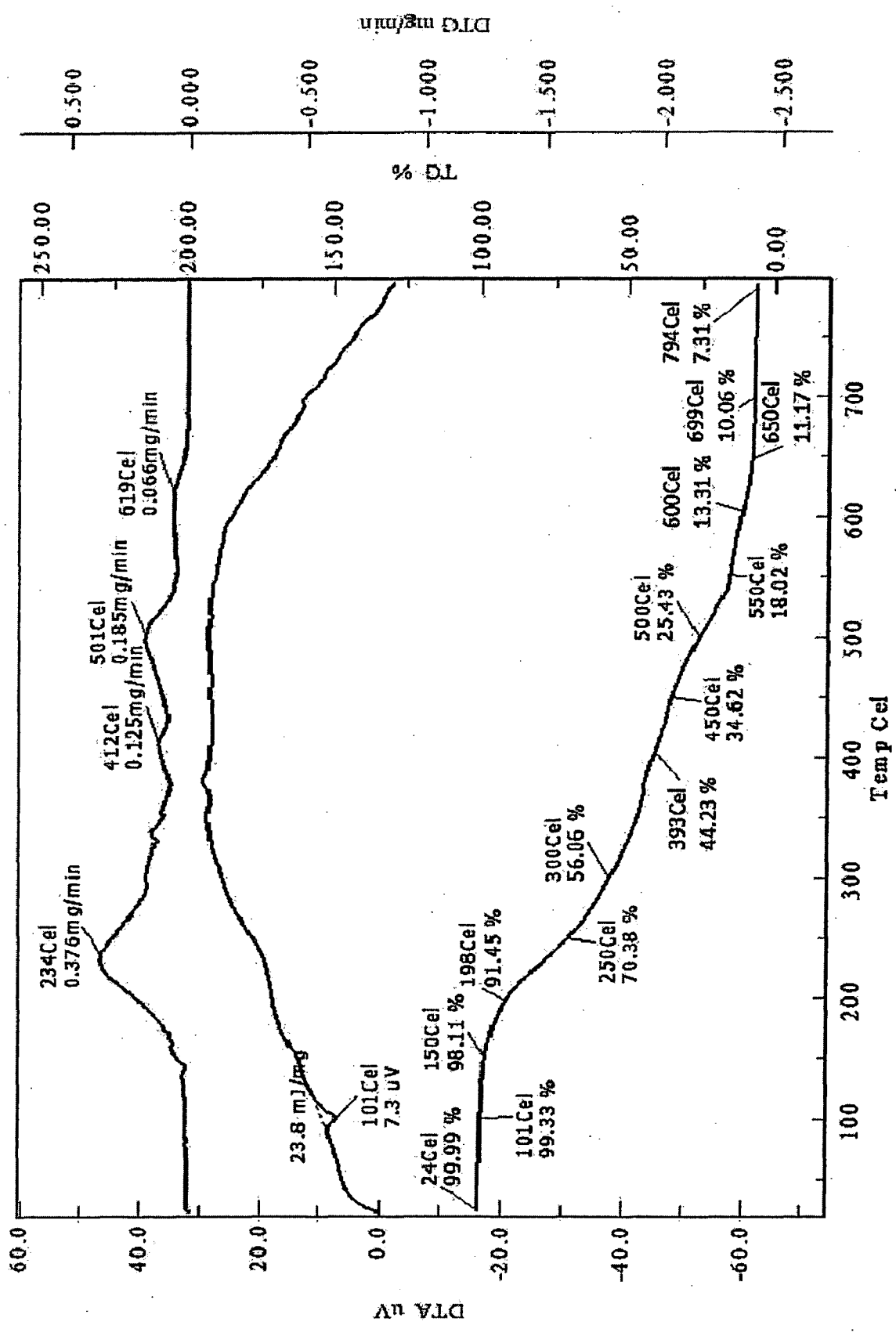


Fig. 5.30 Thermal decomposition data of $[Ni(Tp^{Ph,Me})(pz^{Ph,Me})(p-NO_2-OBz)]$ complex

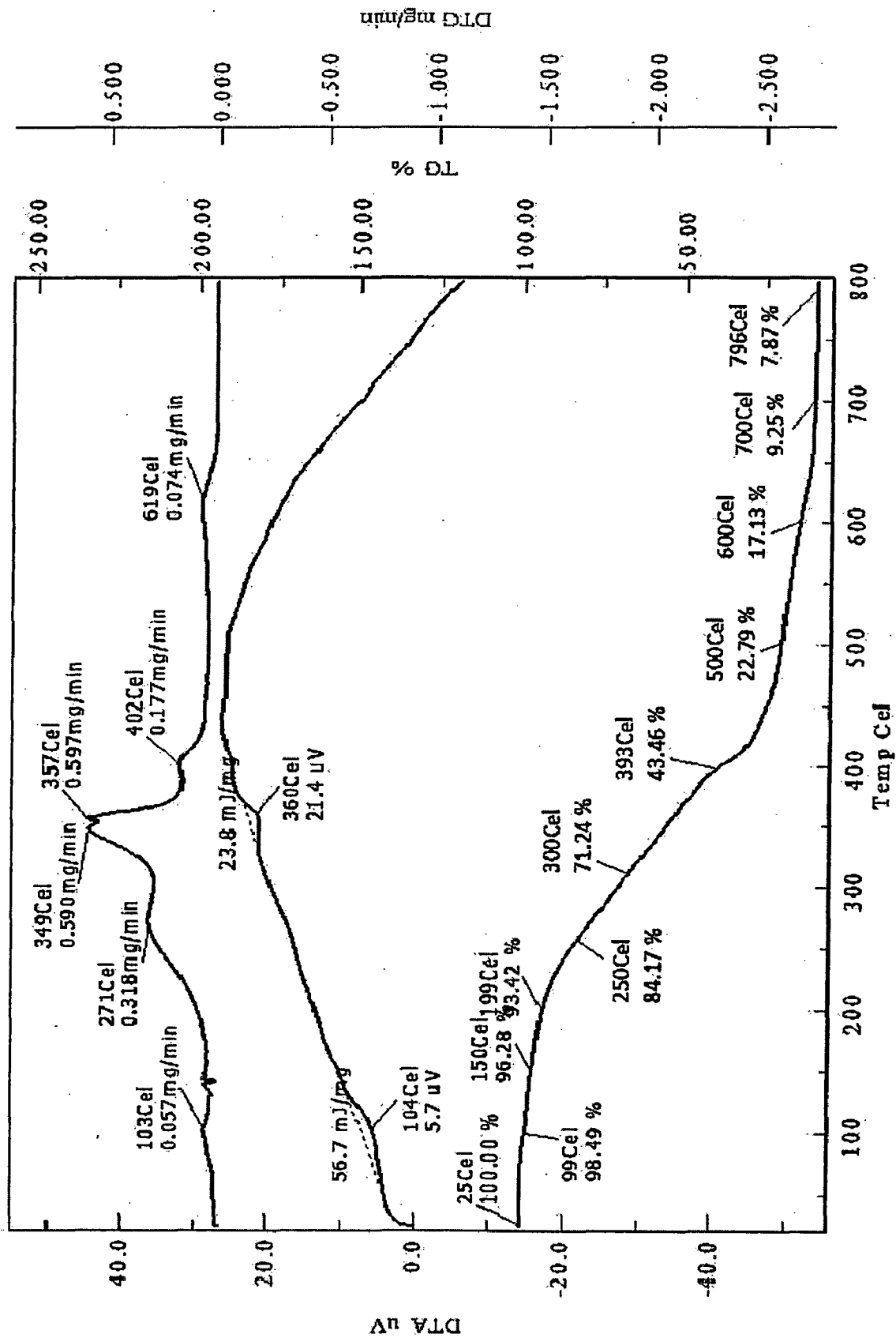


Fig. 5.31 Thermal decomposition data of $[\text{Ni}(\text{Tp}^{\text{Ph,Me}})(\text{pz}^{\text{Ph,Me}})(p\text{-Me-OBz})]$ complex

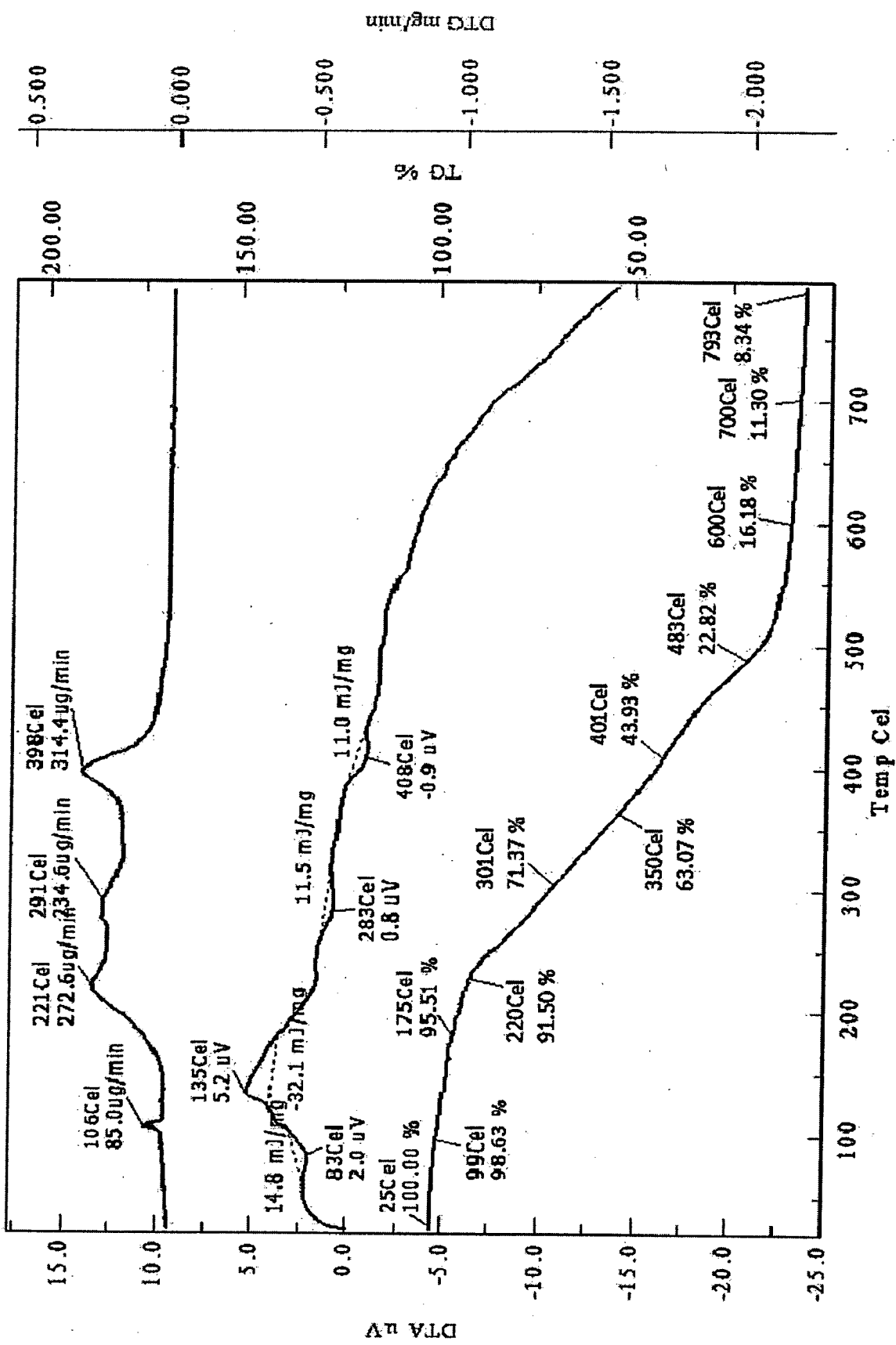


Fig. 5.32 Thermal decomposition data of $[\text{Ni}(\text{Tp}^{\text{Ph,Me}})(\text{pz}^{\text{Ph,Me}})(p\text{-OH-OBz})]$ complex

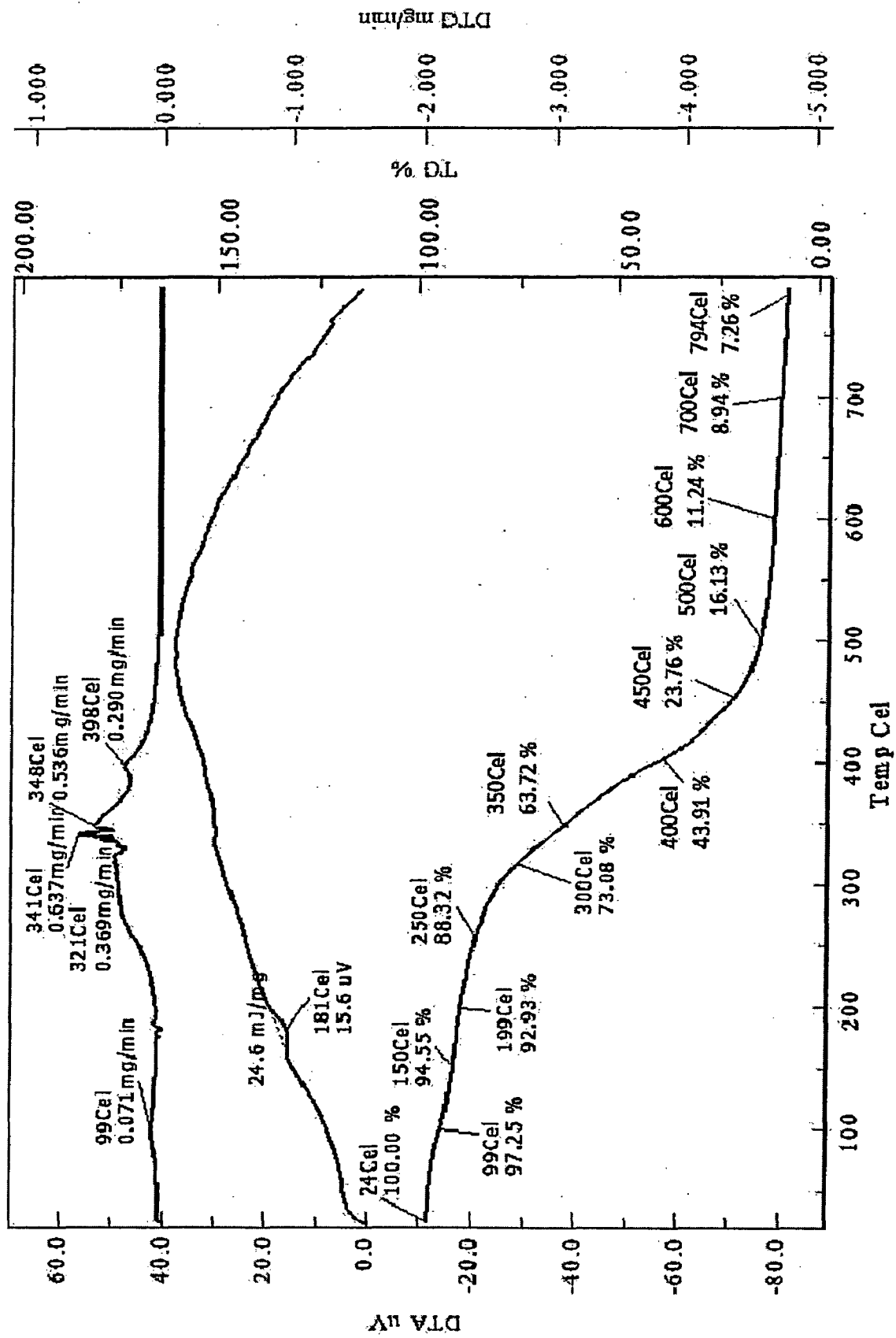


Fig. 5.33 Thermal decomposition data of $[\text{Ni}(\text{Tp}^{\text{Ph,Me}})(\text{pz}^{\text{Ph,Me}})(p\text{-CHO-OBz})]$ complex

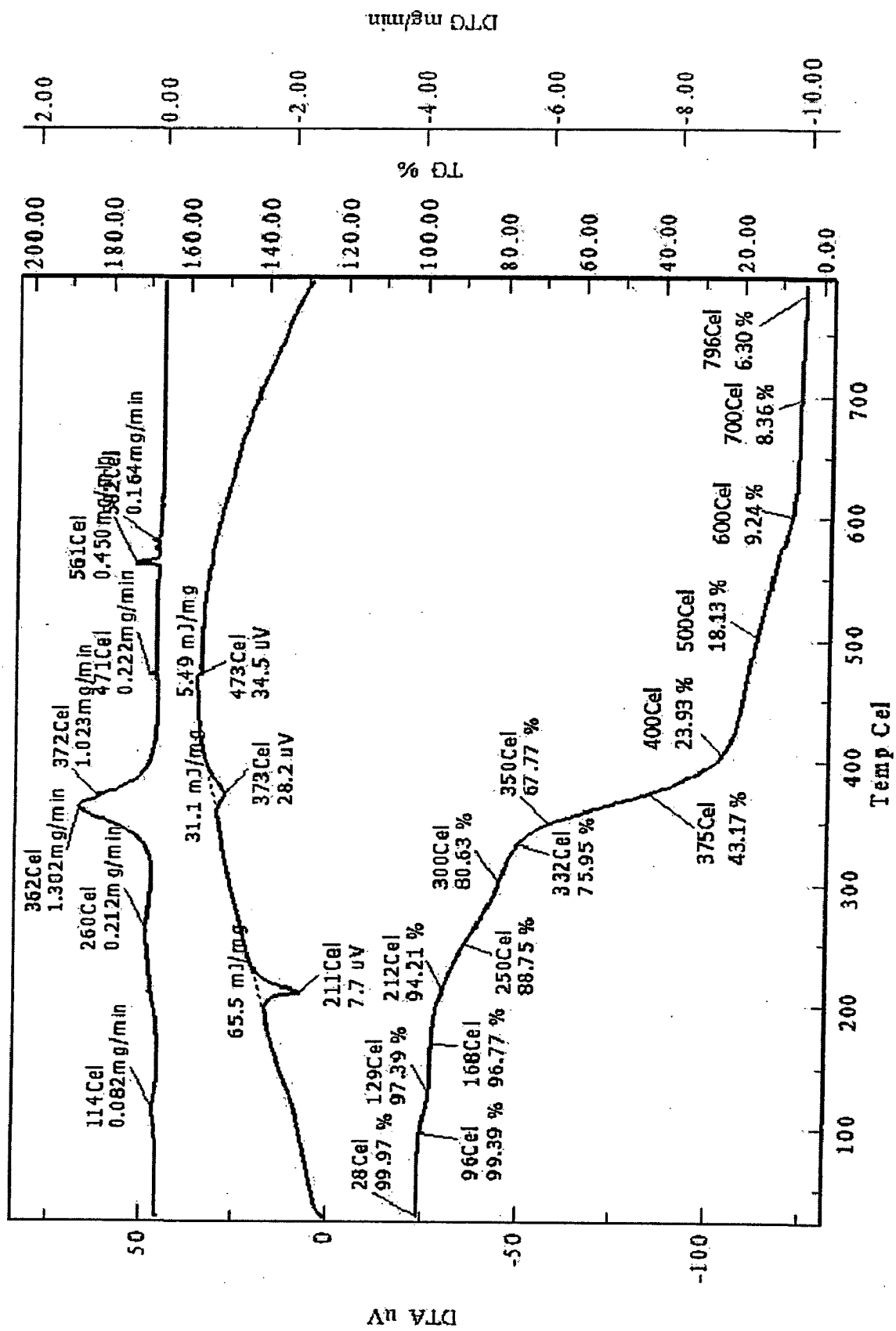


Fig. 5.34 Thermal decomposition data of $[\text{Ni}(\text{Tp}^{\text{Ph,Me}})(\text{pz}^{\text{Ph,Me}})(p\text{-CN-OBz})]$ complex

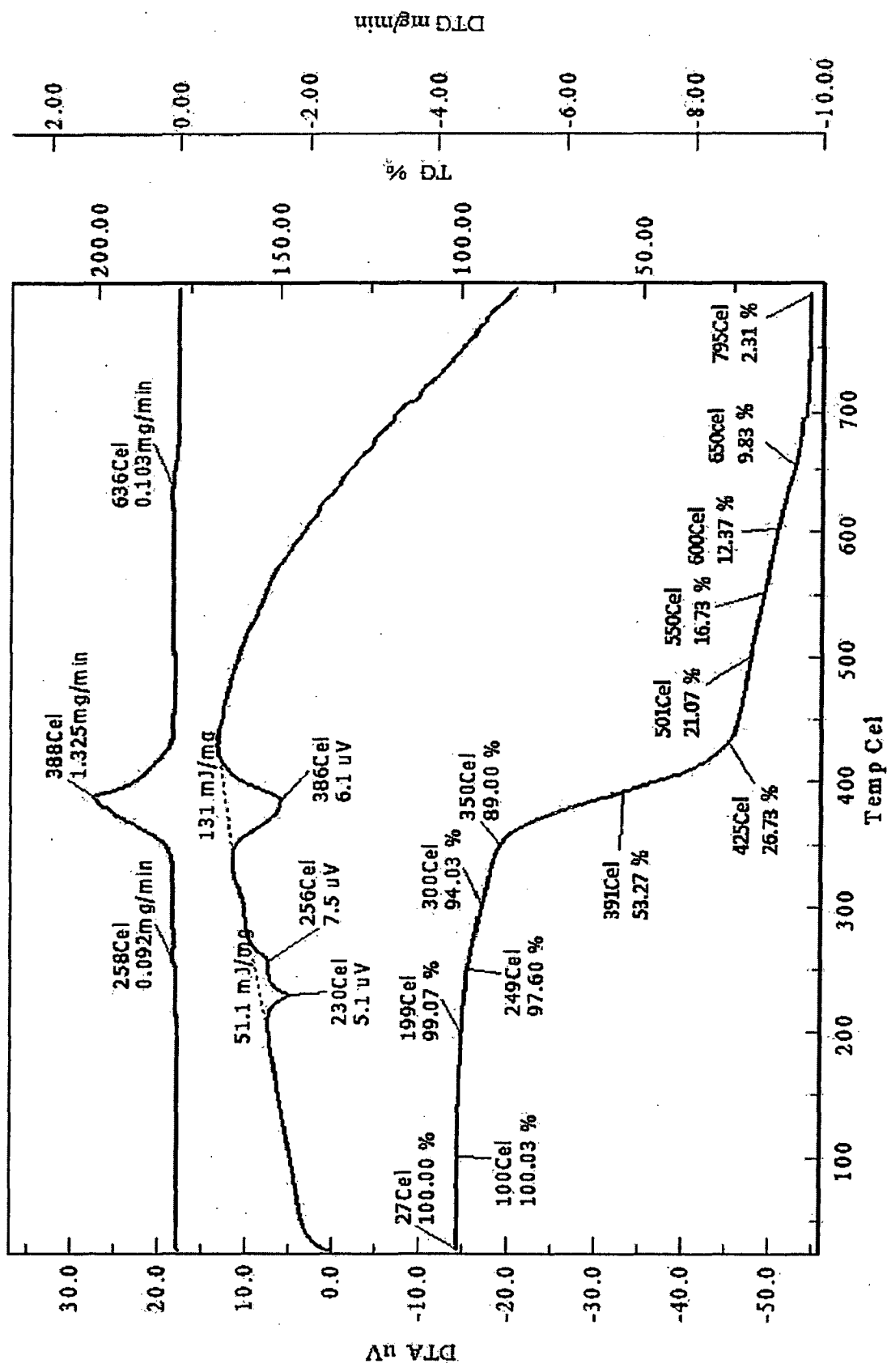


Fig. 5.35 Thermal decomposition data of $[Ni(Tp^{Ph,Me})_2]$ complex

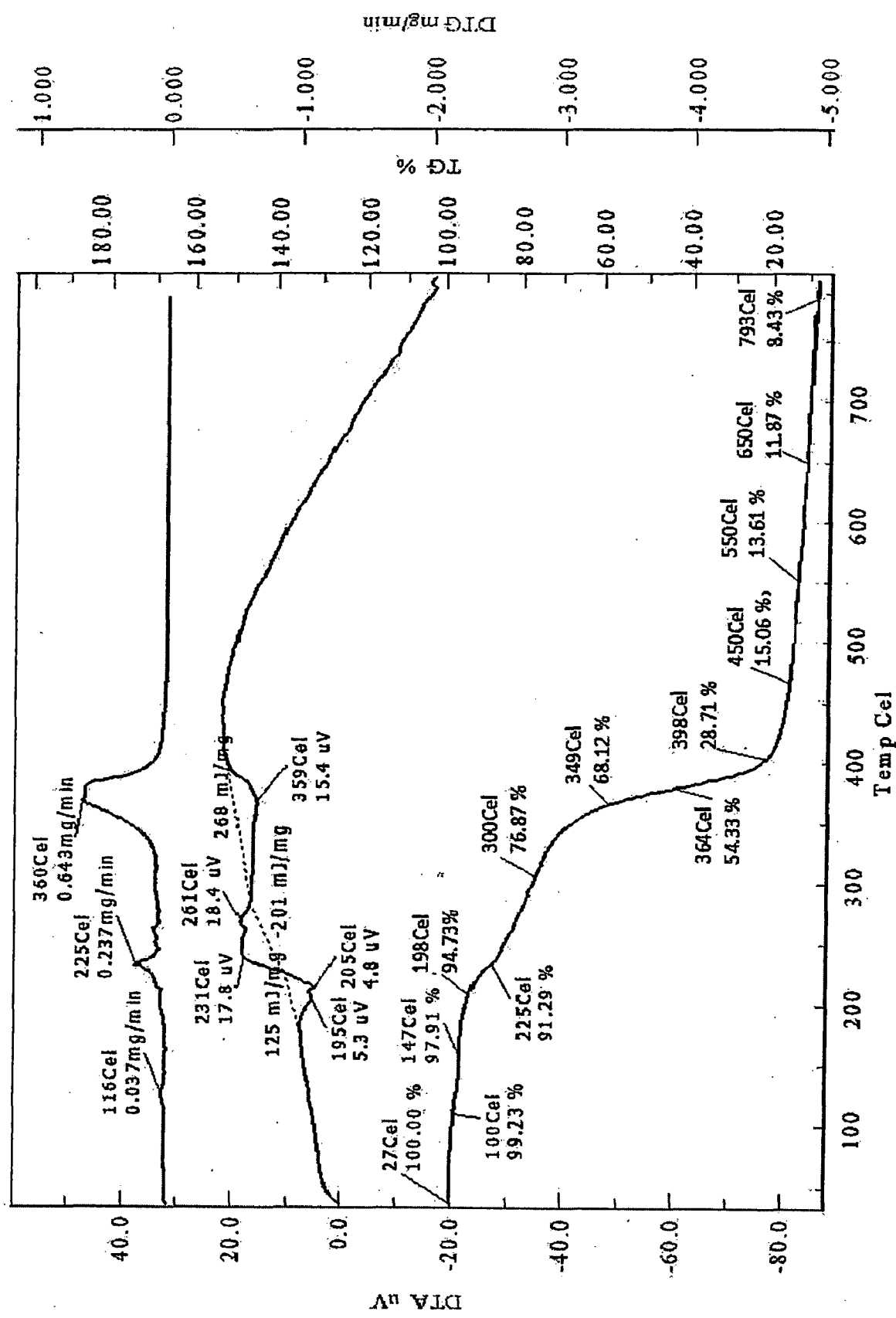


Fig. 5.36 Thermal decomposition data of $[\text{Ni}(\text{Tp}^{\text{Ph,Me}})(\text{pz}^{\text{Ph,Me}})(\text{N}_3)]$ complex

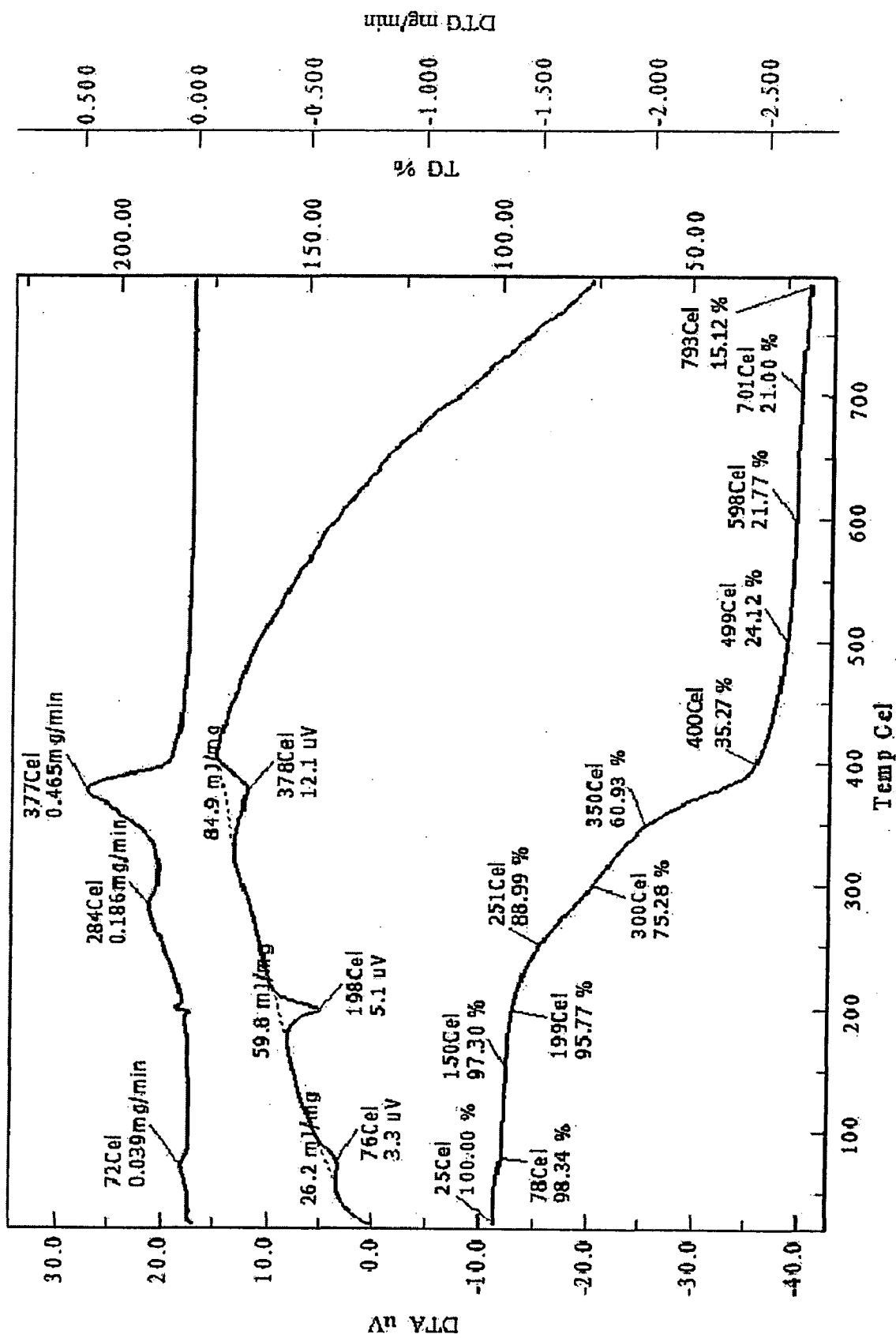


Fig. 5.37 Thermal decomposition data of $[\text{Ni}(\text{Tp}^{\text{Ph,Me}})(\text{pz}^{\text{Ph,Me}})(\text{NCS})]\text{complex}$

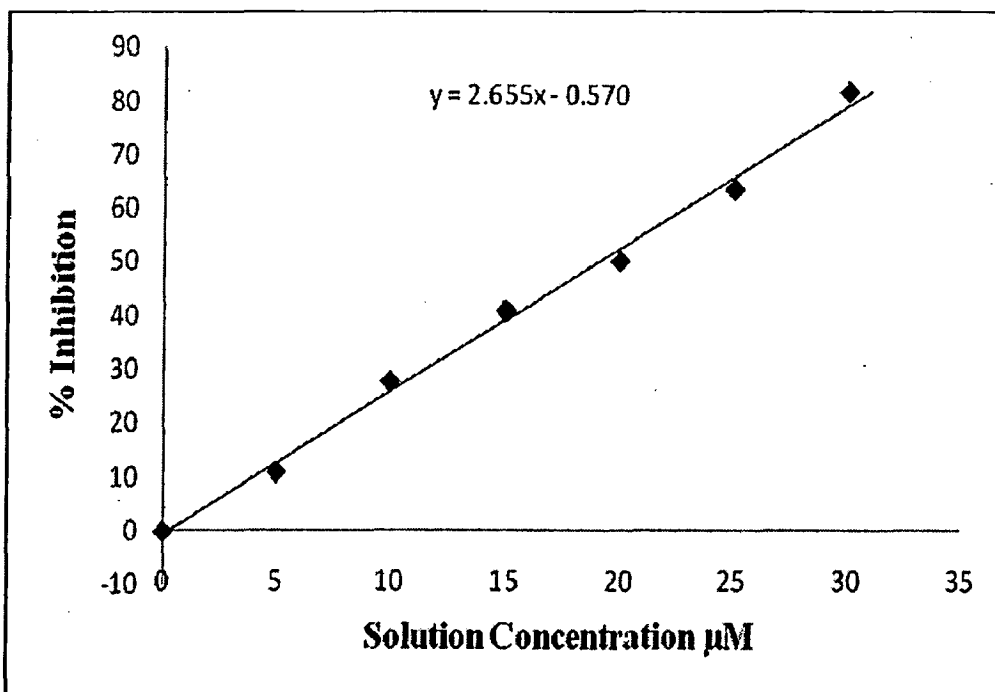


Fig. 5.38 SOD activity of complex 2 in xanthene oxidase-NBT assay

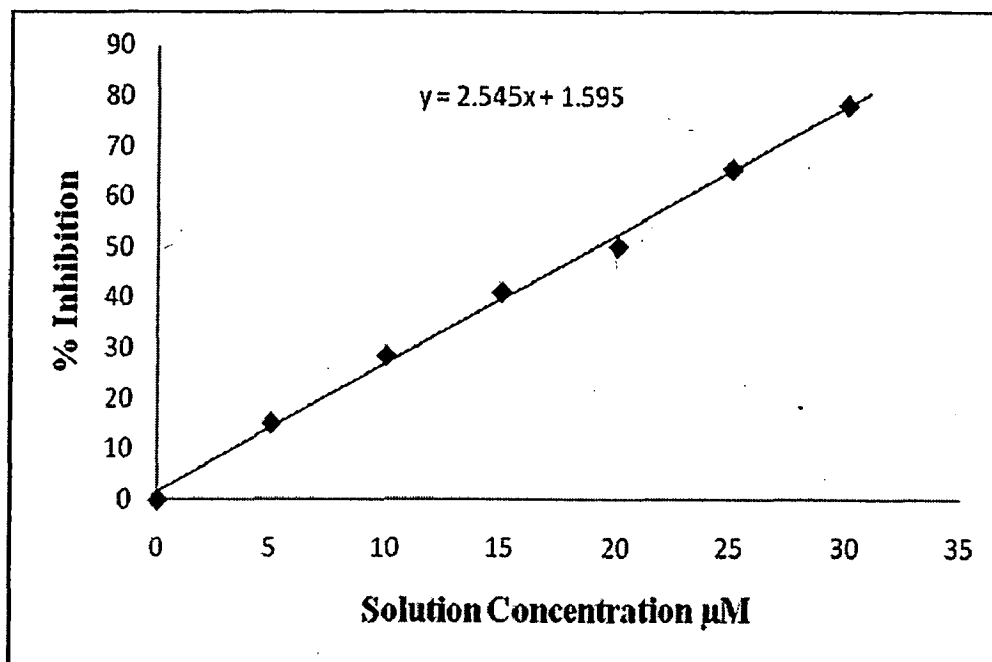


Fig. 5.39 SOD activity of complex 3 in xanthene oxidase-NBT assay

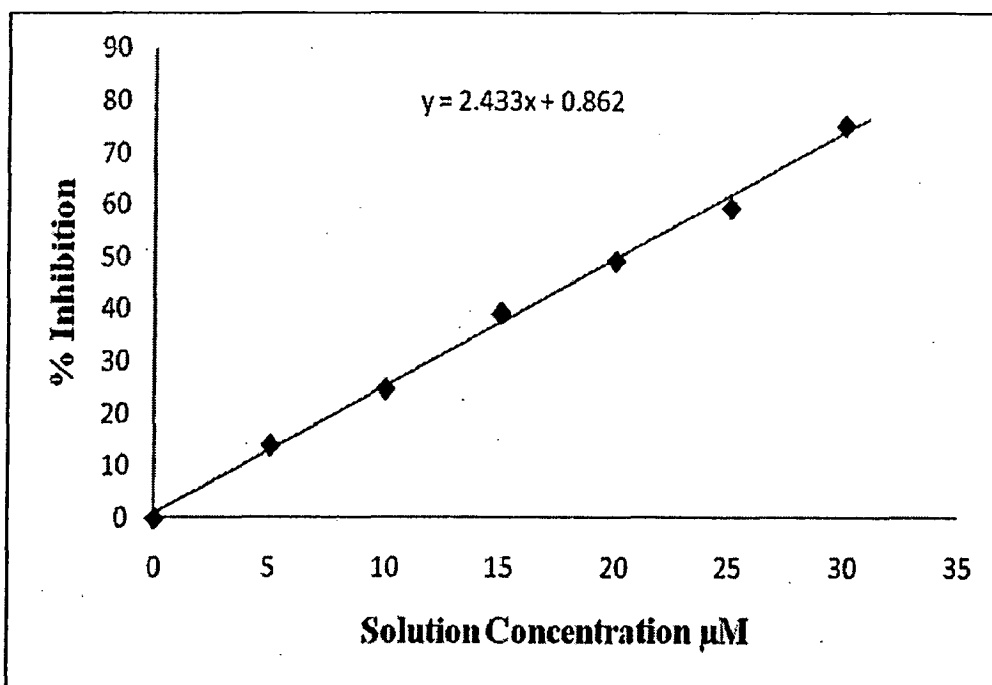


Fig. 5.40 SOD activity of complex 4 in xanthene oxidase-NBT assay

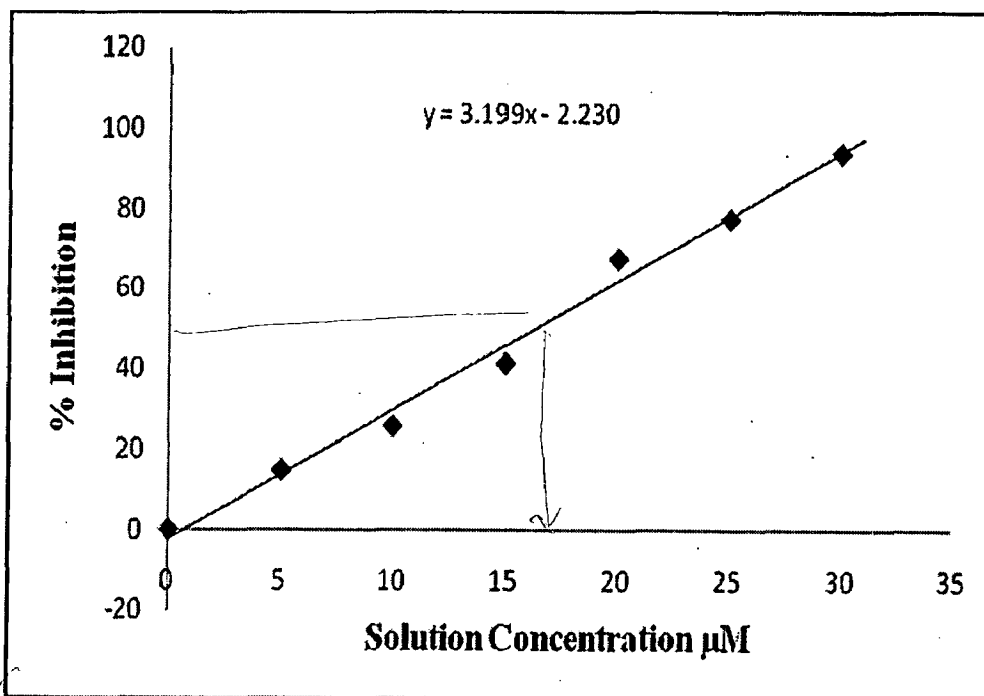


Fig. 5.41 SOD activity of complex 5 in xanthene oxidase-NBT assay

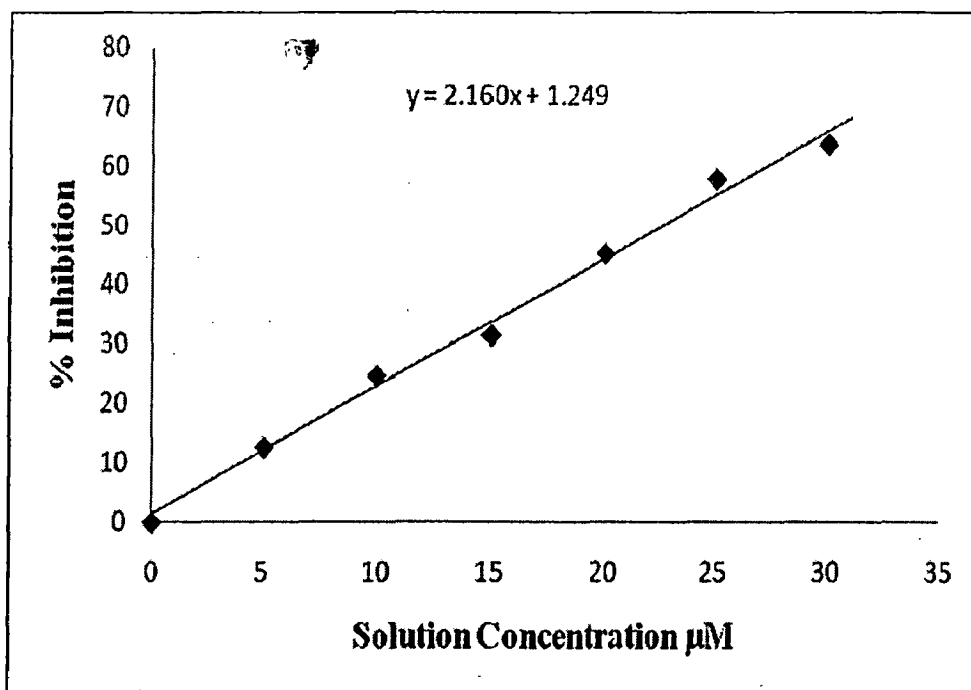


Fig. 5.42 SOD activity of complex 6 in xanthine oxidase-NBT assay

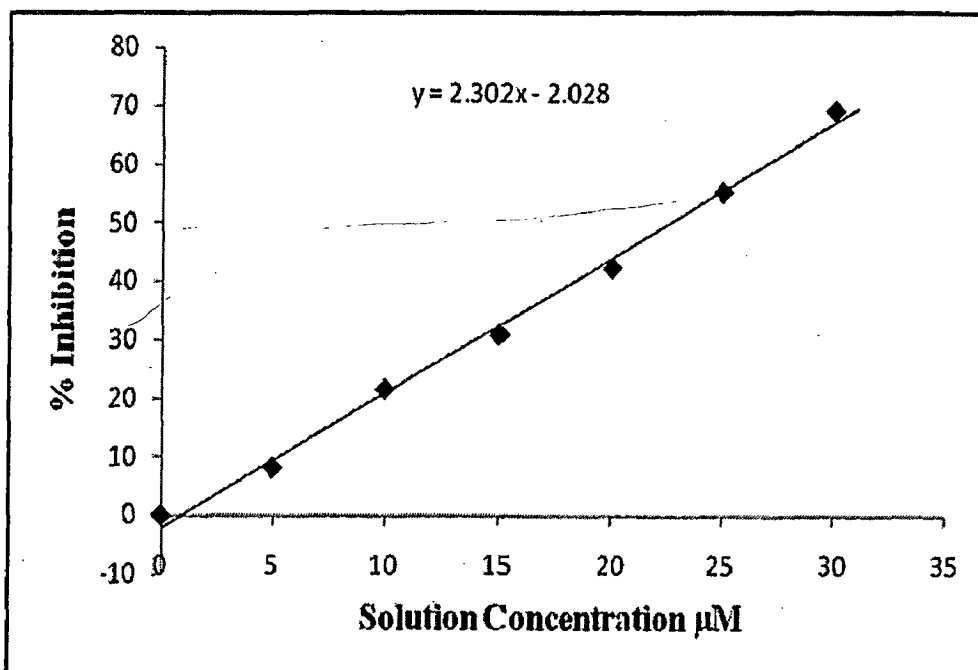


Fig. 5.43 SOD activity of complex 7 in xanthine oxidase-NBT assay

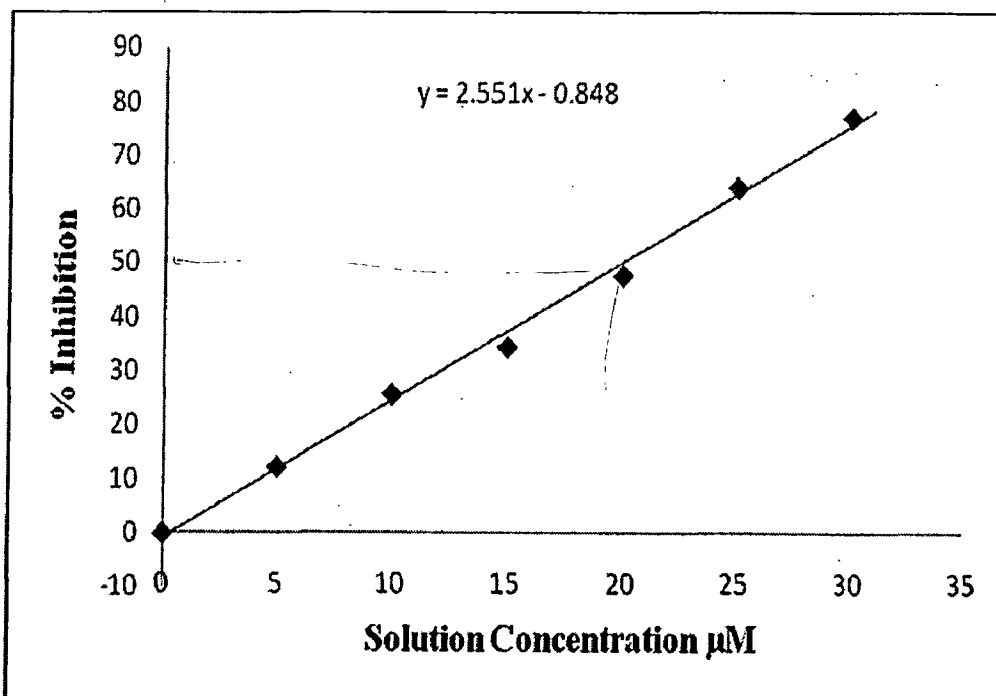


Fig. 5.44 SOD activity of complex 8 in xanthene oxidase-NBT assay

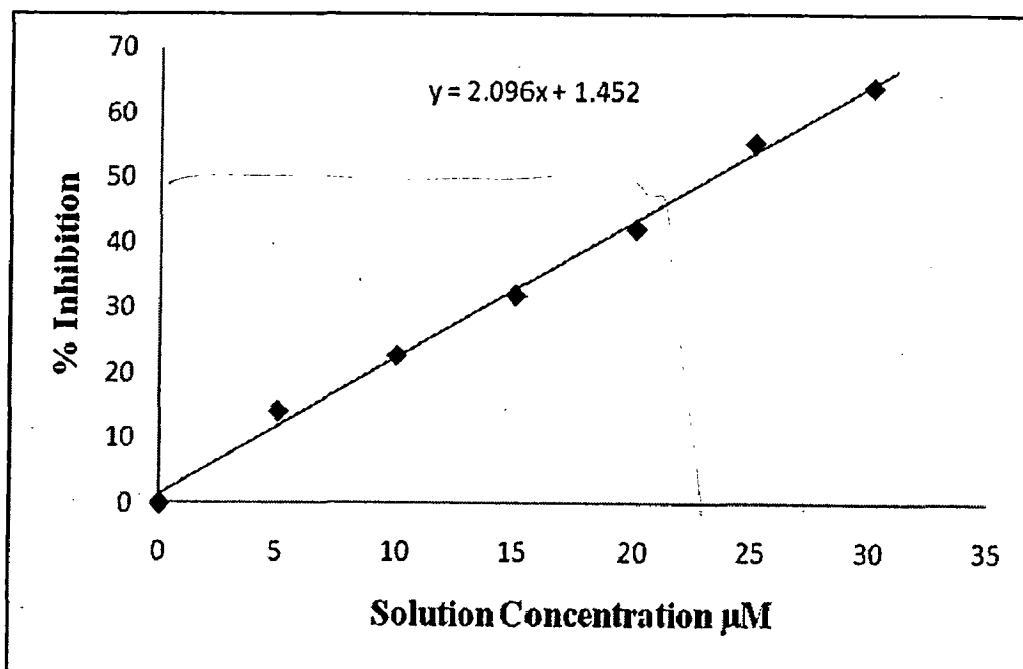


Fig. 5.45 SOD activity of complex 9 in xanthene oxidase-NBT assay

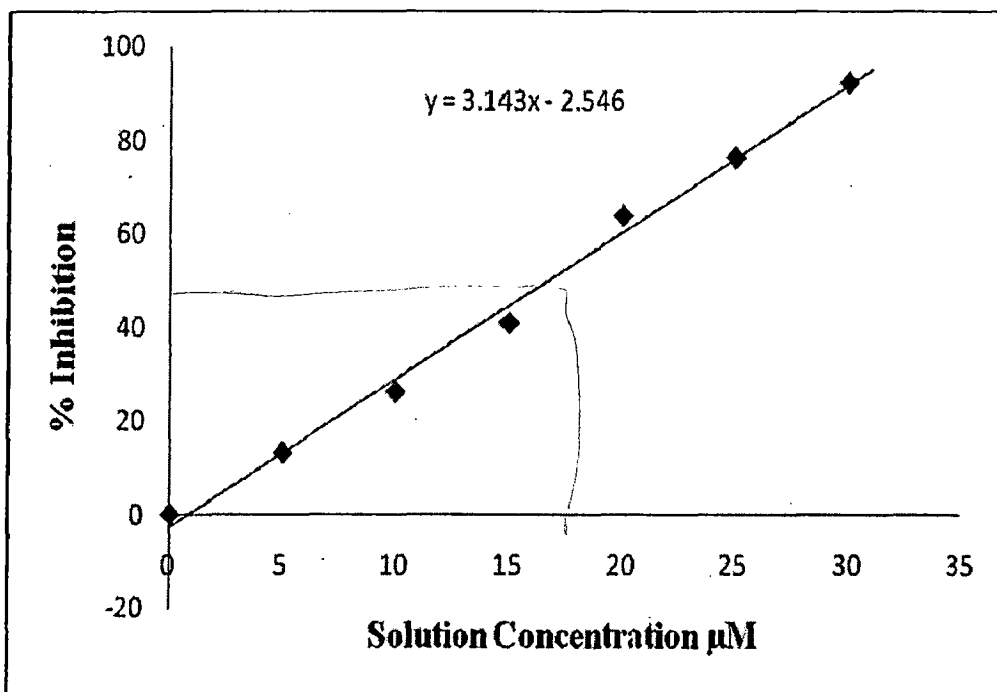


Fig. 5.46 SOD activity of complex 10 in xanthene oxidase-NBT assay

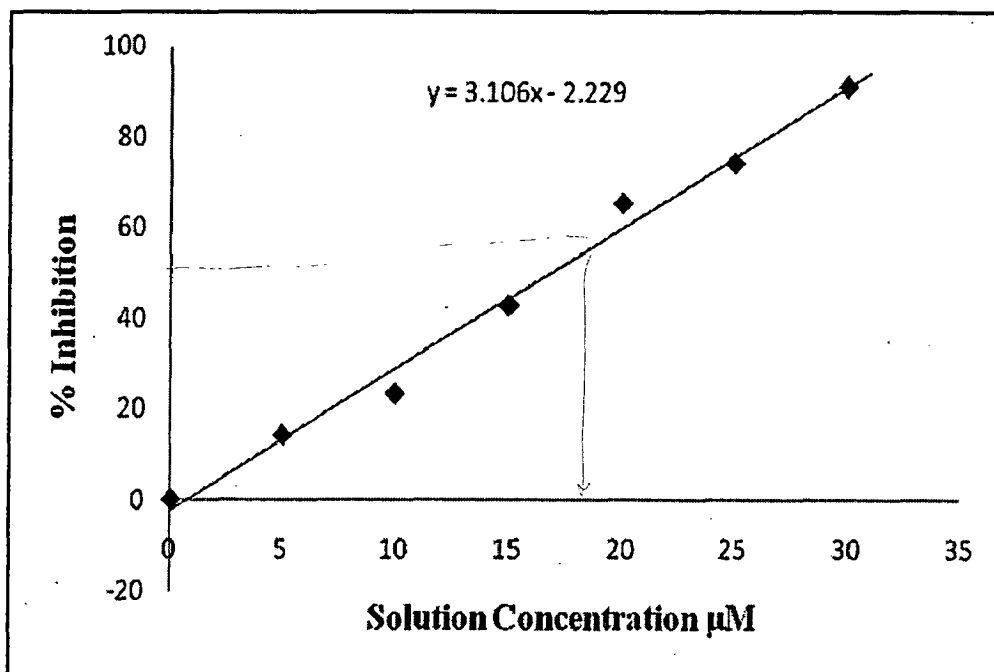


Fig. 5.47 SOD activity of complex 11 in xanthene oxidase-NBT assay

1. Arthur J. R., Bremner I. and Chesters J. K., "Trace elements in animal nutrition", *Inorg. Biochemistry*, H. A. O. Hill, (Ed.), **2**, 283 (1979).
2. Dixon N. E., Gazzola C., Blakeley R. L., and Zerner B., "Jack bean urease (EC 3.5.1.5). Metalloenzyme. Simple biological role for nickel", *J. Am. Chem. Soc.*, **97**, 4131 (1975).
3. Scott B. M. and Robert P. H., "Nickel uptake and utilization by microorganisms", *Nat Struct Biol.*, **10**, 234 (2003).
4. Bible K. C., Buytendrop M., Zierath P. D. and Rinehart K. L., "Tunicchlorin: a nickel chlorin isolated from the caribbean tunicate *Trididemnum soalidum*", *Proc. Natl. Acad. Sci., USA*, **85**, 4582 (1988).
5. Malcolm A. H. and Christou G., "Bioinorganic chemistry of nickel", *Chem. Rev.*, **94**, 2421 (1994).
6. Pearson M. A., Hausinger R. P. and Karplus P. A., "Crystallographic studies of the nickel metalloenzyme urease and insight into the catalytic mechanism", *J. Inorg. Biochem.*, **67**, 179 (1997).
7. Jabri E., Carr M. B., Hausinger R. P. and Karplus P. A., "The crystal structure of urease from *Klebsiella aerogene*", *Science*, **268**, 998 (1995).
8. Day E. P., Peterson, Sendova M. S., Todd M. J. and Hausinger, R.P., "Saturation magnetization of urease from *Klebsiella aerogenes* and Jack bean: No evidence for exchange coupling between the two active site nickel ions in native enzymes", *Inorg. Chem.*, **32**, 634 (1993).
9. Wages R. H. F., Tan. K, L. and Lippard S. J., "[Ni₂(OAc)₃(urea)-(tmen)₂](Otf) and Ni(OAc)(urea)₂(tmen)](Otf), model complexes for the enzyme urease", *Inorg. Chem.*, **32**, 4985 (1993).
10. Chaudhuri P., Kuppers H., Wieghardt K., Gehring S., Haase W., Nuber B. and Weiss J., "Synthesis, magnetic properties, redox ,behaviour and crystal structure of the bridged binuclear nickel(II) complex [Ni₂(μ-OH)(μ-O₂CCH₃)₂L₂](ClO₄).H₂O", *J. Chem. Soc.,Dalton Trans.*, 1367 (1988).
11. Buchanan R. M., Mashuta M. S., Oberhausen K. J., Richardson J. F., Li Q. and Hendrickson D. N., "Active site model of urease: Synthesis, structure and magnetic

- properties of a binuclear Ni(II) complex containing a polyimidazole ligand", *J. Am. Chem. Soc.* **111**, 4497 (1989).
12. Holman T. R., Hendrich M. P. and Que L. Jr., "EPR studies of a dinickel complex in its I, II and III oxidation states", *Inorg. Chem.* **31**, 937 (1992).
 13. Holligan B. M., Jeffery I. C. and Ward M. D., "The coordination chemistry of mixed pyridine-phenol and phenanthroline-phenol ligands;" Effects of π -stacking interactions and ligand rigidity on complex structures ", *J. Chem. Soc.. Dalton Trans.*, 3337 (1992).
 14. Mikuriya. M., Murase I., Asato E. and Kida S., "A novel Mn-carbonato- bridged binuclear nickel(II) complex with N, N', N'', N'''- tetrakis(2-aminoethyl)-1,4,8,11-tetraazacyclotetradecane", *Chem. Lett.*, 497 (1989).
 15. Rawle S. C., Harding C. J., Moore P. and Alcock N. W., "Crystal structure of an antiferromagnetically coupled μ -carboxylato-bridged dinickel(II) complex containing the pendent-arm macrocycle 1-(3-dimethylaminopropyl)-1,5,9-triazacyclododecane (L'); a system which readily sequesters carbon dioxide from air", *J. Chem. Soc., Chem. Commun.*, 1701 (1992).
 16. Eemler U., Grabarse W., Shima S., Goubeaud M. and Thauer R. K., "Crystal structure of methyl-CoM reductase containing a Niporphinoid," *J. Inorg. Biochem.*, **67**, 180 (1997).
 17. Thauer R. K., "Structure and function of the nickel enzyme methyl coenzyme M-reductase", *J. Inorg. Biochem.*, **74**, 54 (1999).
 18. Higuchi Y. and Yasuoka N., "Novel nickel-iron active center found in hydrogenase", *J. Inorg. Biochem.*, **67**, 190 (1997).
 19. Cammack R., Fernandez V. M. and Schneider K., (Ed.), "Title Bioinorganic chemistry of nickel", VCH Publishers (1988).
 20. Voo. J. K., Riordan C. G., Yap G. P. A. and Rheingold A. L., "Models for the active sites of carbon monoxide dehydrogenase/acetyl coenzyme synthase", *J. Inorg. Biochem.*, **74**, 330 (1999).
 21. Russell. W., Stalhandske K., Xia J., Scott R. A. and Lindahl P. A., "Spectroscopic, redox and structural characterization of the Ni-labile and nonlabile forms of the

Chapter-6

REFERENCES

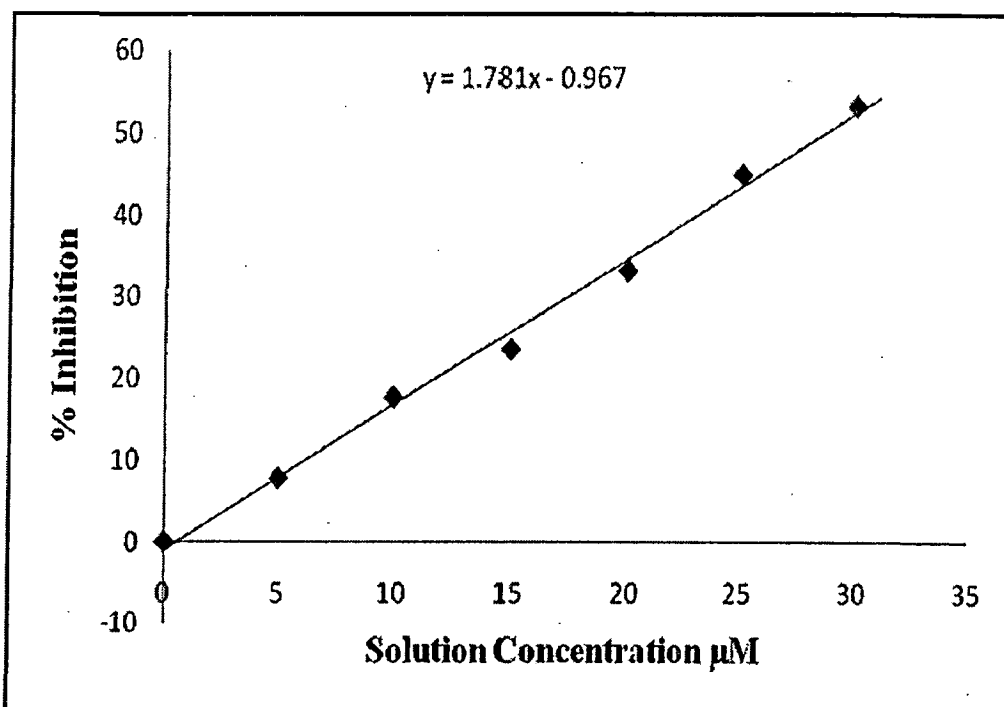


Fig. 5.50 SOD activity of complex 14 in xanthene oxidase-NBT assay

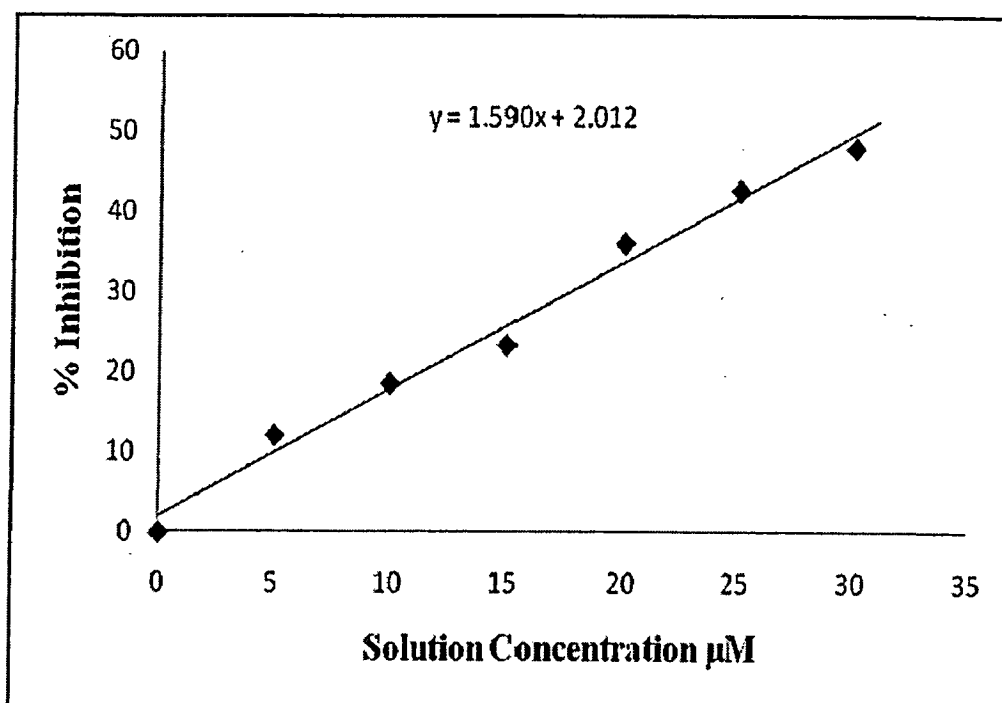


Fig. 5.51 SOD activity of complex 15 in xanthene oxidase-NBT assay

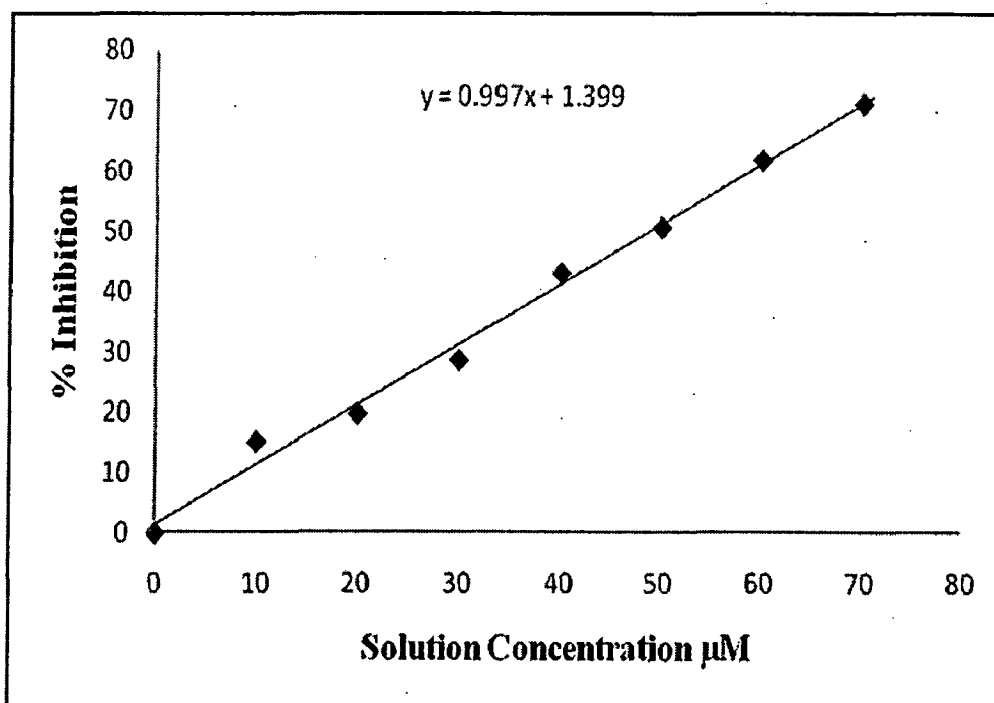


Fig. 5.48 SOD activity of complex 12 in xanthene oxidase-NBT assay

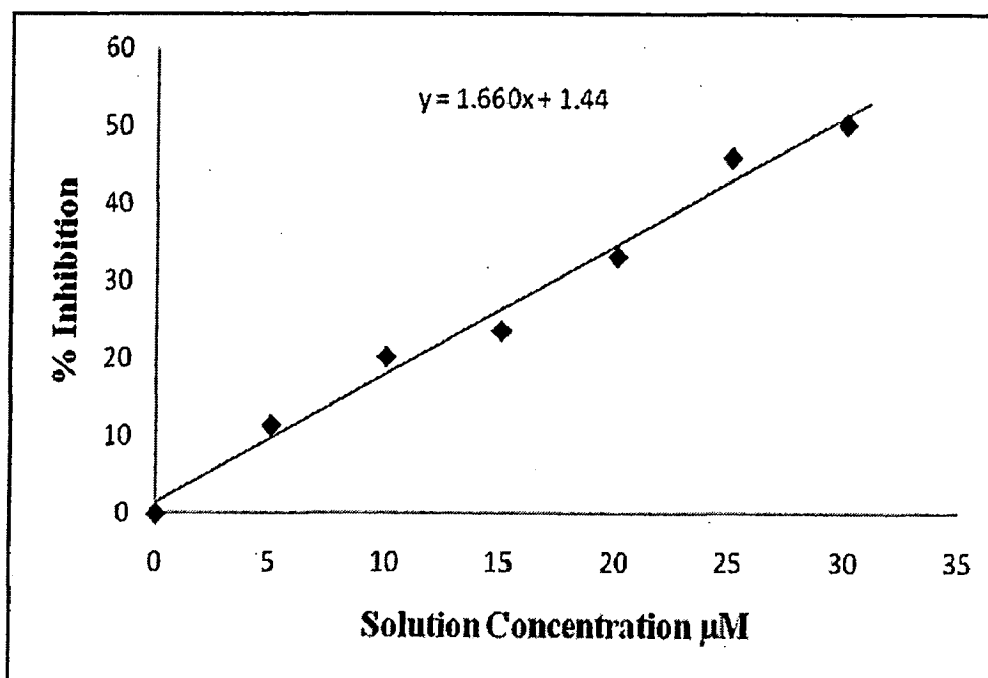


Fig. 5.49 SOD activity of complex 13 in xanthene oxidase-NBT assay

- acetyl-CoA synthase active site of carbon monoxide dehydrogenase", *J. Am. Chem. Soc.*, **120**, 7502 (1998).
22. Fridovich I. "Superoxide dismutases. An adaptation to a paramagnetic gas", *J. Biol. Chem.*, **264**, 7761 (1989).
 23. Fridovich I. "Oxygen toxicity: a radical explanation", *J. Exp. Biol.*, **201**, 1203 (1998).
 24. Rosen D. R., Siddique T., Patterson D., Figlewicz D. A., Sapp P., Hentati A., Donaldson D., Goto J., O'Regan J. P. and Deng H. X. "Mutations in Cu/Zn superoxide dismutase gene are associated with familial amyotrophic lateral sclerosis", *Nature*, **362**, 59 (1993).
 25. Orrell R. W. "Amyotrophic lateral sclerosis: copper/zinc superoxide dismutase (SOD1) gene mutations", *Neuromuscular Disord.*, **10**, 63 (2000).
 26. Stathopoulos P. B., Rumfeldt J. A., Scholz G. A., Irani R. A., Frey H. E., Hallewell R. A., Lepock J. R. and Meiring E. M. "Cu/Zn superoxide dismutase mutants associated with amyotrophic lateral sclerosis show enhanced formation of aggregates in vitro", *Proc. Natl. Acad. Sci., U.S.A.*, **100**, 7021 (2003).
 27. Liochev S. I. and Fridovich I. "Mutant Cu₂Zn superoxide dismutases and familial amyotrophic lateral sclerosis: evaluation of oxidative hypotheses", *Free Radical Biol. Med.*, **34**, 1383 (2003).
 28. Bordo D., Pesce A., Bolognesi M., Stroppolo M. E., Falconi M. and Desideri A. "Copper-zinc superoxide dismutase in prokaryotes and eukaryotes". In *Handbook of Metalloproteins*, Messerschmidt, A., Huber, R., Poulos, T., and Wieghardt, K., Eds.; Wiley & Sons: Chichester, New York, Weinheim, Brisbane, Singapore, Toronto., **2**, 1284 (2001).
 29. Youn H.-D., Youn H., Lee J.-W., Yim Y.-I., Lee J.-K., Hah Y. C. and Kang S.-O. "Unique isozymes of superoxide dismutase in *Streptomyces griseus*", *Arch. Biochem. Biophys.*, **334**, 341 (1996).
 30. Youn H.-D., Kim E.-J., Roe J.-H., Hah Y. C. and Kang S.-O. "A novel nickel-containing superoxide dismutase from *Streptomyces* spp.", *Biochem. J.*, **318**, 889(1996).

31. Kim E.-J., Kim H.-P., Hah Y. C. and Roe J.-H. "Differential expression of superoxide dismutases containing Ni and Fe/Zn in *Streptomyces coelicolor*", *Eur. J. Biochem.*, **241**, 178 (1996).
32. Palenik B., Brahamsha B., Larimer F. W., Land M., Hauser L., Chain P., Lamerdin J., Regala W., Allen E. E., McCarren J., Paulsen I., Dufresne A., Partensky F., Webb E. A. and Waterbury J. "The genome of a motile marine synechococcus", *Nature*, **424**, 1037 (2003).
33. Maroney M. J., Choudhary S. B., Lee J. -W., Davidson G., Yim Y -I., Bose. K., Sharma M. L., Kang S.-O. and Cabelli D. E. "A SOD story: the structure and function of the NiSOD active site," *J. Inorg. Biochem .*, **74**, 39 (1999).
34. Wuerges, J., Lee, J.-W., Yim, Y.-I., Yim, H.-S., Kang, S.-O. and Carugo, K. D. "Crystal structure of nickel-containing superoxide dismutase reveals another type of active site." *Proc. Natl. Acad. Sci. U.S.A.*, **101**, 8569 (2004).
35. Barondeau D. P., Kassmann C. J., Bruns C. K., Tainer J. A. and Getzoff E. D. "Nickel superoxide dismutase structure and mechanism", *Biochemistry*, **43**, 8038 (2004).
36. Barondeau D. P. and Getzoff E. D. "Structural insights into protein-metal ion partnerships", *Curr. Opin. Struct. Biol.*, **14**, 765(2004).
37. Vladimir P. and Per E. M. Siegbahn, "Nickel Superoxide Dismutase Reaction Mechanism Studied by Hybrid Density Functional Methods", *J. Am. Chem. Soc.*, **23**, 7475 (2006).
38. Christianson D. V. and Lipscomb W. N., "Carboxypeptidase A", *Acc. Chem. Res.*, **22**, 62(1989).
39. Bertini. J., Donaire. A., Monnanni R., Moratal J. M. and Salgado J., "Spectroscopic characterization of nickel(II) carboxypeptidase", *J. Chem. Soc.. Dalton Trans.*, 1443 (1992).
40. Moratal J. M., Castells J., Donaire A., Salgado J. and Jimenez H. R., "Interaction of carboxylate inhibitors with the active site of nickel(II) carboxypeptidase A", *J. Chem. Soc., Dalton Trans.*, 3317(1992).

41. Bertinin I., Borghi E., Luchinat C. and Monnanni R., "Nickel carbonic anhydrase: A re-examination of the electronic spectra with the help of CD spectra", *Inorg. Chim. Acta*, **67**, 99(1982).
42. Moratal J. M., Martinez-Ferrer M. J., Donaire A., Castells J., Salgado J. and Jimenez H. R., "Spectroscopic studies of nickel(II) carbonic anhydrase and its adducts with inorganic anions", *J. Chem. Soc., Dalton Trans.*, 3393 (1991).
43. Kitajima N., Hikichi S., Tanaka M. and Moro-oka Y., "Fixation of atmospheric CO₂ by a series of hydroxo complexes of divalent metal ions and the implication for the catalytic role of metal ion in carbonic anhydrase. Synthesis, characterization and molecular structure of [LM(OH)]_n (n = 1 or 2) and LM(μ-CO₃)ML, (M(II) = Mn, Fe, Co, Ni, Cu, Zn; L = HB(3,5-iPr₂pz)₃)", *J. Am. Chem. Soc.*, **115**, 5496(1993).
44. (a) Looney A., Saleh A., Zhang Y. and Parkin, G., "Tris(pyrazolyl)hydroborato complexes of cadmium: A bidentate nitrate derivatives and its relevance to carbonic anhydrase activity", *Inorg. Chem.*, **33**, 1158 (1994). (b) Looney, A. and Parkin, G., "Molecular structure of {η³-HB(pz)₃}ZnNO₃: Comparison between theory and experiment in a model carbonic anhydrase system", *Inorg. Chem.*, **33**, 1234 (1994).
45. Trofimenko S., "The coordination chemistry of pyrazole-derived ligands", *Chem. Rev.*, **72**, 497(1972).
46. Trofimenko S., "Coordination chemistry of pyrazole-derived ligands", *Prog. Inorg. Chem.*, **34**, 115 (1986). (b) Trofimenko, S., "Recent advances in poly(pyrazolyl)borate (scorpionate) chemistry", *Chem. Rev.*, **93**, 943 (1993).
47. Akita M. and Hikichi S. "Inorganic chemistry based on Tp ligands from dioxygen complexes to organo-metallic systems". *Bull. Chem. Soc. Jpn.*, **8**, 1657(2002).
48. Santi R., Anna M. R., Anna S., Manuela G., Claudio B. and Giuseppe M., "Catalytic polymerisation of ethylene with tris(pyrazolyl) borate complexes of late transition metals". *J. Mol. Catal. A: Chemical*, **229**, 191 (2005).
49. Parkin G., "Bis(pyrazolyl)hydroborato ligands are represented by the abbreviations[BpR,R] with the 3- and 5-alkyl substituents listed respectively as superscripts", *Adv. Inorg. Chem.* **42**, 291 (1995).

50. Ruggiero C.E., Carrier S.M. and Tolman W.B., "Reductive Disproportionation of NO Mediated by Copper Complexes: Modeling N₂O Generation by Copper Proteins and Heterogeneous Catalysts", *Angew. Chem.*, **33**, 895(1994).
51. Cho S.H., Whang D., Han K.N. and Kim K., "Convenient synthesis, structure and properties of trichloro(hydrotripyrazolylborato)ferrate(1-)", *Inorg. Chem.* **31**, 519(1992).
52. Sun Y.-J., Cheng P., Yan S.-P., Jiang Z.-H., Liao D.-Z. and Shen P.-W., "New half-sandwich nickel(II) complex with mono-hydrotris-(3,5-dimethylpyrazolyl) borate ligand and nitrite". *Inorg. Chem. Commun.*, **3**, 289 (2000).
53. Kunrath F. A., de Souza R. F., Casagrande O. L., Brooks N. R. and Young V. G. J., "Highly Selective Nickel Ethylene Oligomerization Catalysts Based on Sterically Hindered Tris(pyrazolyl)borate Ligands", *Organometallics*, **22**, 4739 (2003).
54. Kitano T., Sohrin Y., Hata Y., Mukai H., Wada H. and Ueda K., "Highly selective extraction of Cu(II) and Zn(II) using [B(3-*i*Prpz)₄]⁻ (*i*Prpz=1-isopropylpyrazolyl)", *Polyhedron*, **23**, 283 (2004).
55. Anastasiya V. Yakovenko, Sergey V. Kolotilov, Anthony W. Addison, Swiatoslaw Trofimenko, Glenn P.A. Yap, Victoria Lopushanskaya and Vitaly V. Pavlishchuk, "Ni(II), Co(II) and Mn(II) tris(pyrazolyl)borate complexes with 2,6-di-*tert*-butyl-4-carboxy-phenol: Formation of coordinated phenoxyl radical", *Inorg. Chem. Commun.*, **8**, 932 (2005).
56. Matsunaga Y., Fujisawa K., Ibi N., Miyashita Y., and Okamoto K., "Structural and Spectroscopic Characterization of First-Row Transition Metal(II) Substituted Blue Copper Model Complexes with Hydrotris(pyrazolyl)borate", *Inorg. Chem.*, **44**, 325 (2005).
57. Harding D. J., Harding P., Adams H. and Tuntulani T., "Synthesis and Characterization of Sterically Hindered Tris(pyrazolyl)borate Ni Complexes", *Inorganica Chimica Acta*, Accepted Manuscript, (2007).
58. McCord J. M. and Fridovich I., "Superoxide dismutase: an enzymic function for erythrocuprein (hemocuprein)", *J. Biol. Chem.* **244**, 6049 (1969).
59. Beauchamp C. and Fridovich I., "Superoxide Dismutase: Improved Assays and an Assay Applicable to Acrylamide Gels", *Anal. Biochem.* **44**, 276 (1971).

60. Patel R. N., Singha N. and Gundla V.L.N. "Synthesis, characterization and superoxide dismutase activity of some octahedral nickel(II) complexes", *Polyhedron*, 26, 757 (2007).